Universidade de Lisboa

Faculdade de Medicina

Malaria and Tuberculosis co-infection: role for Hemozoin immunosuppression?

Rosangela Maria Rodrigues Carvalho Frita

Doutoramento em Ciências Biomédicas
Especialidade em Microbiologia e Parasitologia

2014

Universidade de Lisboa

Faculdade de Medicina

Malaria and Tuberculosis co-infection: role for Hemozoin immunosuppression?

Rosangela Maria Rodrigues Carvalho Frita

Tese orientada pelo Professor Doutor Thomas Hänscheid e
Professora Doutora Maria M Mota

Doutoramento em Ciências Biomédicas
Especialidade em Microbiologia e Parasitologia

Todas as afirmações efectuadas no presente documento são da exclusiva responsabilidade do seu autor, não cabendo qualquer responsabilidade à Faculdade de Medicina de Lisboa pelos conteúdos nele apresentados.

A impressão desta dissertação foi aprovada pela Comissão Coordenadora do Conselho Científico da Faculdade de Medicina de Lisboa em reunião de 28 de Janeiro de 2014.

Dissertação apresentada à Faculdade de Medicina da Universidade de Lisboa, para obtenção do grau de Doutor em Ciências Biomédicas.

Todas as experiências realizadas foram feitas com a Aprovação do Comité de Ética da Faculdade de Medicina e pela Direcção Geral de Veterinária.

A presente dissertação foi realizada na Unidade de Microbiologia Molecular e Infecção do Instituto de Medicina Molecular, Faculdade de Medicina da Universidade de Lisboa.

O trabalho aqui apresentado foi realizado no âmbito do projecto PIC/IC/83214/2007.
Bolsa de Doutoramento da Fundação para a Ciência e a Tecnologia (referência: SFRH/ BD/61174/2009).

Á minha mãe e pai

Abstract

Malaria and tuberculosis (TB) endemic regions overlap considerably, especially in sub-Saharan Africa. Although it is very likely that co-infections occur in these regions, not much is known about malaria-TB co-infections in humans, and how the interplay between these two infections might affect the prognosis of co-infected individuals. Furthermore, multiple *Plasmodium* infections will likely result in accumulation of malaria pigment (hemozoin) in host organs. Hemozoin was first thought of as an inert waste product resulting from hemoglobin digestion. However, several studies have associated the presence of hemozoin with host immunosuppression. Thus, the subject of this thesis was the study of Malaria-Tuberculosis co-infections with a particular focus on a possible role for hemozoin induced immunosuppression.

For this, protocols for hemozoin production and characterization were first established. Then, *in vitro* studies to investigate how hemozoin ingestion affected cellular functions of human peripheral blood mononuclear cells (PBMC) were performed. For the first time hemozoin effects at the single cell level were investigated by flow-cytometry, using a novel method developed by us, which uses Side Scatter Depolarization for hemozoin detection.

Following *in vitro* studies, we investigated hemozoin dynamics in host tissues of two murine models, post-malaria clearance. Hemozoin deposition in host organs was evaluated both by flow-cytometry, as well as by observation of histological preparations. Finally, the murine model was used to evaluate the susceptibility of *Plasmodium* infected mice to subsequent tuberculosis infection. Tuberculosis infection was evaluated during acute malaria, and during chronic *Plasmodium* infection.

Results from *in vitro* studies suggested that hemozoin impaired cell functions and that these effects could be propagated to non-hemozoin containing cells. Hemozoin-induced impairment decreased microbicidal activity, as shown by higher mycobacterial load in these cells. Our investigation of hemozoin kinetics in host organs revealed that hemozoin is dynamic within and between host organs, with very little signs of it being eliminated over time.

Malaria-tuberculosis co-infection *in vivo* demonstrated that mice presenting with acute malaria, have a poor prognosis when co-infected with tuberculosis. Mice infected with tuberculosis during chronic malaria did not become as sick as mice during acute infection however, they still exhibited symptoms of malaria-induced anaemia. Thus, in

our model of co-infection hemozoin did not seem to contribute significantly to immunosuppression of the host nor to increased susceptibility to tuberculosis infection.

Overall, we present a novel method for the detection of hemozoin that allowed functional investigation of hemozoin-containing and non-hemozoin containing leukocytes at the single cell level, in the same sample. This might be useful for further studies using leukocytes from malarious patients, who usually only have a few percent of these cells in circulation. We also provide evidence for poor prognosis of malaria-tuberculosis co-infection. Furthermore, we demonstrated that following a malaria episode, hemozoin deposition in host organs did not seem to contribute to immunosuppression of the host nor to increased susceptibility to tuberculosis infection by *M. bovis* BCG. However, we observed that hemozoin-containing macrophages participated in granuloma formation in response to tuberculosis infection. This might prove relevant in the context of a tuberculosis infection by the virulent strain *M. tuberculosis*, in which tighter control by immune cells is necessary to prevent tuberculosis dissemination.

Keywords: Hemozoin, Malaria, Tuberculosis, Immunosuppression, Co-infection.

Resumo

As regiões endémicas da malária e tuberculose sobrepõem-se consideravelmente, especialmente na África sub-Saariana. Embora seja bastante provável que co-infecções entre malária e tuberculose ocorram nestas regiões, pouco se sabe sobre a sua incidência, ou como a sua interação poderá afectar o prognóstico de indivíduos co-infectados. Episódios consecutivos de malária poderão levar à acumulação do pigmento malárico (hemozoína) nos órgãos do hospedeiro. Inicialmente, a hemozoína era considerada um sub-produto inerte, resultante da digestão da hemoglobina pelo parasita. No entanto, vários estudos têm associado a presença da hemozoína com imunossupressão do hospedeiro. Assim, o tema desta tese foi o estudo da co-infecção malária-tuberculose, com especial foco no possível papel da hemozoína na indução de imunossupressão no hospedeiro.

Neste projecto, começou por estabelecer-se protocolos para produção e caracterização de hemozoína. Consequentemente, foram realizados estudos *in vitro* para investigar o impacto da ingestão de hemozoína nas funções celulares de células mononucleadas do sangue periférico (PBMC) humanos. Pela primeira vez, os efeitos da hemozoína foram investigados por citometria de fluxo, utilizando um novo método desenvolvido por nós, que utiliza a detecção da despolarização da luz para a identificação de células que contêm hemozoína.

Após esta caracterização *in vitro*, a dinâmica da hemozoína em tecidos do hospedeiro após a infecção por *Plasmodium* foi investigada, usando dois modelos de ratinho. A acumulação de hemozoína em órgãos do hospedeiro foi avaliada por citometria de fluxo, e pela observação de preparações histológicas, ao longo do tempo.

Finalmente, o modelo de murino foi usado para avaliar a susceptibilidade de ratinhos com malária a uma subsequente infecção por tuberculose. A infecção por tuberculose foi avaliada durante as fases aguda e crónica de malária.

Os resultados dos estudos *in vitro* sugerem que a hemozoína compromete funções celulares importantes e que estes efeitos podem ser propagados a células que não têm hemozoína. A inibição de funções celulares levou à redução da capacidade microbicida, como mostrado pelo aumento da carga bacteriana nestas células. Relativamente à avaliação da cinética da hemozoína nos tecidos do hospedeiro, este estudo revelou que a hemozoína tem uma distribuição dinâmica tanto dentro do mesmo órgão, como entre

diferentes órgãos do hospedeiro. Também se observou que, ao longo do tempo, a hemozoína não parece ser eliminada dos órgãos do hospedeiro.

Os ensaios *in vivo* de co-infecção malária-tuberculose demonstraram que ratinhos com malária desenvolvem uma doença fulminante, quando co-infectados com tuberculose. Este fenótipo agravado não foi observado em ratinhos infectados com tuberculose durante uma infecção crónica de malária, ainda que estes apresentassem sinais de anemia associada à malária. Tendo em conta os resultados obtidos com o nosso modelo, a hemozoína não parece contribuir de forma significativa para a imunossupressão do hospedeiro nem para um aumento de susceptibilidade à infecção por tuberculose.

Em resumo, este trabalho apresenta um novo método para a detecção de hemozoína. Este método permitiu a investigação de funções celulares em leucócitos com e sem hemozoína na mesma amostra, ao nível celular. Esta metodologia poderá ser aplicada noutros estudos, nomeadamente na análise de leucócitos com hemozoína de doentes com malária, cujas percentagens são normalmente baixas. Os resultados apresentados nesta tese também sugerem que co-infecções de malária-tuberculose resultam numa deterioração rápida do hospedeiro. No entanto, como observado durante a infecção crónica de malária, a deposição de hemozoína nos órgãos do hospedeiro não parece contribuir para um aumento da imunossupressão do hospedeiro, não tendo sido observada uma maior susceptibilidade à infecção por tuberculose. Ainda assim, foi observado que macrófagos com elevado conteúdo em hemozoína contribuem significativamente para a formação de granulomas, em resposta à infecção por *M. bovis* BCG. Isto pode ser relevante no contexto de uma infecção de tuberculose pela estirpe virulenta *M. tuberculosis*, em que é necessário um controlo mais restrito por células do sistema imunitário para prevenir a disseminação da tuberculose.

Palavras-chave: Hemozoína, Malária, Tuberculose, Imunossupressão, Co-infecção.

Acknowledgements

I would like to thank Prof. Thomas Hänscheid for supervising and advising me during the course of my PhD. I'm especially thankful for all our conversations that taught me how to think "outside the box". I would also like to thank Prof. Maria Mota, my co-supervisor, for all her advice and welcome into her group.

I would also like to acknowledge, Prof. José Melo Cristino (Director of the Instituto de Microbiologia) and Prof. Mario Ramirez (Instituto de Medicina Molecular) for welcoming me in their facilities.

Thank you to Prof. Cevayir Coban (Osaka, Japan), for providing me with hemozoin for my studies.

A very warm Thank You to all the people who have made my work possible: everyone at the Animal Facility, Joana Marques and Dolores Bonaparte for their helpful advice, and Iolanda and Carlos, for taking good care of my mice and always finding me "spare" mice when I needed them! In the Histology unit, I would like to thank Andreia and Ana Margarida for doing my histological preparations and to Tânia for evaluation of my slides. Thank you to António Temudo and Ana for helping me with the Axiovert and for helpful advice. I also have to thank many other people whom I pestered with technical questions or asking for bits of reagents. Thanks to you I learned many new things and was able to take my work forward.

To the malaria unit for accepting me as part of your group. Thank you for advice, reagents and motivation! Thanks to Ana Parreira, Inês Albuquerque and Patricia Meireles for all your help, support, putting up with my grumpiness and more importantly for being my friends!

Thank you, Maria Rebelo, Ana Góis, Márcia, Cláudia and Carolina for all the fun moments, support and friendship.

Thank you to Miguel Prudêncio, for being my Tutor and help in revising this thesis and to Russel Foxal for English corrections!

I would also like to acknowledge Fundação para a Ciência e a Tecnologia for the financial support through the PhD Scholarship (SFRH/BD/61174/2009) and co-financed by the project PIC/IC/83214/2007 both from the Fundação para a Ciência e Tecnologia (FCT).

Rita T., Rita A. e Adriana (mais o macaquinho), thank you for our "sushizadas" and making me believe that surviving this was possible and everything would be alright. To Rita Moura for our conversations and kind words in unlikely places, even when you were busy you had always time to hear me out.

Finalmente gostaria de agradecer à minha Mãe e Pai, por fazerem de mim o que sou hoje e por me sempre terem apoiado. Dedico esta tese a vocês.

Index

Figure Index

Introduction

Chapter I. Hemozoin production and characterization

Chapter II. Detection of Hz-containing cells using flow-cytometry

Chapter III. Long term kinetics of hemozoin

Chapter IV. *In vivo* Malaria and Tuberculosis co-infection in a murine model

Table Index

Abbreviations

15-HETE: 15-(S,R)-hydroxy-6,8,11,13-eicosatetraenoic acid

AIDS: Acquired immunodeficiency syndrome

BCG: *Mycobacterium bovis* Bacillus Calmette–Guérin

CFUs: Colony forming unit(s)

cHz: Crude native Hz

CQ: Chloroquine

CSP: Circumsporozoite protein

CTCF: Corrected total cell fluorescence

DC: Dendritic cell(s)

DDT: Dichloro-diphenyl-trichloroethane

DHR 123: Dihydrorhodamine 123

DMSO: Dimethyl sulfoxide

DNA: Deoxyribonucleic acid

EBV: Epstein-Barr virus

EEF: Exoerythrocytic form

ERK1/2: Extracellular-signal-regulated kinase 1 and 2

FITC: Fluorescein isothiocyanate

FSC: Forward scatter

GFP: Green fluorescent protein

GMEP: Global Malaria Eradication Program

gMFI: Geometric mean fluorescence intensity

H&E: Hematoxylin and eosin

H_2O_2: Hydrogen peroxide

HCM: Human cerebral malaria

HCT: Hematocrit

HDP: Heme detoxification protein

HEPES: 4-(2-hydroxyethyl)-1-piperazineethanesulfonic acid

HGB: Hemoglobin

HIV: Human immunodeficiency virus

HLA-DR: Human leukocyte antigen – DR

HNE: Hydroxynonenal

HO1: Heme oxygenase-1

HRPs: Histidine-rich proteins

HSP27: Heat shock protein 27

Hz: Hemozoin

ICAM-1: Intercellular Adhesion Molecule 1

IFN-γ: Interferon gamma

Ig: Immunoglobulin

IL: Interleukin

IP: Intraperitoneally

IPS: Instituto Português do Sangue

iRBC: Infected red-blood cells

LPS: Lipopolysaccharide (Endotoxin)

LT-α: Lymphotoxin-alpha

MA-ARDS: Malaria-associated acute respiratory distress syndrome

malERA: Malaria Eradication Research Agenda

MAPK: Mitogen activated protein kinase

MCH: Mean corpuscular hemoglobin

MCHC: Mean corpuscular hemoglobin concentration

MCP-1: Monocyte chemotactic protein-1

MCV: Mean corpuscular volume

MHC-class II: Major histocompatibility complex

MIP: Macrophage Inflammatory Protein

MMP9: Matrix metalloproteinase-9

MOI: Multiplicity of infection

MR4: Malaria Research and Reference Reagent Resource Center

mRNA: Messenger RNA

NF-κB: Nuclear factor kappa B

nHz: Native Hz

NK: Natural killer cell(s)

NOX: NADPH oxidase

NTD: Neglected tropical diseases

NTS: Non-typhi *Salmonella*

OADC: Oleic-albumin-dextrose-catalase

p38 MAPK: p38 mitogen-activated protein kinases

PAS: p-aminosalicylic acid

PbA: *Plasmodium berghei* ANKA

PBMC: Peripheral blood mononuclear cell(s)

PbNK65: *Plasmodium berghei* NK65

PBS: Phosphate buffer saline

PcAS: *P. chabaudi* AS

PD-1: Programmed cell death protein-1

PE: Phycoerythrin

PFA: Paraformaldehyde

PKC: Protein kinase C

PMA: Phorbol myristate acetate

PPD: Purified protein derivative

pRBC: Parasitized erythrocytes

PRRs: Pattern recognition receptors

PV: Parasitophorous vacuole

RANTES: Regulated on activation, normal T cell expressed and secreted

RBC: Red-blood cells

RNA: Ribonucleic acid

ROI: Region of interest tool

ROS: Reactive oxygen species

RT: Room temperature

SCGF: Stem cell growth factor

SDS: Sodium dodecyl sulfate

SEM: Scanning Electron Microscopy

sHz: Synthetic hemozoin

SMA: Severe malaria anaemia

SSC-1: Side scatter

SSC-2: Depolarized side scatter

TB: Tuberculosis

TGF-β: Transforming growth factor beta

Th1: Type 1 T helper cell(s)

Th17: T helper cell(s) producing IL-17

Th2: Type 2 T helper cell(s)

TLC: Thin layer chromatography

TLR: Toll-like receptor

TNF-α: Tumor necrosis factor-α

T_{reg}: Regulatory T-cell(s)

VSA: Variable surface antigens

WHO: World Health Organization

XRD: X-ray diffraction

General Introduction

Malaria in ancient times

Malaria's history extends into antiquity and like many other parasitic infections has evolved hand in hand with humans. The first records of 'periodic fevers' can be found in Chinese manuscripts as early as 2700 BC. Later descriptions can also be found in manuscripts of Greek, Roman, Indian, Arabic and European physicians, up to the 19th century[1]. In the 5th century BC Hippocrates made detailed accounts of the disease including the association with splenomegaly and classification of the fevers as tertian and quartan[2]. Furthermore, development of molecular techniques allowed the identification of ancient DNA from *Plasmodium falciparum*, one of the species causing malaria, in a 4000 year old Egyptian mummy[3]. Another study reported findings that support the hypothesis that a particular lethal form of malaria in the 5th century A.D. contributed to the fall of the Roman Empire[4].

Discovery of the malaria parasite

The name malaria comes from medieval Italian *mal'aria* meaning bad air since it was believed, until late in the 19th century, to be caused by miasmas coming from swamps and marsh lands[5]. It was only after the work of Pasteur and Robert Koch and the establishment of the germ theory that the miasma theory fell out of grace and the search for the causative agent of malaria intensified[6]. In 1880 Charles Laveran, knowing that the spleens of malaria patients contained pigment (hemozoin), started to look for pigment in fresh unstained blood of patients. Laveran described different forms of erythrocytic organisms including crescents, spherical motionless bodies with pigment, spherical moving bodies with pigment and bodies that extruded flagella-like structures. He noted that these forms were present in all patients with malaria and that quinine removed these stages from the blood. He named this protozoan parasite *Oscillaria malariae* and presented his findings to the French Academy of Medical Sciences in 1880[7]. However, it was only four years later that it was accepted that malaria was caused by a protozoan and not a bacterium. By 1890 three species of malaria were recognized, according to their specific periodicities and other characteristics: *Haemamoeba vivax* (benign tertian), *Laverania malariae* (malignant tertian) and

Haemamoeba malariae (quartan), now known as *Plasmodium vivax*, *P. falciparum* and *P. malariae*, respectively. Later in 1918, John Stephens discovered a forth human species that he named *P. ovale*[6]. More recently, *P. knowlesi*, previously known as one of the plasmodia infecting apes and monkeys[8], was reported as a frequent natural human infection in the Malaysian Borneo[9]. Although, human-to-human transmission has yet to be documented conclusively, *P. knowlesi* is now recognized as a fifth plasmodia species infecting humans, with a transmission apparently restricted to Peninsular Malaysia[10].

Gabon, Lambaréné.

Figure I1. ***Mal'aria*.** It was early recognized that proximity to swamps and marsh lands was associated with the occurrence of febrile illness and hence the name Mal'aria meaning bad air was given to the disease today know as Malaria.

Malaria transmission

At the end of the 19th century no malariologist could explain how the parasite spread from human to human. Before the discovery that mosquitoes were responsible for the transmission, the findings of William MacCallum were of great significance. MacCallum, in 1897 was the first to observe flagellated structures in the blood of crows infected with *Haemoproteus columbae* (a species closely related to malaria parasites). He also described how this flagellated structures fused with non-motile bodies to form a *vermicule* (now known as an ookinete) and suggested that he was observing sexual reproduction. He further suggested that sexual reproduction also occurred in human malaria parasites[11]. Meanwhile, Patrick Manson was increasingly convinced that mosquitoes could be involved in the transmission of malaria. However, he was under the misconception that mosquitoes would then contaminate drinking water and thus

indirectly infect humans. Since Manson himself was unable to go to malarious countries he convinced Ronald Ross, an army surgeon working in India, to pursue this investigation. So it was that in 1897, by combining Laveran's idea of 'following the pigment' and Manson's descriptions of the flagellum, that Ross showed that mosquitoes fed on the blood of malaria patients contained pigmented structures which ruptured and released rods that could then invade the mosquitoes' salivary glands. Ross later demonstrated that mosquitoes fed on *Plasmodium relictum*-infected birds, took up male and female gametocytes which fused in the mosquito, developing into spores in the mosquito's gut. From the spores, rod like structures could be produced that had the ability to invade the mosquito salivary glands and be injected into a new host when the infected mosquito fed[12]. Ross suggested that human malaria was probably transmitted in the same way but it was the work of Grassi, Bignami and Bastianelli that provided the definite proof. Grassi and his colleagues fed *Anopheles claviger* mosquitoes on infected patients and successfully transmitted the infection to uninfected individuals by the bite of these mosquitoes[6].

Malaria liver stage

To complete the life cycle of the malaria parasite it remained necessary to discover what happened to the parasite in the first 10 days post-infection, during which it could not be observed in the blood. Although Grassi was the first to suggest that some sort of development must take place in cells other than the erythrocytes, it wasn't until 1937 that Sydney James and Parr Tate shed some light on the exoerythrocytic development of malaria. Their work demonstrated that, in chickens infected with *Plasmodium gallinaceum* there was a phase of parasite multiplication that occurred in reticuloendothelial cells, prior to the appearance of parasites in the blood[13]. Ten years later, in 1947, Henry Shortt and Cyril Garnham infected rhesus monkeys with *P. cynomolgi* and showed that a phase of development in the liver preceded the appearance of parasites in the blood. They further proved, using human volunteers, that *P. vivax*, *P. falciparum* and *P. ovale* also had an exoerythrocytic stage of development in the liver [14–16].

The life cycle of the malaria parasite in the mammalian host

The life cycle of the *Plasmodium* parasite in the mammalian host starts with the bite of an infectious female mosquito, and the deposition of sporozoites in the dermis of the mammalian host. The sporozoites then follow an erratic forward movement through the dermis that culminates with their entry into the lumen of a capillary or lymph vessel (Figure I2). Recent data from a murine model estimates that sporozoites actually reaching the lymph vessels or capillaries are only 15 to 25%, respectively, whilst around 60% of them remain at the bite site[17]. Sporozoites that enter lymph vessels are carried to the proximal lymph node where they are degraded or partially develop, delivering early exoerythrocytic form (EEF) antigens[18]. Sporozoites that enter blood vessels, reach the liver where they will first glide along the sinusoids that are lined by endothelial and Kupffer cells. To cross the sinusoidal barrier, sporozoites are thought to wound Kupffer cells, and reach hepatocytes, although there are other possible mechanisms of sinusoidal barrier crossing[19].

Once across this barrier, sporozoites traverse several hepatocytes before invading a final one where they will further develop into the next infective stage[20]. Following this final hepatocyte invasion the sporozoite develops inside a parasitophorous vacuole and undergoes a series of morphological changes that culminate in the generation of thousands of merozoites[21]. These merozoites are packaged together inside vesicular structures known as merosomes which are surrounded by the hepatocyte membrane. Merosomes bud off and detach from hepatocytes into the sinusoidal lumen[22]. Once in circulation, merosomes reach the lung microvasculature where they accumulate and eventually disintegrate, disseminating merozoites into the bloodstream[23].

The erythrocytic stage begins when merozoites released from the lung attach to specific receptors on the membrane of red-blood cells (RBC) and initiate asexual development. This stage is characterized by cyclic development of the parasite inside RBC from early ring stage, to early and late trophozoite stage and finally to schizont stage[24]. Depending on the parasite species schizonts may contain 6-32 merozoites[25]. The rupture of the schizont releases new merozoites into the bloodstream and these will then infect new erythrocytes and re-initiate the asexual cycle. During the repeated cycle of asexual development, some merozoites differentiate into male and female gametocytes. These can be taken up by female mosquitoes during a blood meal, thus

initiating the sexual blood stage of parasite development, and eventually be transmitted into a new host[26].

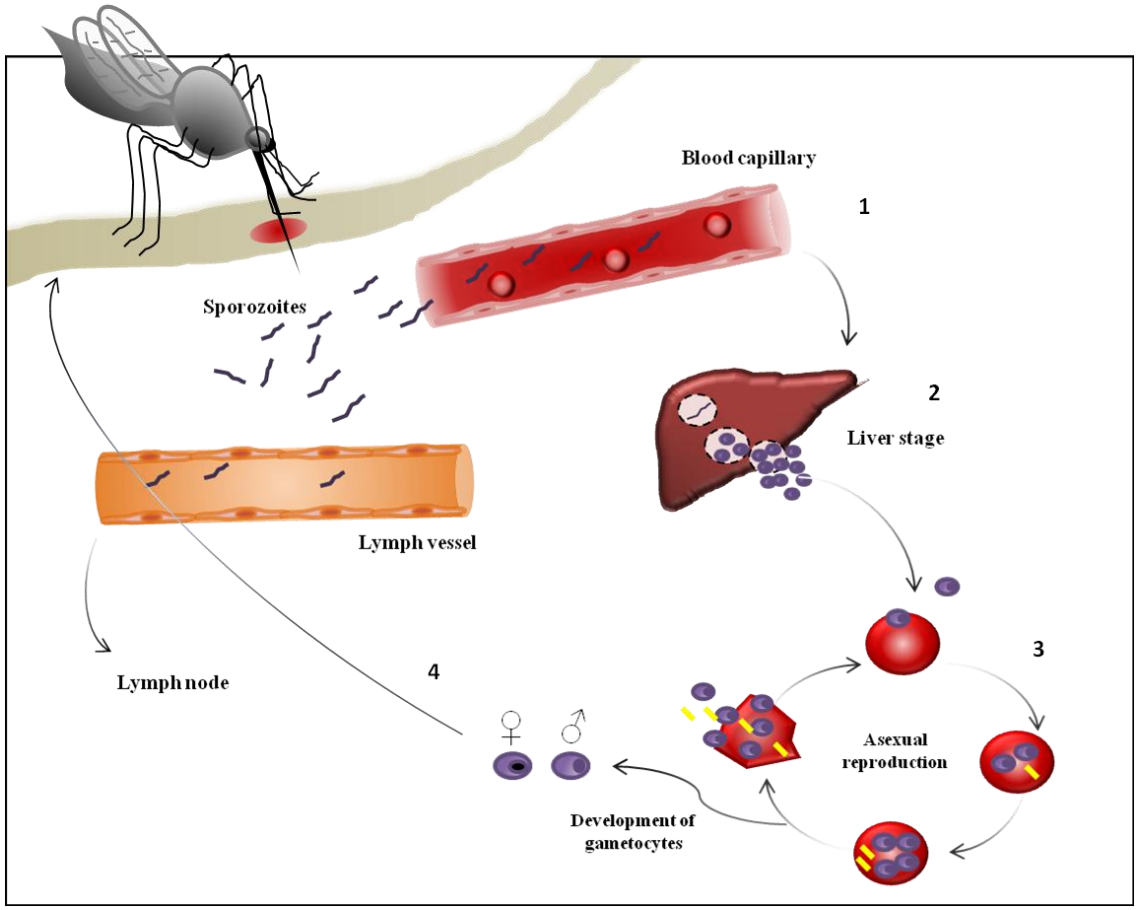

Figure I2. *Plasmodium* life cycle. In the mammalian host, infection starts through the bite of an infected *Anopheles* mosquito. Sporozoites are injected into the dermis and migrate rapidly from the region of the bite. Some sporozoites will enter lymph vessels and establish themselves in lymph nodes. Other sporozoites enter blood capillaries (1) and migrate to liver cells where they will establish the liver stage (2). This is the first stage of intracellular development where thousands of merozoites will be generated. Merozoites generated during the liver stage will then invade erythrocytes, and subsequently undergo cycles of asexual reproduction (3). During the blood stage some merozoites will differentiate into gametocytes (4) thus completing the life cycle when the sexual stages are ingested by a new *Anopheles* mosquito.

Malaria: early 20th century to today

The discovery that mosquitoes played an essential role in the transmission of malaria provided malariologists with a new weapon against the disease. The first decades of the 20th century saw concerted efforts to control malaria via reducing contact with infected mosquitoes. These efforts included drainage of swamps and free-laying water to eliminate mosquito breeding sites, and by promoting the protection of individuals from mosquito bites. Another strategy implemented was to make quinine

widely available to treat fever attacks in malaria-endemic areas, and later the use of quinine as a prophylactic measure[27,28]. These efforts contributed to the elimination of malaria from most northern countries in Western Europe. Further progress was achieved with the advent of dichloro-diphenyl-trichloroethane (DDT) and chloroquine. DDT's success in reducing mosquito transmission and chloroquine's efficacy against human malaria fuelled the belief that malaria could be eradicated globally. Thus, in 1955 the World Health Organization launched the Global Malaria Eradication Program (GMEP). As a result, by 1978, malaria was eliminated from 37 of the 143 countries in which it was endemic in 1950[29]. In other countries, although elimination was not achieved, the burden of disease and deaths due to malaria was greatly reduced. Despite the initial success of the GMEP, the program was closed by 1969, with the emergence of drug resistance, malaria resurgence in areas where its transmission had already been interrupted, reports of avoidance of vector contact with DDT, and the later ban on DDT use, fuelled by Rachel Carson's 'Silent Spring'[30]. As it became clear that there were countries where eradication was not feasible in the short term, and that control measures were more appropriate for the future eradication of malaria in those areas, a renewed interest in malaria research increased[31].

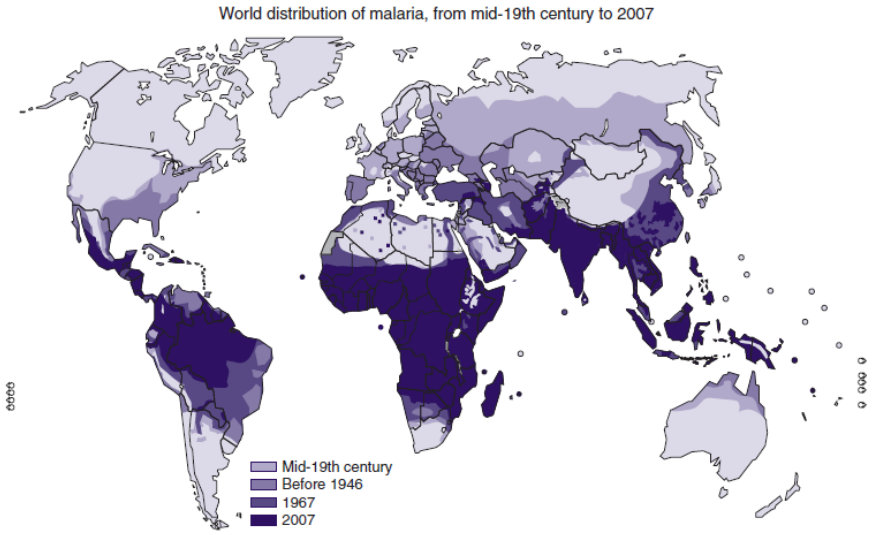

Figure I3: Malaria risk areas from mid 19th century to present. In the 19th century approximately 90% of the world population lived in malarious regions. Later in the same century and likely as a result of improved housing and changes in agricultural land use, large areas of North America and Northern and central Europe became malaria-free. Other events such as the discovery of the malaria parasite and its mode of transmission, discovery of DDT and chloroquine and the use of focal mosquito control measures resulted in the eradication of malaria in 37 out of the 143 countries in which it was endemic in 1950. The implementation of the Global Malaria Eradication Programme played a major role in this. (Source: From malaria control to eradication: The WHO perspective.)[29]

Today, malaria is still transmitted in 106 countries, with 1.2 billion people living in high transmission areas that account for 225 million cases of clinical malaria and 781,000 malaria-related deaths, mainly in children under age 5[32]. Malaria transmission occurs primarily in tropical and subtropical regions in Sub-Saharan Africa, Asia, Middle East, Eastern Europe, Central and South America, Caribbean, the Indian subcontinent and Oceania[33]. However, the intensity and risk of malaria transmission is quite variable within tropical and subtropical areas, and even within the same endemic country. Highest transmission is found in warmer regions closer to the equator, whereas in cooler regions, transmission is likely to be less intense and more seasonal[34,35]. Within endemic regions, malaria transmission will depend on factors such as urbanization, altitude, proximity to sea, river or floodplain, local climate, land use, local vector species and vector breeding sites, waste management, human movement patterns, socioeconomic factors and local malaria intervention programs[36].

The current research agenda aims primarily to control and reduce morbidity and mortality. Others, such as the Malaria Eradication Research Agenda (malERA), aim at identifying strategies, which will ultimately lead to the complete eradication of the parasite. Past failures have helped to recognize that malaria eradication will only be possible with concerted efforts to develop not only new tools for malaria control, but also with a sustained commitment from local communities, civil society, policy leaders, and the scientific community, to implement the necessary strategies for control and elimination of malaria[32].

Tuberculosis – brief overview

Evidence of tuberculosis (TB) disease has been found in 5000 year old Egyptian mummies[37,38]. Contrary to the earliest view of an animal origin for TB, there is now evidence to support the idea that the *Mycobacterium tuberculosis* complex originated as a human pathogen in Africa, and spread throughout the world via the Out-of-Africa migrations of modern humans[39]. During the seventeenth and eighteenth centuries, tuberculosis increased dramatically in Europe and North America[40]. This was likely fuelled by the industrial revolution and the extremely poor socio-economic conditions, such as overcrowding, malnutrition, lack of hygiene and sanitation and poor access to medical care[41]. In 1882 the etiologic agent of tuberculosis was first identified by Robert Koch[42]. Later, he would develop tuberculin and present it as a remedy against

tuberculosis. Although the use of tuberculin for the treatment of tuberculosis would prove a failure it would later lead to the development of the tuberculin skin test (also known as purified protein derivative (PPD) or Mantoux)[43]. Mortality rates began to decline by the mid-nineteenth century, perhaps due to improved living conditions, better nutrition and increased social conditions[44]. With the isolation of streptomycin in 1944, the first antibiotic effective against tuberculosis became available[45]. However, streptomycin only became available in Europe later and the first treatment report was only published in 1950[46]. Meanwhile, another compound, *p*-aminosalicylic acid (PAS), became available for the treatment of tuberculosis in conjunction with streptomycin[47,48]. However, it was the discovery of isoniazid's superior activity against tuberculosis[49,50] that soon brought an end to sanatoriums and collapse therapy, and started a new era for the control of tuberculosis.

Today, tuberculosis still remains a global problem with an estimated 8.7 million new cases and 1.4 million deaths in 2011. Geographically, the burden of tuberculosis is highest in Asia and Africa, with 60% of cases in South-East Asia and Western Pacific regions whilst the African region accounts for 24% of the world's cases. Almost 80% of tuberculosis cases among people with HIV occur in Africa[51]. WHO's (World Health Organization's) current goal for tuberculosis care and control, endorsed by the Stop TB Strategy, is to reduce tuberculosis prevalence and deaths by 50% by 2015 and to eliminate tuberculosis as a public health problem by 2050[51].

Tuberculosis, the disease and immunity

Tuberculosis disease

Tuberculosis (TB) is spread by the inhalation of airborne droplet nuclei, which are small size particles of 1-5 µm in diameter containing *M. tuberculosis* bacilli. Their small size allows them to pass into the lower respiratory tract[52]. Ingestion of *M. tuberculosis* by alveolar macrophages in the lung leads to a series of events that either results in the successful containment of the infection, or progression to active disease (primary TB disease). The risk of developing active disease will depend on factors such as time since infection, age and host immunity[53]. One third of the world population is estimated to be latently infected with *M. tuberculosis* and of those only 5-10% will ever develop active disease[54].

Typical symptoms developed during tuberculosis disease vary from development of fever, weight loss and night sweats, to persistent cough and development of radiological abnormalities such as thoracic lymphadenopathy and lung cavities or densities[55]. Development of primary tuberculosis weeks or months following first exposure occurs frequently in young children, the elderly or immunodeficient patients. This is often characterized by disseminated infection to other organs, such as liver, kidney, bone marrow and meninges. In other individuals, tuberculosis infection develops only years later after exposure from a previous latent asymptomatic infection. This is normally characterized by a predominant pulmonary infection of the upper lungs, which in some cases can progress to extra-pulmonary tuberculosis *via* lymphatic and/or hematogenous spread (reviewed by Brändli[56]).

Innate immnuity

The initial response to *M. tuberculosis* infection is thought to involve phagocytosis by alveolar macrophages, neutrophils and dendritic cells[57–60]. Macrophages and neutrophils are thought to act as the initial line of defense against TB by producing and secreting antimicrobial peptides, cytokines, and chemokines[61]. Phagocytosis of *M. tuberculosis* by macrophages involves various receptors, including the mannose receptor, scavenger receptors and complement receptors[62]. Within infected macrophages, lipid mediators, such as prostaglandin E2 (proapoptotic) or lipoxin (pronecrotic) will determine downstream events that will either lead to the induction of apoptosis or necrosis. Necrotic death of macrophages is associated with immune evasion and cell-to-cell spread of the bacilli whilst apoptotic death is associated with enhanced immunity and diminished pathogen viability[63].

The role of neutrophils in tuberculosis infection is still not clear, with reports suggesting that they can participate in granuloma formation[64] and facilitate the activation of adaptive immune responses by delivering bacilli to dendritic cells in a form that enables dendritic cells to more effectively activate CD4 T-cells[65]. Other reports suggest that neutrophils play a detrimental role in the pathogenesis of tuberculosis, with increased neutrophil numbers associated with respiratory failure and mortality in active tuberculosis patients[66]. In the murine model, susceptible mouse strains feature higher numbers and accelerated recruitment of neutrophils into the lungs, as compared to more resistant mouse strains[67]. *M. tuberculosis* can inhibit apoptosis of

both macrophages and neutrophils which in turn can result in delayed activation of naïve CD4 T-cells in the lymph nodes [68].

Intracellular mycobacteria within macrophages can be killed by different mechanisms, such as production of reactive oxygen and nitrogen species[69–71]. Another potential mechanism of mycobacterial killing is macrophage activation, which leads to phagosome maturation and fusion with the lysosome[72,73]. However, *M. tuberculosis* has developed mechanisms to counteract the bactericidal activity of macrophages. Studies have demonstrated that mycobacteria are capable of inhibiting phagosome-lysosome fusion and can also produce ammonia which could further help mycobacteria cope with phagosome acidification[74]. Sulfatides, a glycolipid produced by mycobacteria can also inhibit phagosome-lysosome fusion[75]. It was also demonstrated that virulent strains of mycobacteria can escape the phagolysosome into cytoplasmic vacuoles that do not fuse further with secondary lysosomes[76,77]. Establishment of an asymptomatic latent state is viewed by some as a resistance mechanism in its own right, enabling mycobacteria to attain a state of dormancy and persist for quite some time in this state in host tissues[78].

During innate response, cytokines such as TNF-α can play a major role in the killing and control of mycobacterial growth. The essential role of TNF-α was demonstrated in humans receiving anti-TNF treatment for rheumatoid arthritis or Crohn's disease. Individuals latently infected with tuberculosis and receiving anti-TNF therapy had higher rates of reactivation of active tuberculosis[79,80]. Experiments in mice in which TNF-α was lacking, either through antibody treatment or by genetically knocking out the TNF receptor, demonstrated that without TNF-α/TNF receptor *M. tuberculosis* infection is lethal, with both increased bacterial load and necrosis within granulomas[81]. It has been demonstrated, in a cynomolgus macaque latency model, that TNF-α neutralization leads to disseminated disease and reactivation in most animals with latent tuberculosis, ultimately leading to fulminant disease[82].

The granuloma

Intracellular killing and control of mycobacteria by macrophages is aided by the action of T-cells. T-lymphocytes can be recruited to sites of mycobacterial infection by the action of TNF-α and further assist macrophages in the growth inhibition and killing of mycobacteria[83]. Macrophages and T-cells come together and form a specialized structure called the granuloma. Although granulomas can be formed in response to

several infectious and non-infectious agents, tuberculosis is the most frequent cause, with granulomas being seen as the hallmark of TB infection[84]. The granuloma is an organized structure of epithelioid cells. These originate from macrophages that underwent a specialized transformation into cells with tightly interdigitated cell-membranes, linked to adjacent cells. Other macrophages in the granuloma fuse into multinucleated giant cells or differentiate into foam cells. Foam cells, derive their name from their high lipid content and are often found at the edge of the necrotic centre in mature granulomas. Mycobacteria are commonly found at the centre of the necrotic regions together with dead/dying macrophages. Other cells participating in the granuloma structure are neutrophils, dendritic cells (DC), B- and T-cells, natural killer (NK) cells, fibroblasts and cells that secrete extracellular matrix components. Epithelial cells are also normally found surrounding the outer region of the granuloma[85].

Classically, the granuloma is seen as a protective structure that helps to contain and kill mycobacteria until effector mechanisms of the adaptive immune response come in play. This idea is supported by evidence from old autopsy studies of individuals who died from unrelated causes, which revealed the presence of healed granulomas that contained no trace of viable bacteria, even after inoculation into the extremely susceptible guinea pig[86,87]. Further evidence is provided by deficiencies in TNF-α which are associated with the presence of disorganized granulomas and increased susceptibility to tuberculosis infection[88–91]. However, recent evidence suggests that mycobacteria exploit granuloma formation for their own proliferation and dissemination in the host[92]. Using a larval-zebrafish model of *M. marinum* infection, it was demonstrated that granulomas could form in the context of innate immunity[93]. Further insight was obtained from dynamic imaging studies which demonstrated that new macrophages arriving at the granuloma show a continuous and dynamic movement throughout the entire structure, instead of the long-held view that they are static within granulomas. The rapid and continuous migration of the newly arrived macrophages provides them access to numerous dying infected cells within the granuloma. The moving macrophages can then phagocytose the contents of dying macrophages, thereby becoming infected themselves and thus increasing the number of infected cells[85,94]. Studies of this dynamic process of macrophage movement also demonstrated that primary granulomas can seed new granulomas via the egress of infected macrophages. Thus, these data implicate the granuloma as a primary mean of disseminating infection[94].

Adaptive immune response

The adaptive immune response to *M. tuberculosis* is initiated not in the lung granuloma but in the draining lymph node. However, the initiation of the adaptive immune response is characterized by a lag in its initiation, which has been attributed to a delay in the migration of infected DC from primary granulomas to lymph nodes[95,96]. Regulatory T-cells (T_{reg}) may also play a role by inhibiting the induction of Th17 cells that would otherwise lead to the recruitment of Th1 effector T-cells to the sites of infection in the lung[97]. It was also demonstrated that *M. tuberculosis*-specific T_{reg} cells present in pulmonary lymph nodes are capable of delaying the priming of effector CD4 and CD8 T-cells and their subsequent accumulation in the lung[98]. On the other hand, even after pathogen-specific effector T-cells arrive in the lung, it seems that mycobacterium-infected macrophages remain unresponsive to T-cell help and fail to increase their microbicidal activity[99]. Eventually, adaptive, Th1-mediated immunity controls *M. tuberculosis* lung infection and the mycobacteria are thought to assume a state of nonreplicating persistence[100]. During chronic infection, effector T-cell responses continuously control infection, hence the risk of disease reactivation if these T-cell responses are lost or suppressed. Recent studies suggest that these effector T-cells responses are maintained from a proliferative population of CD4 T-cells expressing PD-1 (programmed cell death protein-1)[101,102]. PD-1 expressing T-cells are normally regarded as functionally exhausted[103], however, in tuberculosis this seems not to be the case. PD-1^+ cells seem to exhibit a high degree of proliferation and continuously give rise to antigen-specific effector T-cells necessary to maintain a protective response during chronic tuberculosis infection[101,102].

Malaria co-infections with other endemic infectious diseases

The considerable geographic overlap between malaria, HIV/AIDS and tuberculosis is well known[104]. However, individuals living in these endemic areas are exposed to several other pathogens causing diseases such as, buruli ulcer, chagas, cholera, dengue, sleeping sickness, leishmaniasis, leprosy, lymphatic filariasis, schistosomiasis, and other helminthiasis[105] (Table I1). Bacteremia is also common in malaria endemic areas and a frequent cause of febrile illness and acute pediatric admissions that may be mistaken as malaria[106]. This can lead to a delay in diagnosis and failure to treat severe bacterial infections. However, more often than not a

significant proportion of the populations living in sub-Saharan Africa will be polyparasitized with helminths, schistosomes, and filarial worms[107]. Occurrence of bacteremia concomitantly with malaria is also common with either malaria predisposing to bacteremia[108,109] or bacteremia causing more severe malaria[110]. Increasing evidence suggests that HIV/AIDS, tuberculosis, and malaria occur predominantly in populations who are polyparasitized[111,112]. Helminths, being the most common parasite found in HIV-, tuberculosis-, and malaria-infected populations[113].

Disease	Pathogen	Approximate global prevalence	Major affected areas
Ascariasis	*Ascaris lumbricoides*	800 million	Asia, Africa, Latin America
Chagas	*Trypanosoma cruzi*	10 million	Latin America
Hookworm	Necator americanus and Ancylostoma duodenale	600 million	Asia, Africa, Latin America
Human African Trypanosomiasis	*Trypanosoma brucei*	<0.1 million	Africa
Leishmaniasis	*Leishmania* sp	12 million	Asia, Africa, Latin America
Leprosy	*Mycobacterium leprae*	<0.5 million	Asia, Africa, Latin America
Lymphatic Filariasis	*Wuchereria bancrofti, Brugia malayi and Brugia timori*	115 million	Asia, Africa, Latin America
Onchocerciasis	*Onchocerca volvulus*	26 million	Asia, Africa, Latin America
Schistosomiasis	*Schistosoma* sp	200-600 million	Asia, Africa, Latin America
Trachoma	*Chlamydia trachomatis*	41 million	Asia, Africa, Latin America
Trichuriasis	*Trichuris trichiura*	600 million	Asia, Africa, Latin America

Table I1. Prevalence of pathogens commonly found in malaria endemic areas. Individuals living in malaria endemic areas are exposed to a variety of other pathogens. The group of pathogens presented in the table is part of a group known as neglected tropical diseases (NTD), common in impoverished tropical regions and for which known preventive measures and/or medical treatments exist in more developed countries. Together NTD have an impact comparable to that of malaria or tuberculosis. Table adapted from Hotez[114].

Malaria and HIV

With respect to malaria-HIV co-infection it has been shown that malaria infection can transiently enhance/reactivate viral replication[115–118]. Thus, it is likely that a positive correlation exists between areas of malaria prevalence and the risk of HIV infection. The first study to provide evidence for this correlation was conducted in East sub-Saharan Africa (including data from Kenya, Malawi and Tanzania) by Cuadros *et al*[119]. In contrast, another study performed by the same group, this time in western sub-Saharan Africa (Burkina Faso, Ghana, Guinea, Mali, Liberia and Cameroon) found no evidence of an association between malaria incidence and HIV infection. The western region of sub-Saharan Africa has a lower prevalence of HIV than the eastern regions, which suggests that malaria might only contribute to the spread of HIV where the

incidence is already high, with malaria acting as a facilitator of HIV transmission rather than as a contributor to HIV dissemination throughout the general population[120].

HIV and malaria co-infection is associated with a higher risk of fetal anemia, cord blood malaria parasitaemia, and low birth weight and post neo-natal mortality[121–123]. The risk of increased malaria severity appears higher in HIV positive individuals, and is further associated with a low $CD4^+$ T-cell count[124,125]. There is little information regarding the impact of malaria on HIV pathology. However, epidemiological data indicates a higher morbidity in malaria-HIV-positive patients and an increased risk of HIV vertical transmission[126]. Malaria infection has been shown to induce cytokine production, leading to the activation of $CD4^+$ T-cells. This may prove detrimental for HIV positive individuals with higher $CD4^+$ T-cell counts, as more T-cells will become available for viral replication[116]. On the other hand, repeated *P. falciparum* episodes have been shown to contribute to a faster decline in $CD4^+$ T-cell counts, potentially leading to more rapid progression to AIDS[127]. There is also evidence that the malaria pigment (hemozoin), which is produced by the malaria parasite during infection, might play an important role in viral transfer of HIV from dendritic cells (DC) to CD4 T-cells. This is thought to involve the induction of a partial maturation phenotype on DC upon exposure to hemozoin, which renders DC less permissive to HIV infection, whilst enhancing viral transfer to CD4 T-cells[128].

Malaria and helminths

The most common parasitic worm found in helminth-malaria co-infections is *Ascaris lumbricoides*, followed by hookworm and *Schistosoma*[129]. While several studies seem to indicate that *Ascaris* co-infection is associated with a reduced prevalence and/or reduced parasitaemia[130–132], others indicate an increase in malaria prevalence [133,134]. *Ascaris*-malaria co-infection has also been associated with improved protection against severe malaria in adults[135,136]. On the other hand, hookworm co-infection seems to mostly be associated with an increase in malaria severity[137–139]. Disparity in results can be explained by variability in the study design, the age groups sampled and on the parameter reported (malaria prevalence, incidence or protection against severe disease).

Helminthic infection is known to skew the immune reaction towards a Th2/Treg type response. This is particularly relevant when considering co-infections with malaria since it has the potential to modify the malaria-specific immune response. Observations

that helminthic infection was protective against more severe forms of malaria may be explained by the induction of high amounts of IgE. This in turn leads to the release of anti-inflammatory IL-10 and nitric oxide which contributes to a reduction in sequestration of parasitized red blood cells, thus decreasing the chances of cerebral malaria[140]. Another explanation is that helminth-infected individuals feature a higher induction of regulatory T-cells, that inhibit Th1 T-cells and their pro-inflammatory activity[141,142]. On the other hand, increased incidence of clinical malaria cases in helminth-infected individuals may be explained by a shift in antibody subclasses, from malaria-protective cytophilic subclasses (IgG1 and IgG3) to a more predominant subclass of non-cytophilic antibodies (IgG2, IgG4 and IgM)[143]. Another aspect to take into consideration is that studies on immunologic effects of helminthic infections tend to pool worms together into a single group, based on the assumption that they induce similar immune responses. However, it is clear from epidemiological studies that different worms can have different interactions with the host, with *Ascaris lumbricoides* contributing to a milder malaria outcome, and hookworm apparently contributing to higher malaria incidence[129].

Malaria and bacterial infections

Together with helminths, bacteremia is also widespread in sub-tropical and tropical regions[105]. However, contrary to what is seen with helminth co-infection, where some appear advantageous to the host (ie, less incidence of severe malaria and protection against allergic and auto-immune diseases), bacteremia-malaria co-infections appear always to be detrimental, with only a few studies reporting no further association between co-infection and disease severity.

Although evidence of an association between *Salmonella* infection and higher incidence of malaria cases had been noted as early as 1929[144], with Japanese investigators reporting malaria-related complications of syphilis therapy due to *Salmonella* infection[145], at this time a direct association between malaria and bacteremia had not been clearly established. Mabey *et al* were the first to conduct a retrospective study showing a direct association between septicemia and malaria incidence[146]. In their study, non-typhi *Salmonella* (NTS) was reported as the most common bacteremia isolated from blood (mostly in children under 4 years of age), followed by *Salmonella* typhi (commonly in older patients), coliforms, *Streptococcus pneumonia* and *Haemophilus influenza.* Malaria or evidence of recent malaria was more

commonly found in patients with NTS septicemia than other septicemias. More importantly, Mabey and colleagues found that, whilst the carriage of *Salmonella* in stool samples did not seem to change throughout the year, a higher incidence of *Salmonella* septicemia cases occurred during the rainy season, concomitantly with malaria. This suggested that malaria predisposed to NTS sepsis[146]. Others have published similar findings, associating malaria with persistent fever due to bacteremia/sepsis[147–151]. Association of bacteremia/sepsis with increased malaria severity was suggested by some of the smaller studies/case reports mentioned above, however this was more clearly demonstrated by a large study in Kenya, performed by Berckley *et al*. In his study, the most prevalent species found in blood cultures were *Streptococcus pneumoniae*, followed by *Staphylococcus aureus*, *Salmonella* non-typhi, *Haemophilus influenzae* and *Pseudomonas aeruginosa*. Children under six months of age were more affected than those between 6 and 30 months. Nonetheless, in both age groups bacteremia was correlated with higher mortality in children with a previous diagnosis of severe malaria[110]. The authors further proposed that young children presenting with severe disease consistent with malaria infection be treated with anti-malarial drugs as well as broad-spectrum antibiotics, to cover cases where disease is actually caused by bacterial infection. Further studies suggested that bacteremia caused by Gram-negative organisms is associated with low-density parasitaemia, higher incidence of severe malaria anaemia (SMA) and increased susceptibility to respiratory distress[106,108,152,153].

Whilst two studies reported reduced rates on invasive NTS and other bacteremia associated with reductions in malaria incidence[109,154], an association between bacteremia and malaria severity, or higher incidence of bacteremia in malarial individuals is not always observed[155,156]. Other confounding factors such as blood culture contaminants, nutritional status and prevalence of HIV and malaria transmission might contribute to different observations.

The mechanisms by which malaria might predispose to bacteremic infections, mainly NTS, were reviewed by Graham *et al*[157]. This include altered antibody responses and humoral immunity to *Salmonella* antigens; low serum complement which is associated to lower bactericidal activity; inhibition of Fc-receptor mediated phagocytosis; increased iron availability due to malaria induced hemolysis; and alteration of bactericidal functions induced by the ingestion of hemozoin, which will be described later in the introduction.

Malaria and Tuberculosis

Molecular studies of ancient DNA suggest that malaria-tuberculosis co-infections were already common place in ancient Lower Egypt. It is likely that the increased agricultural development at the time, together with increased population density, contributed to the spread of both malaria and tuberculosis[158]. However, the information available today regarding incidence of malaria-tuberculosis co-infections, their possible interactions and potential outcomes are still very limited. It is possible, that this limitation comes from the generalized idea that the two diseases do not spatially overlap. Even though both malaria and tuberculosis are endemic in sub-Saharan Africa (Figure I4), malaria incidence is greater in rural areas whilst tuberculosis incidence is higher in crowded urban areas[159,160]. A recent review on tuberculosis-parasitic disease co-infections found 44 studies, of which 22 were case reports, five were epidemiological studies and 17 were immunological research/reviews. However, on malaria-tuberculosis co-infection specifically, only one case report, one epidemiological study and three immunological research/reviews were found[161]. The epidemiological report refers to a study in Tanzania where 3% of tuberculosis infected patients also had malaria[162]. A more recent report showed incidence of malaria co-infection in 37.5% of tuberculosis infected patients in Angola[163]. Only one study has associated malaria with increased mortality among tuberculosis infected individuals, by demonstrating that the outcome of severely ill tuberculosis patients could be improved by preventing/reducing malaria transmission[164].

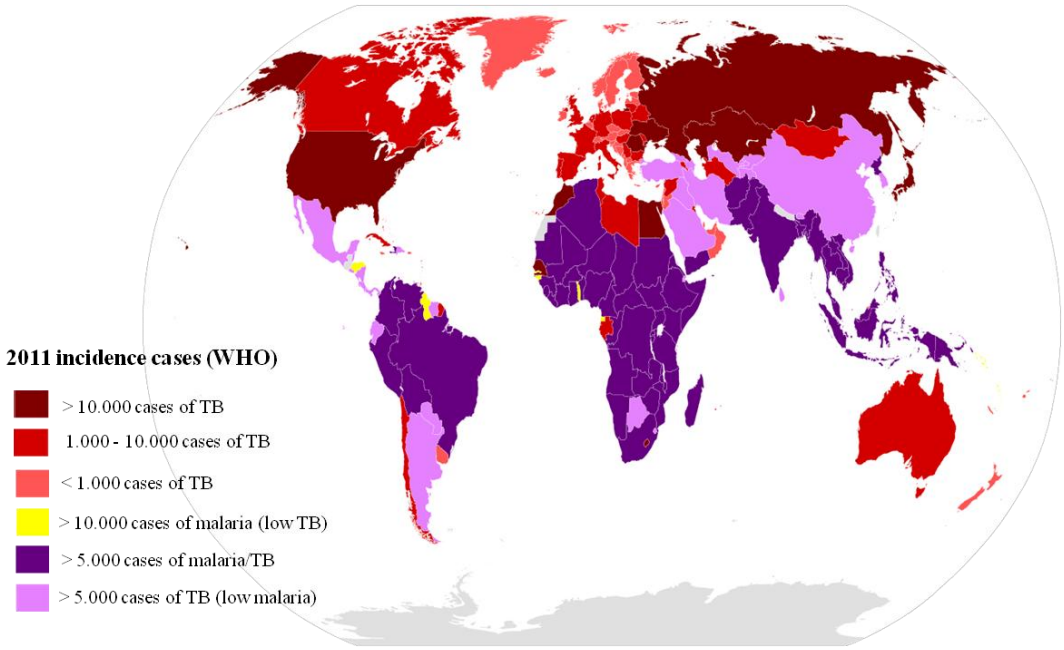

Figure I4. Overlap of Malaria-Tuberculosis endemic regions. Shown, are estimated incidences of malaria and tuberculosis for 2011, according to the WHO 2013 report. Shades of purple represent regions endemic for both malaria and tuberculosis. Dark-purple represent regions with high incidence of both malaria and tuberculosis; light-purple represent regions in which tuberculosis' incidence is higher than malaria (<5.000).

Even though malaria-tuberculosis interactions in humans are poorly characterized several studies have been performed using animal models. Early studies reported that *M. tuberculosis* infection could confer protection against *Plasmodium* infection in non-human primates[165,166]. In the murine model, *M. bovis* BCG was also shown to confer protection against several murine *Plasmodium* species[167–169]. This suggested that the immune response elicited by infection with mycobacteria could have desirable protective effects against malaria. Further investigation suggests that the protective effect of BCG vaccination is possibly due to a shift towards a Th-1 type response following parasite infection. Thus, susceptible A/J mice vaccinated with BCG become more resistant to infection with the lethal strain *P. yoelii* 17XL[170]. Conversely, a different study demonstrated that C57BL/6 mice infected with *M. tuberculosis* became more susceptible to an otherwise non-lethal infection with *P. yoelii* 17X. Co-infected mice had increased mortality compared to control mice infected with *P. yoelii* alone, higher mycobacterial loads than control mice infected with *M. tuberculosis*, and higher numbers of IFN-γ producing CD4 T-cells[171]. Work by the same group also demonstrated that mice normally susceptible to *P. yoelii* 17XL became resistant if they were pre-infected with *M. tuberculosis*; this protection was associated with a higher

magnitude of a Th-1 type response. Contrastingly, BALB/c mice gained no protection against malaria following *M. tuberculosis* pre-infection[172]. To add to these findings, a different study again showed that C57BL/6 mice normally resistant to *P. chabaudi* infection became susceptible if they were previously infected with *M. bovis* BCG. In parallel, A/J mice normally succumb to *P. chabaudi* infection but became resistant following *M. bovis* BCG infection[173].

The effect of malaria-tuberculosis co-infection on the progression of tuberculosis disease has also been investigated. One study reported that malaria exacerbates tuberculosis, with co-infected mice exhibiting higher bacterial loads, and higher levels of circulating inflammatory cytokines. In this study it was also suggested that malaria, and possibly hemozoin accumulation in granulomas, might promote tuberculosis reactivation in a model of latent tuberculosis[174]. A second study reported that, even though malaria-tuberculosis co-infected mice were more resistant to malaria, the concomitant tuberculosis disease was more severe. Co-infected mice had lower levels of malaria parasitaemia but increased mycobacterial loads and inflammation in the lungs. The inflammatory response in these mice was significantly altered with cytokines in tissue and sera increased to levels similar to those observed in sepsis[175]. The different tuberculosis/parasite *versus* host strain combination and consequent outcome of the above studies are summarized in Table I2.

Mycobacterium sp	*Plasmodium* sp	Mice strain	Findings/Outcome	Reference
M. bovis BCG (Tokyo)	*P. yoelii* 17XL	A/J	BCG protects mice from lethal infection with *P. yoelii*. Protection was associated with higher levels of Th1 cytokines.	Matsumoto S. (Yamada T.), 2001[170]
M. tuberculosis (CDC1551)	*P. yoelii* 17X NL	C57BL/6	22% co-infected mice died vs 10% in *P. yoelii* group. Lethality was associated with higher bacterial burdens and higher levels of IFN-γ in co-infected animals	Scott C. (Manabe Y.), 2004[171]
M. tuberculosis (CDC1551)	*P. yoelii* 17XL	C57BL/6 BalbC	Exposure to *M. tuberculosis* conferred protection to C57BL/6 but not BalbC mice through enhancement of Th-1 response	Page K, (Manabe Y.), 2005[172]
M. bovis BCG, (Copenhagen)	*P. chabaudi* AS	C57BL/6 A/J	*P. chabaudi* infection in previously BCG infected animals became lethal in C57BL/6 mice whilst it conferred protection to A/J mice. Lethality was associated with an earlier and stronger Th-1 type response in C57BL/6 mice than A/J	Leisewitz A., 2008[173]
M. bovis BCG (Pasteur)	*P. chabaudi* AS	C57BL/6	Infection of C57BL/6 mice with *P. chabaudi* exacerbated acute BCG infection and promoted reactivation of latent mycobacterial infection	Hawkes M. (Kain K.), 2010[174]
M. tuberculosis (H37Rv)	*P. berghei* NK65	C57BL/6	Co-infection exacerbated chronic tuberculosis while protecting mice against *Plasmodium* infection. Exacerbation of tuberculosis was associated with uncontrolled production of inflammatory cytokines by innate cells.	Mueller A-K (Schneider B.), 2012[175]

Table I2. Malaria-Tuberculosis co-infection studies in the murine model. Co-infection studies in the murine model suggest that tuberculosis infection can modulate the immune response to a subsequent infection by the malaria parasite and influence the outcome of co-infection.

Other work has focused on the potential effect of BCG infection on experimental vaccination against malaria or the effect of malaria on novel tuberculosis vaccines. An initial study investigated the interaction of BCG vaccination administered together with irradiated sporozoites. As BCG infection was shown to confer some protection to malaria, the idea was that it may have an adjuvant effect when given together with irradiated sporozoites (an experimental anti-malaria vaccine). The authors found that BCG infected mice survived the first challenge with live sporozoites, but not subsequent challenges, whilst those mice vaccinated with irradiated sporozoites alone, that survived the first challenge, all survived subsequent challenges. Vaccinating mice both with BCG and irradiated sporozoites appeared to have a synergistic effect on them, with increased protection against a first challenge, however they were unable to survive subsequent challenges. These results suggests that although BCG infection can induce a non-specific protection against malaria, this protection in short lived and, more importantly,

it appears to interfere with the protective immunity induced by other live vaccines[176]. A second study evaluated if malaria co-infection would disrupt the protective anti-tuberculosis immunity induced by BCG vaccination or other experimental tuberculosis vaccines. Results seem to indicate that protective immunity induced by either of the anti-tuberculosis vaccines tested was not affected by malaria co-infection. Mice infected with the *Plasmodium* parasite malaria after tuberculosis vaccination remained resistant to tuberculosis infection upon challenge at the same level as vaccinated mice that were not co-infected with malaria[177].

Taken together, studies in animal models suggest that malaria and tuberculosis infections can mutually influence each other and the outcome of co-infection will ultimately depend on the overall immune response elicited in the host.

Malaria, the disease and immunity

Malaria disease

Of the five *Plasmodium* species known to infect humans, *P. falciparum* is the most deadly. Overall, infection by *Plasmodium* frequently results in a mild, uncomplicated febrile illness characterized by intermittent episodes of fever and peaks of parasitaemia. Other symptoms such as chills, nausea, headaches, diarrhea and muscular pain are also common and usually occur just before or at the time of schizont rupture. In endemic regions of Africa where *P. falciparum* is predominant some malaria infections, particularly in young children, progress to severe disease and may lead to death. Malaria severe disease can be divided in three overlapping syndromes: cerebral malaria, metabolic acidosis and severe anaemia[178]. Another form of severe disease is placental malaria a common complication of malaria infection during pregnancy that may result in fetal loss or babies of low birth weight[179].

Sequestration of infected RBC to endothelial cells causes cell injury, promotes disruption of blood flow and leads to the development of tissue hypoxia and lactic acidosis. These mechanisms can contribute to the development of cerebral malaria due to sequestration of parasites in the brain. Severe anaemia may develop not only due to the hemolysis of infected and uninfected RBC but also due to inhibition of erythropoiesis[178]. Whilst cerebral malaria is more common in 3- to 4- year old children, living in lower endemic regions, severe malaria anaemia occurs more frequently in children younger than 3 years of age, living in higher endemic regions[179].

Malaria acidosis affects children of all age groups equally. Children with acidosis often present with respiratory stress and other clinical symptoms resembling sepsis such as hypovolaemic shock. Metabolic acidosis, especially when occurring concomitantly with impaired consciousness, is considered as strong predictor of death. The majority of malaria related deaths occur within 12 hours of admission before antimalarial medication can have its full effects. Therefore, implementation of supportive therapies together with fast acting antimalarial drugs is important to improve the outcome of severe malarial cases[180].

Exo-erythrocytic stage immunity

As mentioned earlier malaria infection in the mammalian host starts with the bite of an infected mosquito. Some sporozoites deposited in the skin enter blood capillaries through gliding motility, whilst most remain in the skin or make their way to lymph vessels, in a recently described "skin stage"[17]. Most lymph parasites are captured and degraded by dendritic cells and, while it was demonstrated that a host response can be induced by these captured parasites[181], it remains unclear if the host possesses an innate immune response able to detect sporozoites in the "skin stage".

Sporozoites that reach blood capillaries circulate to hepatocytes where they will eventually develop into merozoites. Wounding of hepatocytes during sporozoite traversal results in the release of cytosolic factors into the microenvironment, which seem to induce an innate pro-inflammatory response[182]. Studies by other groups also suggest that sporozoite infection in the liver induces innate inflammatory responses, as demonstrated by the presence of macrophages, neutrophils and eosinophils surrounding infected hepatocytes[183–185]. While it seems clear that the *Plasmodium* parasite is detected, and a weak inflammatory response induced during the liver stage, several questions remain unanswered. What are the parasite molecules recognized by the host? Which host pattern recognition receptors (PRRs) sense the parasite? How is the parasite detected by the host during its development inside the parasitophorous vacuole (PV)? What type of innate response is induced?[186]

The *Plasmodium* parasite appears to have evolved host evasion mechanisms that could explain why, during the liver stage, only weak inflammatory responses are induced. One of these putative mechanisms is the release of circumsporozoite protein (CSP) – the most abundant protein on the surface of sporozoites – into the host-cell cytoplasm. The CSP protein was shown to be able to outcompete NF-κB for nuclear

translocation thereby inhibiting the transcription of NF-κB-dependent pro-inflammatory genes[187]. Another possible mechanism by which host immunity is evaded, is the induction of the anti-inflammatory enzyme heme oxygenase-1 (HO1), which appears to reduce the frequency of inflammatory cells and cytokines[185]. While developing inside the hepatocyte the parasite is able to inhibit host cell apoptosis[184], and once it has fully matured into thousands of merozoites, is released into circulation inside merosomes: structures surrounded by the hepatocyte membrane and thereby protected from the host immune system[188].

Erythrocytic stage immunity

It is during the erythrocytic stage of *Plasmodium* infection that clinical symptoms of the disease manifest, and it is also during this stage that severe malaria disease may develop. Human and animal studies (mainly using the murine model) suggest that the optimal anti-malarial immune response is characterized by an early, intense, pro-inflammatory response, mediated by cytokines and effector mechanisms that lead to the destruction and clearance of parasite-infected cells. Once parasite replication is under control, the inflammatory response must be rapidly suppressed by anti-inflammatory mediators to avoid adverse pathological effects to the host[189].

Studies suggest that IFN-γ is a key cytokine for the control of initial parasite levels, and for the induction of protective immunity against blood stage malaria, both in the murine model[190,191], and in humans[192,193]. The earliest source of IFN-γ are NK cells. These cells are activated by IL-12, and to some extent IL-18, cytokines produced by activated DC and macrophages[194]. Optimal activation of NK cells appears to require further contact between NK cells and infected erythrocytes[195]. Production of large amounts of IFN-γ may further activate macrophages and promote non-opsonic phagocytosis of infected erythrocytes, as well as intra-erythrocytic killing of the parasites[196,197]. Within this highly inflammatory environment, the adaptive acquired immune response is initiated, with mature DC and activated monocytes/macrophages presenting parasite antigens to naïve T-cells, resulting in Th1 polarization of CD4 T-cells[198]. Activation of Th1 responses promotes the activity of γδ T-cells, which help inhibit the growth of intra-erythrocytic parasites[199], and further induces B-cell and humoral responses necessary for the complete clearance of plasmodium parasites[200].

Although an early robust pro-inflammatory response is seen as beneficial for the host, as it allows the control of the infection until the adaptive immune response kicks

in, it may also promote increased disease severity. In the murine model, overproduction of IFN-γ and TNF-α/LT-α[201] was associated with increased pathology in a process that seemed to involve IL-12[202]. The host mechanisms involved in the control of cytokine levels, such that parasite clearance is facilitated without promoting pathology, are unclear at present. However, key cytokines that might be involved in the immunoregulation of innate immunity appear to be IL-10 and/or TGF-β, both of which can be produced by innate (macrophages) and adaptive (T-cells) responses[200].

Evidence suggests that during the blood stage the parasite is able to modulate the immune system to its own advantage. The expression of variable surface antigens (VSA) is thought to promote sequestration of parasitized erythrocytes (pRBC), preventing their removal by the spleen[203–205]. Also, rosetting (adherence of pRBC to uninfected RBC) seems to protect pRBC from the immune system[206]. Macrophage function seems to be impaired by interactions with pRBC and/or parasite products (mainly hemozoin)[207,208]. Urban *et al*[209] demonstrated that DC incubated with pRBC were unable to fully mature and present antigens to T-cells. This was later linked to binding of pRBC to CD36 on DC[210]. Furthermore, the same study showed that DC incubated with pRBC developed a polarized anti-inflammatory phenotype, and produced IL-10[210]. Evidence for modulation of DC function by plasmodium parasites during acute infection was also observed in Kenyan children, in whom a significant proportion of DC had low expression of HLA-DR: an important molecule for DC-T-cell interactions[211]. However, this does not necessarily reflect a detrimental action of the parasite on the host, but rather, might reflect a beneficial homeostatic process, in which harmful inflammatory responses are down-regulated and immunopathology is prevented[212].

Malaria infection and host immunosuppression

The idea that malaria infection could cause immunosuppression of the host immune system was fuelled by vaccine studies carried out in highly malaria-endemic regions. One of these first studies was carried in 1962 by Mcgreggor and Barr[213] in a group of Gambian children, which had been kept malaria free by chemoprophylaxis treatment. In this study, children that received no chemoprophylaxis had lower antibody responses to tetanus toxoid vaccination than children kept malaria free. At the same time however, these authors showed that despite frequent malaria infections, Gambian

children had high antibody titers against diptheria toxin[214]. Later studies also observed diminished responses to *Salmonella* typhi O antigen, tetanus toxoid and meningococcal vaccine in children with acute malaria[215–217]. Febrile illness due to malaria or other acute illness was also associated with lower antibody titers in response to vaccination with *Haemophilus influenzae* type b conjugate vaccine[218].

Further evidence for malaria induced immunosuppression was the association of malaria endemicity with a higher occurrence of Burkitt's lymphoma[219]. This was later associated with malaria induced reduction of T-cells during infection, that in turn promoted abnormal proliferation of Epstein-Barr virus (EBV) infected B-cells. High numbers of EBV infected B-cells are correlated with a higher risk of developing Burkiit's lymphoma[220]. Initially, several mechanisms were proposed to explain malaria-induced immunosuppression including: depletion of antigen-reactive cells, disruption of lymphatic tissue architecture, polyclonal activation, macrophage dysfunction, antigenic competition and activation of non-specific suppressor cells[221]. Today, it is still a matter of great debate as to whether regulatory mechanisms such as inhibition of antigen presentation, switching from a polarized pro-inflammatory to an anti-inflammatory response and massive apoptosis of splenic T- and B-cells following malaria infection, are truly immunosuppressive and harmful to the host, or are important regulatory mechanisms to prevent harmful pathology[212].

Hemozoin role in the modulation of the immune system

What is hemozoin?

The presence of hemozoin (Hz) was first described at autopsy, by Giovanni Lancisi, in brains and spleens of patients that had died of malaria, in 1717; and in the blood, liver and spleen of an insane woman, by Meckel in 1847. Later, Virchow would associate the presence of this pigment with the causative agent of malaria (reviewed in[222]). The recognition that Hz was associated with malaria and its presence, not only in patients suffering from malaria, but also in the invertebrate host, played a pivotal role in the identification of the *Plasmodium* parasite, as well as its mode of transmission[6,7,12]. Hz was initially described as a melanin pigment – hence, it also being known as malaria pigment – but was later found to be derived from heme[223]. Hz is a paramagnetic crystal with an average size of 0,5-1 μm[224]. The crystal is composed of cyclic dimers of ferriprotoporphyrin IX (heme), via the coordination of the propionate group of each heme monomer to the Fe(III) centre of its partner. The dimers

are then linked via hydrogen bonds between the propionic groups[225,226]. Hz is produced during the blood stage of the *Plasmodium* parasite as a result of haemoglobin catabolism. As the parasites mature inside erythrocytes, up to 80% of the haemoglobin is digested[224]. Haemoglobin degradation occurs inside the digestive vacuole of the parasite and results in the release of amino acids and heme. It has been proposed that haemoglobin degradation is necessary, both to provide amino acids as a food source, and also as a requirement to maintain osmotic balance whilst the parasite matures and increases in size[227]. The released heme is toxic not only to the parasite, but also the host and, apparently, Hz formation is the end product of a detoxification mechanism employed by the parasite to pack a potentially damaging molecule into a highly insoluble and seemingly innocuous crystal[226]. The process of Hz biocrystallisation is still unexplained. Initially it was thought to be mediated by histidine-rich proteins (HRPs), which are secreted by some *Plasmodium* species and can bind very efficiently to heme molecules. However, this seems unlikely since Hz production in *P. falciparum* clones, in which HRPII has been silenced, is identical to wild-type parasites[228]. It is now thought that neutral lipid nanospheres, also located in the digestive vacuole, promote Hz formation at the surface interface between the acidic environment of the food vacuole and the lipid nanosphere[229]. This hypothesis is further supported by the fact that other Hz producing species, such as *Schistosoma mansoni* and *Rhodnius prolixus*, also biosynthesize Hz in lipid droplets[230]. Recent evidence points to a possible role for heme detoxification protein (HDP). This recently described protein is thought to be involved in the formation of the heme dimer and to contribute to the seeding of crystal growth[231].

Hz and the immune system

The first evidence that Hz might be involved in the pathology of malaria was provided by W.H. Brown in 1912, when he observed that rabbits injected with a hematin precipitate solution (possibly resembling synthetic Hz) exhibited symptoms typical of malaria, such as fever and shaking chills[232]. However, for a long time Hz was only regarded as an inert waste product resulting from the detoxification of the heme liberated during hemoglobin digestion[233,234].

Although impairment of macrophage function during malaria infection had been demonstrated by Loose *et al* in 1972[235], it was Schwarzer *et al* that in 1992 associated the ingestion of Hz by macrophages with their functional impairment[208]. Defects in

function resulting from ingestion of Hz by monocytes/macrophages include: reduced phagocytic capacity; inhibition of phorbol myristate acetate (PMA)-induced oxidative burst due to the inhibition of protein kinase C (PKC) activity and NADPH oxidase (NOX) assembly at the cell membrane, both of which are important for the generation of oxidative burst; reduced ability to kill bacteria, fungi or tumor cells; and inability to induce expression of ICAM-1, integrin-CD11c and MHC-class II in response to IFN-γ[208,236–239].

Further studies demonstrated that high levels of lipidperoxides are generated during Hz ingestion. Hydroxynonenal (HNE) and other derivatives of lipid peroxidation were shown to directly interact with key cellular enzymes, thus leading to the inhibition of several cellular functions[240–242]. Lipid peroxide derivatives were further associated with the inhibition of monocyte maturation to dendritic cells[243,244], inhibition of erythroid progenitors development[245,246], and increased destruction of non-parasitized erythrocytes resulting in the promotion of malaria anaemia[247,248]. The importance of lipid peroxidation catalyzed by Hz was further demonstrated by Carney *et al*, whereby β-hematin (synthetic Hz) was unable to inhibit PMA-induced oxidative response in RAW macrophages. Previous reaction of β-hematin with RBC membranes (erythrocyte ghosts) before incubation with macrophages restored the inhibitory effects normally observed with native Hz[249].

Work by Urban *et al* explored the inhibitory effects of Hz on dendritic cells. *P. falciparum* infected erythrocytes were shown to inhibit the up-regulation of MHC-II, ICAM-1 and the important co-stimulatory molecules CD83 and CD86 following LPS stimulation[209]. This inhibitory effect was apparently mediated by binding of infected RBC to CD36 on dendritic cells[210]. At the same time, experiments by Millington *et al* provided evidence that splenic DC isolated from *P. chabaudi* infected animals had an activated phenotype when isolated shortly after infection (4 days), but when isolated from infected animals later during infection (12 and 20 days) featured decreased expression of DC maturation markers and were unresponsive to LPS *in vitro*. It was further demonstrated that the parasite component responsible for DC inhibition was Hz ingestion by DC during malaria[250]. In a separate study, synthetic Hz was found to induce partial maturation of DC, with upregulation of CD80, CD83 and CXCR4 but not HLA-DR or CCR7. This, coupled with a lower production of IL-12, suggests that, although DC migrate to lymphoid organs, their subsequent activation of T-cell responses might be impaired[251]. Hz inhibition of HLA-DR upregulation might explain

clinical findings in Kenyan children suffering from mild to severe malaria, in whom a significant proportion of DC were found to express lower levels of HLA-DR than healthy children[211].

Several *in vivo* studies correlate natural acquisition of Hz by human monocytes with altered chemokine profiles – mainly MIP-1α, MIP-1β and RANTES – with disease severity[252,253]. These studies demonstrated that increased levels of Hz deposition were associated with increased severity of malaria anaemia and lower levels of RANTES. Incubation of peripheral blood mononuclear cells (PBMC) from healthy volunteers with Hz in a Cytokine Expression Array identified human stem cell growth factor (SCGF) – an important hematopoietic growth factor – as one of the most dysregulated genes. Indeed, in children with higher deposition of Hz, SCGF levels were lower, and this was associated with reduced erythropoietic responses in children with malaria anaemia[254]. In other studies, elevated levels of Hz are positively associated with severity of malaria anaemia and decreased levels of IL-12[255,256]. These studies demonstrated that IL-12 is regulated by IL-10, and more importantly, that Hz was able to induce production of both pro-inflammatory (TNF-α) and anti-inflammatory cytokines (IL-10).

Despite all of the aforementioned studies supporting the idea that Hz plays an important role in malaria-induced immunosuppression, data implicating Hz as a pro-inflammatory mediator also exists. Ingestion of Hz by monocytes was shown to induce the production of high levels of inflammatory cytokines, such as TNF-α and IL1-β[257,258]. In a different study, Hz was shown to induce IL1-β and TNF-α together with the anti-apoptotic cytokines MCP-1 and IL-8. Expression of HSP27, another inhibitor of apoptosis was also induced, thus suggesting that ingestion of Hz might promote induction of inflammatory cytokines and prolong survival of impaired monocytes[259]. Jaramillo *et al,* demonstrated that Hz injection in a murine model led to increased recruitment of leukocytes and increased levels of IL-1β, IL-1α, IL-6, MIP-1α, MIP-1β, MIP-2 and MCP-1 mRNA[260]. Hz phagocytosis by macrophages *in vitro* enhanced iNOS production in response to IFN-γ stimulation[261]. In a different study, Hz phagocytosis by macrophages was associated with increased mRNA levels of MIP-1α, MIP-1β, MIP-2 and MCP-1 chemokines, but not IL-1β, IL-1α or IL-6. Induction of chemokine mRNA was dependant on ERK1/2 MAPK pathway activation and nuclear translocation of NF-κB[262].

A series of studies demonstrated that Hz promotes the expression and activity of matrix metalloproteinase-9 (MMP9)[263]. MMPs belong to a family of proteolytic

enzymes able to degrade basement membranes, cleave pro-forms of inflammatory molecules, and disrupt inter-endothelial tight junctions[264]. There is growing evidence for a possible involvement of MMPs in severe malaria[265,266]. *In vitro*, it was shown that Hz or trophozoite fed monocytes had increased levels of MMP-9 and enhanced matrix invasion ability. Activity of MMP-9 seemed to be mediated by Hz-induced TNF-α[267]. Further studies demonstrated that Hz-induced MIP-1α and IL-1β were also mediators of MMP-9 expression and activity[268,269]. The Hz-enhanced effects on MMP9 could be mimicked by 15-HETE, suggesting a role for the lipid moiety of Hz. Moreover the Hz induction of MMP9 and related cytokines (TNF-α, IL-1β and MIP-α) were dependant on the nuclear translocation of NF-κB, and on the p38 MAPK pathway[270,271]. Monocyte incubation with Hz also seems to promote degranulation, resulting in the release of lysozyme. As was shown for Hz-enhancement of MMP-9 activity, lysozyme release is apparently dependent on the NF-κB and p38 MAPK pathways, which lead to induction of TNF-α, IL-1β and MIP-α[272–274]. Recently, it was found that host fibrinogen is frequently bound to Hz and might be responsible for increased levels of TNF-α and MCP-1. Hz-bound fibrinogen induced a rapid oxidative burst, peaking at 7 minutes post-Hz addition, and lasting for 20 minutes, declining thereafter[275].

Hz recognition was shown to require TLR-9[276] however, this is controversial as another study demonstrated that Hz-induced NF-κB nuclear translocation was TLR independent[277]. In parallel to TLR studies, several groups have investigated the role of the inflammasome in the response elicited by Hz. To this end it was demonstrated that Hz-induced IL-1β and neutrophil recruitment were dependent upon the NLRP3 inflammasome[278,279]. Griffith *et al* also demonstrated that Hz-induced recruitment of neuthrophils into the peritoneal cavity of mice occurred in a NLRP3 inflammasome-dependant manner. However, in this study *in vitro* phagocytosis of Hz did not result in induction of IL-1β by THP-1 cells, a commonly used cell line for the study of inflammasome activation and IL-1β production[280].

Overall, studies demonstrate that Hz is responsible for modulating several aspects of the innate and adaptive immune response. Nonetheless, some studies argue against a role for Hz as an immune modulator. One study demonstrated that Hz purified from *P. falciparum* culture had no *in vitro* stimulatory activity when fed to DC, and that protein-DNA complexes were the component responsible for activating DC[281]. Pichyangkul also demonstrated that the stimulatory activity of Hz was abolished following treatment with proteases, further supporting the idea that proteins on Hz surface are responsible

for the effects and not the crystal itself[257]. Another study demonstrated that Hz itself is inert but enhances immune responses by presenting malaria DNA to TLR-9 on DC[282]. Yet another series of studies suggest that *in vivo* Hz is naturally released inside intact food vacuoles, stimulates oxidative burst and drives neutrophils to a state of functional exhaustion; Hz itself is not ingested by phagocytes[283–285]. Some contradictory findings were also observed, for example, Hz was shown to induce production of ROS in RAW murine macrophages[286], but in a different study no ROS production was observed following Hz stimulation[249]. Similarly, synergistic production of NO by Hz and IFN-γ/LPS co-stimulation was observed by some groups[261,277], in contrast to another study in which Hz pre-incubation, prior to stimulation with IFN-γ/LPS, prevented NO induction[287]. Although some of these discrepancies between studies might be explained by the different cell types used, or differences in protocols (ie pre-incubation of Hz or Hz used as a stimulus), it also raises the question of what is the "true Hz". It is likely, that Hz released from schizont rupture is covered in multiple proteins and lipids. Thus, some studies use Hz extracted from culture, with different degrees of purification to remove DNA and proteins, whilst others favor the use of synthetic Hz, which, whilst virtually free of proteins/lipids/DNA, may vary in crystal size and quality[224,288].

Aims

Individuals living in malaria-endemic regions acquire anti-malaria immunity against severe life-threatening disease early in childhood, and eventually also develop immunity to uncomplicated febrile malaria by early adulthood. However, this immunity is not sterile and individuals often carry blood-stage parasites without symptoms[289]. As reviewed earlier, effective control of malaria parasites involves innate immune responses, as well as activation of a polarized Th1 adaptive response that must be tightly regulated to avoid immune pathology. However, repeated malarial episodes will lead to increased Hz deposition in host organs with potential detrimental effects. If Hz impairs cellular functions, such as phagocytosis and oxidative burst, the ability to kill intracellular bacteria might be impaired. On the other hand, Hz phagocytosis by DC also seems to impair antigen presentation and activation of T-cells, therefore it might impair the immune system's ability to properly control an infection such as the one produced by *M. tuberculosis*. Still, not much is known about malaria-tuberculosis co-infections and how their interaction might impact upon the disease outcome in co-infected individuals.

Thus, this project aimed to:

1) Produce and characterize Hz from different sources.
2) Use flow cytometry to identify Hz containing cells
3) Analyze the cellular function of human PBMC from healthy donors after the ingestion of Hz.
4) Using a murine model, investigate the kinetics of Hz deposition in host organs.
5) Using a murine model, investigate the *in vivo* susceptibility to tuberculosis infection during both acute malaria episodes, and during chronic malaria.

CHAPTER I

Hemozoin production and characterization.

Introduction

The exact processes involved in hemozoin (Hz) biosynthesis remain unknown, although it is thought that lipid droplets, and some as yet to be identified proteins, may have an important role in the initial nucleation of Hz crystal growth[224]. Studies of Hz are performed either with Hz extracted from *Plasmodium falciparum* cultures (natural-hemozoin) or β-hematin produced from hemin (synthetic-hemozoin). Although nHz and sHz are structurally identical[225,290], the lack of standardised protocols for the production of either type of Hz may account for the discrepant results found in the literature[224,288,291]. Extraction of Hz from *P. falciparum* cultures normally involves some kind of cell lysis[208,237,239] or the natural release of the crystals into the culture medium[283,284]. Either of these processes may result in Hz contacting any one of several biomolecules such as proteins, DNA or lipids, all of which can easily attach to Hz due to its amphilic nature[224]. Further purification procedures can be employed to remove these attaching molecules. On the other hand, synthetic hemozoin (sHz) can be produced *via* several different protocols which may lead to the production of a crystalline material that differs in size and shape to natural Hz.

This chapter describes the standardization of in house protocols for the production of Hz. The different Hz preparations were then quantified, and characterized with respect to the presence of common biomolecules, such as DNA and proteins and unreacted heme contamination. They were further characterized by scanning electron microscopy (SEM) and X-ray diffraction.

Results

Production and quantification of Hz.

Hz was produced either by synthesizing β-hematin (sHz) from hemin as described by Slater[292] or by isolating Hz from *P. falciparum* cultures[276,293]. Hz crystals are dark brown in colour and when in suspension have a blackish colour as shown in Figure 1. To the naked eye all these preparations appear very similar. Hz was quantified in terms

of heme-equivalents using the QuantiChrom™ Heme Assay Kit, which correlates absorbance at 400 nm with the concentration of total heme in solution. The ranges obtained were 0.2 mM-1 mM for sHz; 0.013-0.29 mM for crude native Hz (cHz) and 1 mM for native Hz (nHz). Here, cHz and nHz refer to *P. falciparum* culture extracts that did not undergo further purification, or to those that were extensively purified to remove protein and DNA, respectively (also see table 1). The differences in yields can be explained by the different volumes used to start the crystallization reaction; by the culture volumes used, and by the extent of purification.

All the different Hz preparations presented a crystalline appearance under light microscopy and depolarized light as observed by microscopy at 1000× magnification (Figure 2). The observed crystals were generally homogeneous in size, with the exception of nHz, which tended to form larger aggregates (Figure 2C) whereas sHz crystals appeared more dispersed and needle-like (Figure 2A).

Hemozoin Type	Description
Synthetic hemozoin (sHz)	Hz synthesized from β-hematin
Crude native hemozoin (cHz)	Hz isolated from *P. falciparum* cultures without extensive purification
Native hemozoin (nHz)	Hz isolated from *P. falciparum* cultures and extensively purified to remove possible protein and DNA contamination.

Table 1. Types of Hz. The table summarizes the types of Hz produced and their designations.

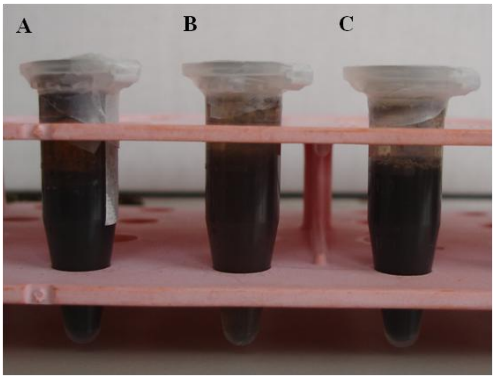

Figure 1. Suspensions of different hemozoin preparations, in water. A – sHz; B – cHz and C – nHz, suspensions in water were quantified in terms of heme equivalents.

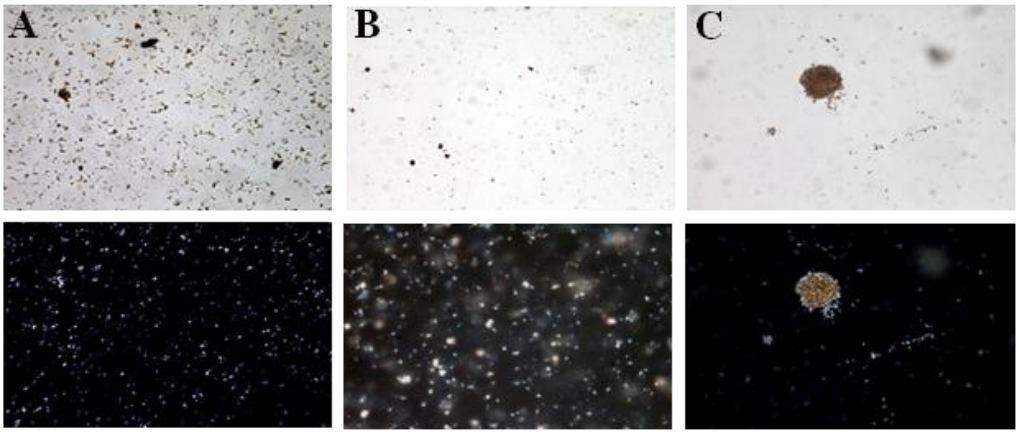

Figure 2. Observation of hemozoin preparations by microscopy. Hemozoin preparations were observed under light (upper pannel) and polarizing-light (lower pannel) microscopy, at 1000× magnification, using a Leica DM2500 optical microscope. A – sHz; B – cHz and C – nHz.

Assessment of Hz: purity and attached biomolecules

The different Hz preparations were assessed for the presence of possible biocontaminants such as DNA, protein and heme. Whereas DNA and protein are frequent contaminants of nHz, heme contamination – resulting from unreacted hemin – is more frequent in sHz.

Heme contamination in Hz samples was assessed by thin layer chromatography (TLC). cHz and nHz were found to be free from contaminating heme (Figure 3B and 3C). sHz was contaminated with a residual amount of free heme which represented less than 1% of total heme content (Figure 3A).

To investigate whether DNA was present, Hz samples were analyzed on an agarose gel and stained for DNA. sHz and nHz samples had no detectable DNA contamination as illustrated in Figure 4 (lanes 1-3). Not surprisingly, the cHz sample was found to be contaminated with DNA (lanes 4 and 5). Interestingly, even after pre-treating the cHz sample with saponin, the contaminating DNA did not migrate beyond the loading site. This may be due to interactions between DNA and other contaminants in the unpurified sample, such as lipids and/or proteins which were resistant to the saponin treatment and remained attached to the cHz crystals.

Hz samples were also assessed for the presence of protein contamination. As indicated by polyacrylamide gel electrophoresis under denaturing conditions (SDS-PAGE), sHz and nHz were free of protein (lane 1 and 2, Figure 5, respectively). cHz on the other hand, contained proteins, as revealed by Coomassie blue staining (lane 3,

Figure 5). The dark band in lane 1 is due to the dark brown color of Hz itself and is not a protein-derived band, as this would be revealed by the Coomassie blue staining.

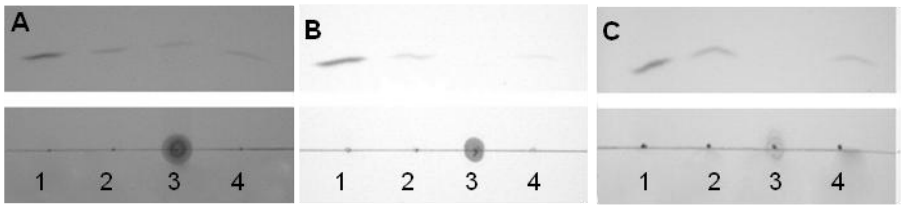

Figure 3: Remaining heme contamination in hemozoin samples as assessed by thin layer chromatography. Samples were eluted on silica gel plates along with 10 µl of 0,2 mM (Lane 1); 0,04 mM (Lane 2) and 0,02 mM (Lane 4) hemin chloride solutions in methanol. Lane 3: 10 µl of 0,2 mM of each hemozoin sample (A – sHz; B – cHz and C – nHz).

Figure 4: DNA contamination assessment of hemozoin samples by agarose gel electrophoresis. L: 1 kb Plus DNA Ladder; 1 – sHz; 2*&3 – nHz and 4*&5 – cHz. Samples denoted with * were pretreated with saponin.

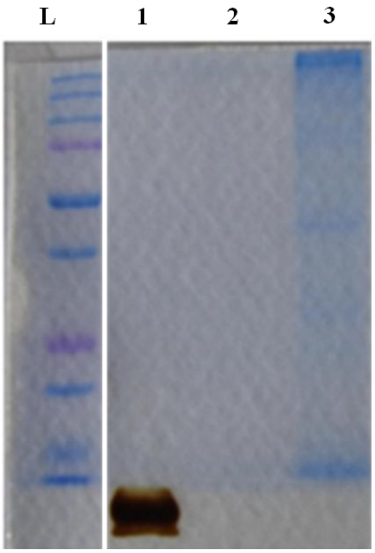

Figure 5: Assessment of protein contamination in hemozoin samples. Hemozoin samples were run on a polyacrylamide gel under denaturing conditions (SDS-PAGE) to assess protein contamination. L – Precision Plus Protein™ Dual Color Standards; 1 – sHz; 2 – nHz and 3 – cHz. Gel was stained with Coomassie blue stain to reveal the presence of proteins.

Scanning Electron Microscopy of Hz samples

The morphology and size of Hz crystals was determined by scanning electron microscopy. As shown in Figure 6, crystals of sHz and nHz were similar in size, ranging from 0.9 to 1.9 μm and 0.7 to 1.5 μm, respectively. The morphology of the nHz crystals featured the characteristic brick-like shape (Figure 6B) whereas sHz presented a more tapered needle-like morphology which can be attributed to a faster growth of the crystal faces (Figure 6A)[294].

A sample of sHz from a different source (our collaborator, Professor Cevayir Coban, Osaka University, Japan) was included in the analysis for comparison (Figure 6C). Although Coban´s sHz produced larger crystals than our preparations (3.8 to 6.3 μm), they were morphologically similar to our sHz, presenting with the same needle-like shape.

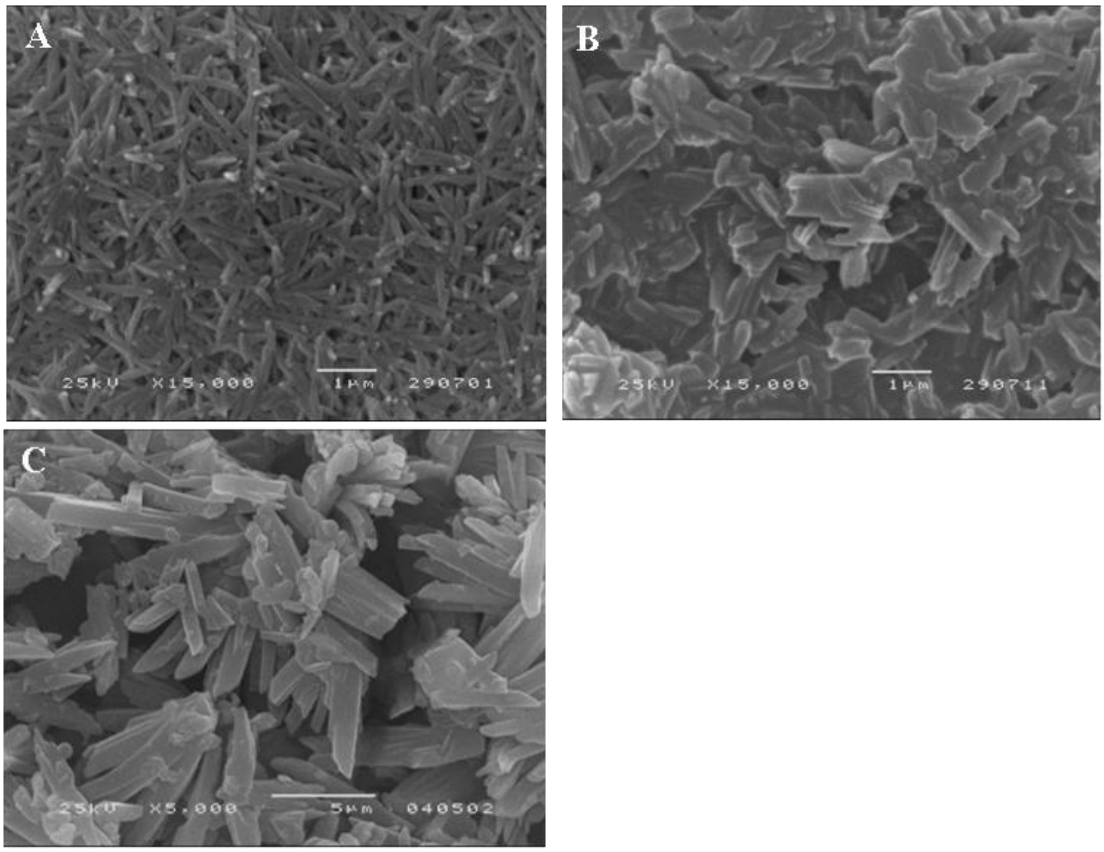

Figure 6: Scanning electron microscopy of Hz. A – sHz; B – nHz and C – Coban sHz at 15000× and 5000 magnification, respectively. Images of air-dried hemozoin samples were obtained with a JEOL, JSM-2500 LV scanning electron microscope. Size bars 1 μm (A and B) and 5 μm (C).

X-ray diffraction of Hz samples

sHz and nHz samples were analyzed with a Philips Analytical PW 3050/60 X' Pert PRO X-ray diffractometer. As shown in Figure 7 their X-ray diffraction peak patterns were identical. These patterns match those obtained by others [225,277,295].

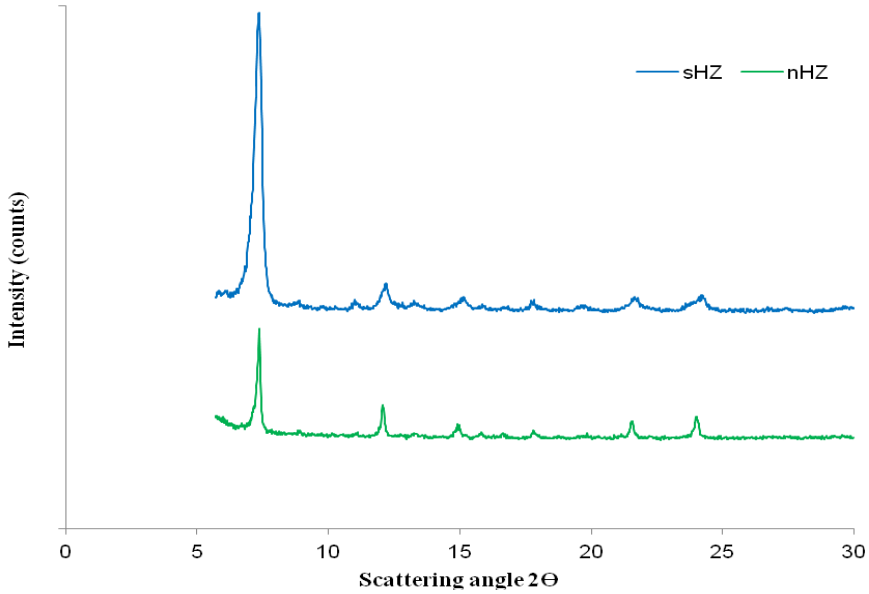

Figure 7: X-ray diffraction of Hz samples. sHz (blue line) and nHZ (green line) air-dried samples were analyzed on silicon sample holders with a Phillips Analytical PW 3050/60 X' Per PRO X-ray diffractometer using a Cu Kα radiation source (λ= 1,54060 Å).

Concluding Remarks

In summary we were able to produce both sHz and nHz and further showed that both Hz obtained were morphologically and physicochemically identical to each other and to preparations obtained by others. cHz differed from sHz and nHz since it contained DNA and protein. Moreover, isolation of Hz from *P. falciparum* cultures is costly and time consuming, even more so if further purification to obtain nHz is performed. Therefore the use of sHz was favoured in subsequent studies.

Materials and Methods

Reagents

Reagents were obtained from Sigma–Aldrich (St. Louis, MO, USA), unless stated otherwise.

Plasmodium falciparum culture

Plasmodium falciparum 3D7 strain was obtained from Malaria Research and Reference Reagent Resource Center (MR4; Manassas, VA, USA) and grown in continuous culture as follows: 10× Albumax stock solution was prepared with 25 g AlbuMAX II® (Invitrogen™ Life Technologies; Carlsbad, USA), 0.1 g hypoxanthine, 1 g glucose, 1.67 g NaHCO3, 2.98 g Hepes (VWR; Radnor, PA, USA), 500 µl gentamincin (Gibco™ Life Technologies; Grand Island, NY, USA) and 5.2 g RPMI 1640 (w L-glutamine, w/o NaHCO3, Gibco™). Each stock was then diluted in 500 ml of RPMI 1640 (no L-glutamine, with NaHCO3, Gibco™) and further supplemented with 500 µl gentamycin (50 mg/ml stock), 5 ml of 200 mM L-glutamine and 12 ml 1 M Hepes (Gibco™). Cultures were incubated at 37ºC, 5% CO_2 and maintained at a parasitaemia < 1% in a hematocrit of 5% according to the recommendations of MR4[296]. Red blood cells for cultures were obtained from discarded buffy coats from healthy blood donors, kindly donated by Instituto Portguguês do Sangue and leucocytes removed by three RPMI 1640 (without L-glutamine, with NaHCO3) washes/centrifugations at 600xg (without brake) for 5 min.

Extraction of crude Hz

P. falciparum Hz was extracted without further purification (cHz), as described by Keller *et al*[293], with some modifications. Briefly, *P. falciparum* cultures (3D7 strain) were grown at 5% hematocrit until a parasitaemia of 2-5% was reached. Then, cultures were centrifuged at 800x*g* for 10 min and the RBC pellet resuspended in 40 ml of 1x PBS (prepared from 10x PBS; Gibco™) containing 1% saponin, for 10 min. Cell lysates were centrifuged at 16000x*g* for 15 min, and the resulting pellet was washed seven times in 1x PBS to obtain the crude Hz extract. After the final wash the pellet was resuspended in 1 ml of ultrapure water, quantified and stored at 4°C.

Purification of crude Hz

Native hemozoin (nHz) was purified after saponin harvesting of parasites from 1 L of *P. falciparum* (3D7 strain) cultures, grown in 1% hematocrit to parasitaemias of at least 10% to enrich in trophozoites, as previously described by Coban *et al*[297]. Culture pellets were extensively washed with 1x PBS, sonicated for 5 min and extensively washed with 2% sodium dodecyl sulfate (SDS). This was followed by an overnight incubation with 2 mg/ml proteinase K (Promega; Madison, WI, USA). The following day pellets were again washed with 2% SDS, and further incubated for 3 h in 6 M urea. Finally, pellets were washed with 2% SDS and ultrapure water. Purified nHz was resuspended in 1 ml ultrapure water, quantified and stored at 4°C.

Production of synthetic Hz

Synthetic hemozoin (sHz) was obtained by the method described by Slater *et al*[292], with some modifications. Briefly, 475 mg of hemin chloride were dissolved in 100 ml of 0.1 N sodium hydroxide and heme was precipitated by slowly adding 35 ml of glacial acetic acid (Merck; Whitehouse Station, NJ). Crystallization was promoted by overnight incubation of the mixture at 80°C. Non-crystalline heme was then removed by washing three times with 1 vol of 100 mM sodium bicarbonate pH 9.1 during 3 h, followed by a 15 min centrifugation at top speed. The pellet was further washed three more times in 1 ml of ultrapure water and finally resuspended in ultrapure water, quantified and stored at 4°C.

Hz concentration measurement

The amount of Hz was quantified as heme-equivalents using QuantiChrom™ Heme Assay Kit DIHM-250 (BioAssay Systems; Hayward CA, USA), by colorimetric determination of total heme at 400 nm. Shortly, after solubilization in an aqueous solution of 20 mM sodium hydroxide for 1 h, samples were added to the Reagent solution for 5 min, after which the absorbance (A) at 400 nm was read. The concentration in μM (heme equivalents) was then determined using the following expression:

Total heme concentration $= \frac{Asample - Ablank}{Acalibrator - Ablank} \times 62.5 \text{x}$ Dilution factor, which correlates absorbance at 400 nm with the concentration of heme present in solution.

Light/Depolarizing microscopy

Hz preparations were observed with light and depolarizing microscopy, using the brightfield microscope Leica DM2500 (Leica Microsystems, Wetzlar. Germany).

Heme contamination assay

Hz preparations were assessed for remaining heme contamination using thin layer chromatography (TLC). Quantified Hz samples were first diluted in absolute methanol (Merck) to the highest concentration of hemin chloride to be eluted (0.2 mM). Then, 10 µl of diluted Hz samples were eluted for 30 to 40 min on silica gel glass plates (Merck) along with hemin solutions of known concentrations (0.2, 0.04 and 0.02 mM), inside a methanol-saturated tank. Images of the plates were acquired with Alpha Imager® HP System (ProteinSimple; Santa Clara, CA, USA). Image analysis was then performed using ImageJ software 1.47v (National Institute of Mental Health, Bethesda MD, USA) to calculate the integrated density of each standard/sample. The standard samples were used to create a standard curve comparing integrated density with hemin concentration and used to calculate the percentage of remaining heme contamination in Hz samples.

DNA contamination

Hz samples were assessed for DNA contamination by agarose gel electrophoresis. Ten microliters of each sample, pretreated or not with 10 µl of 1% saponin for 10 min, were loaded with 3.5 µl of Gel Loading Buffer on a 0.8% agarose gel with 10000x GelRed® Nucleic acid gel stain (Biotium; Hayward CA, USA) diluted 1:20000, and ran in 1x TAE Buffer for 30 min at 100 mA.

Protein contamination

Hz samples were assessed for protein contamination by polyacrylamide gel electrophoresis under denaturing conditions. Twenty microliters of each sample were boiled for 5 min at 100°C with 20 µl of 2x Loading buffer and then loaded onto a SDS-polyacrylamide gel (5% Acrylamide resolving gel/4% Acrylamide stacking gel) and ran in 1x Running buffer, for 40 min at 180 V. The gel was stained in 1% Coomassie Brilliant Blue staining solution (Bio-Rad; Hercules, CA, USA) for 20 min, destained overnight in Destain solution (constituted by 30% ethanol and 10% acetic acid in distilled water). An image of the gel was acquired with Alpha Imager® HP System. Gels

were dried on a filter paper with the DrygelSr Slab Gel Dryer SE1160 (Hoefer® Scientific Instruments, Holliston MA, USA), for at least 40 min at 70°C.

Scanning Electron Microscopy (SEM)

Ten microliters of each Hz sample were allowed to air dry overnight on top of a carbon tape placed on a metallic sample holder. Air dried samples were then metalized for 30 min using JEOL, JFC-1200 with a gold target. Scanning electron microscopy was performed with JEOL, JSM-2500 LV scanning electron microscope (JEOL, Tokyo, Japan), at Faculdade de Ciências da Universidade de Lisboa.

X-ray diffraction

Hz samples were subjected to X-ray diffraction (XRD) analysis. Crystals were resuspended in 10 μl of absolute ethanol (Merck) and allowed to air dry on silicon sample holders. XRD patterns were then acquired at Faculdade de Ciências da Universidade de Lisboa, with the automatic X-ray diffractometer Philips Analytical PW 3050/60 X' Pert PRO (Θ /2Θ) (PANalytical, Almelo, The Netherlands), with an X'Celerator detector and automatic data acquisition with X'Pert Data Collector, version 2.0b. Cu Kα radiation (λ= 1.54060 Å) was used, operating with 30 mA and 40 kV. The diffractograms were recorded in the 2Θ range between 5° and 30° with a step size of 0.0170° (2Θ) and scan step time of 100 seconds.

Discussion

Synthetic Hz (sHz) can be obtained from hemin by reaction with acid producing β-hematin, the chemical equivalent of hemozoin. Alternative methods for production of sHz use a rather long anhydrous base reaction[224]. Hemozoin can also be obtained from *P. falciparum* cultures (natural hemozoin) however, this can be a time consuming and expensive process[297]. Moreover, the different protocols implemented and the source of hemozoin (synthetic or culture) can generate preparations that are quiet different in terms of crystal morphology, size and in the case of natural hemozoin, the type of biomolecules present on the crystal surfaces after isolation[277,295]. Thus, it is important to characterize hemozoin preparations before performing further studies.

Results presented in this chapter demonstrated that hemozoin preparations resulting from three distinct protocols were indistinguishable to the naked eye. Microscopic observation using polarizing light gave little information as to the ultra-

structure of hemozoin crystals, although it served to confirm the birefringent nature of the hemozoin preparations. To further evaluate the ultra-structure of hemozoin it was necessary to perform SEM and X-ray diffraction. This allowed the confirmation of crystal size and morphology of the different hemozoin preparations and their structural arrangement. Hemozoin preparations were identical, morphologically and structurally to those obtained by others[298,299]. Thus, careful standardization of protocols can yield both sHz and natural hemozoin that are equivalent in terms of crystal size, morphology and structural properties. However, as noted by the presence of protein and DNA in hemozoin that was not extensively purified (cHz), extra steps may be required to produce hemozoin that is equivalent in terms of the molecules adsorbed to its surface. Heme contamination was also evaluated by TLC to demonstrate that remaining heme (either from unreacted hemin or from RBC lysis) was not present in our preparations. This is important since remaining heme could exert toxic cellular effects and confound the interpretation of results.

It is important to highlight that whilst many studies reported different findings on the modulatory properties of hemozoin[277], very few of these studies performed extensive hemozoin characterization, using SEM and X-ray diffraction[293,295]. Many earlier studies did not perform any characterization at all[261,268,300]. On the other hand, some studies report that hemozoin itself is inert and that effects normally associated to hemozoin are exclusively due to the presence of other biomolecules on its surface, such as DNA[282]. Fibrinogen has also been shown to bind to crude hemozoin and to induce strong initial stimulation of ROS, TNF-α and MCP-1 *in vitro*[275]. Additionally, it was reported that whilst hemozoin itself appears inactive, it can exert immune effects when in the presence of RBC ghosts. This was interpreted as resulting from interactions between hemozoin and RBC lipids[249]. Thus, some studies suggest that hemozoin serves as a vehicle of diverse biomolecules that then exert their immune effects[282]. Others suggest that hemozoin is released within digestive vacuoles, and that it is the ingestion of these vacuoles and not hemozoin itself that contribute to immune effects[283,284].

These observations raise the question as to what is the 'true hemozoin' *in vivo*. How is natural hemozoin released into circulation upon schizont rupture in the mammalian host? Another important question is what happens to ingested hemozoin once phagocytes reach the end of their natural life span. Natural hemozoin is likely released into circulation upon schizont rupture either as a free crystal or inside the food

vacuole. In any case, it is likely that hemozoin comes in contact with host-derived and/or parasite-derived biomolecules. Then, due to the highly amphiphilic nature of hemozoin these biomolecules easily adsorb to hemozoin crystals. Hemozoin is very resistant to degradation and withstands treatments with acids, alcohols, dimethyl sulfoxide (DMSO) and hydrogen peroxide (H_2O_2)[301]. Thus, acidification or H_2O_2 production in the phagocytic compartment is unlikely to contribute to significant hemozoin degradation, and as phagocytes reach the end of their natural life span it is likely that hemozoin is re-ingested by new phagocytic cells. In such a scenario, it is reasonable to assume that the nature and/or amount of biomolecules attaching to hemozoin changes over time. Eventually, in the long term hemozoin might become free of contaminants, such as proteins and lipids, as these are degraded inside phagolysosomes. In our studies, the use of synthetic hemozoin over hemozoin isolated from cultures was favored because it probably reflects better the hemozoin present in host organs in the long term. Moreover, synthetic hemozoin used in our studies (either synthesized by us or supplied by Professor C. Coban) was thoroughly characterized before being used in functional studies. As discussed, hemozoin characterization is important as many protocols are available for its production and as emphasized by Jaramillo *et al*[277], some may even yield hemozoin with poor crystalline nature.

CHAPTER II

1. Detection of Hz-containing cells using flow-cytometry

Introduction

Hz has been the focus of a substantial amount of research in recent years. However, identification of Hz-containing leucocytes and/or parasitized erythrocytes normally involves microscopy, with all its inherent limitations, which are mostly related to the difficulties in counting relatively low cell numbers[302,303]. Alternatively, Hz can be detected by flow-cytometry using depolarized side-scatter[304,305]. Hz is a birefringent crystal, and is able to rotate the plane of polarized light, a property known as depolarization. Thus, a conventional flow cytometer can detect depolarization via the combination of an orthogonally placed polarization filter (90º rotated) located in front of a second side-scatter detector. Haematology analysers, such as the Cell-Dyn® (Abbott, Santa Clara, CA, USA) already incorporate depolarized SSC detection to distinguish eosinophils from granulocytes. When blood samples from malaria patients were processed in these analysers, the lobularity-granularity plots showed characteristic abnormalities, such as the appearance of monocytes in the eosinophil area and a widely scattered eosinophil population[306]. This was most likely caused by the presence of Hz in monocytes and neutrophils, respectively[307]. The use of this system for further studies is, however, limited by the fact that software analysis, the analyser's analytical algorithms, and the raw data are inaccessible to the operator.

The Cyflow® Blue laser (Partec, Münster, Germany) instrument was adapted to detect depolarized SSC as described in the Methods section of this thesis. With this simple modification it was possible to detect Hz in different cell types including human whole-blood, peripheral blood mononuclear cells (PBMC), murine peripheral blood (described in this chapter) and single-cell suspensions of murine tissues (see also Chapter 3). This allows for the first time to look at possible Hz effects at the single-cell level, whereas previous studies rely on the assumption that all cells being studied contain Hz or that Hz effects are propagated to all cells.

Results

Detection of Hz in human whole-blood

Whole blood from healthy human volunteers was incubated with anti-CD14 and anti-CD16 antibodies to identify monocyte and granulocyte populations, respectively. Hz containing cells were then identified based on their depolarized side scatter (SSC-2) vs. side scatter (SSC-1). The upper panel of Figure 8 shows the gating strategy used for analysing blood from a healthy donor without Hz; the lower panel shows the analysis of the same donor's blood after six hours incubation with sHz. As expected, the sample without Hz had negligible depolarizing events whereas in the sample incubated with sHz, depolarizing events were detected both in the monocyte and granulocyte populations (Figure 8, upper rows). Importantly, Hz-containing monocytes (red dots) showed much higher side-scatter than normal monocytes (blue dots), which overlapped with the granulocyte population (Figure 8, bottom rows). Thus, the use of a classical monocyte gate, based on forward scatter (FSC)/SSC-1 should be avoided at the risk of excluding Hz-containing monocytes. Instead, monocytes and granulocytes were identified exclusively based on the expression of CD14 and CD16 (Figure 8).

A time course incubation of whole blood from healthy volunteers with sHz further showed that the percentage of Hz-containing monocytes and granulocytes depended upon the initial Hz dose and time of incubation. Furthermore, the monocyte population was the main population to phagocytose Hz (Figure 9).

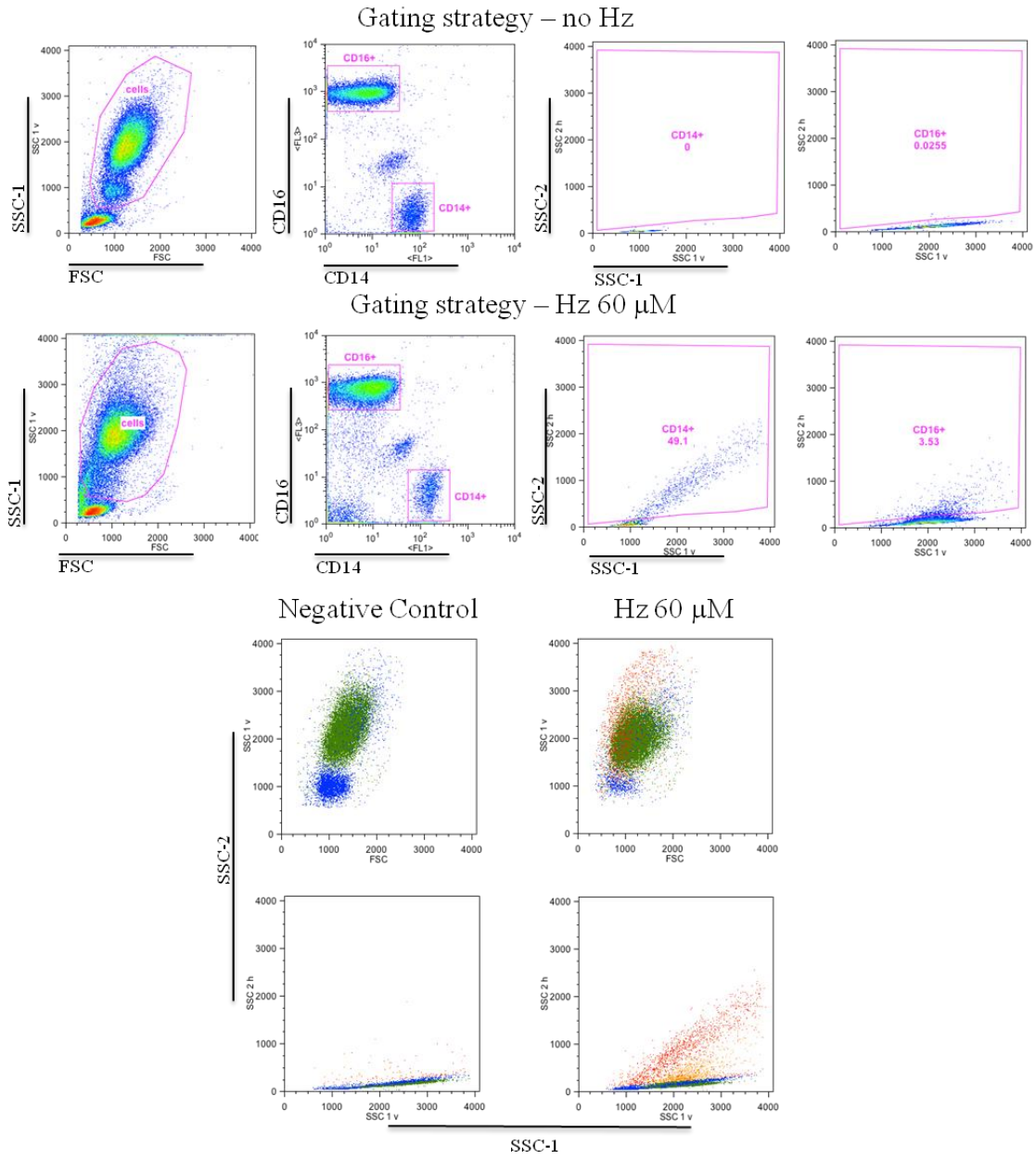

Figure 8. Detection of Hz in human whole blood. Top two rows show the gating strategy used for the detection of Hz in human whole blood. Monocytes and granulocytes were identified based on the expression of CD14 and CD16, respectively, and then analysed in terms of their side scatter (SSC-1) and depolarized side scatter (SSC-2). The first row is representative of blood from a healthy donor without Hz; the second row is the same sample incubated for 6 hours with sHz (60 µM heme equivalents). Bottom two rows: Colour back-gating for samples shown in row one and two. Blue: non-depolarizing monocytes; red: depolarizing monocytes; green: non-depolarizing granulocytes and orange: depolarizing granulocytes. FSC: forward scatter; SSC-1: Side scatter and SSC-2: depolarized side scatter.

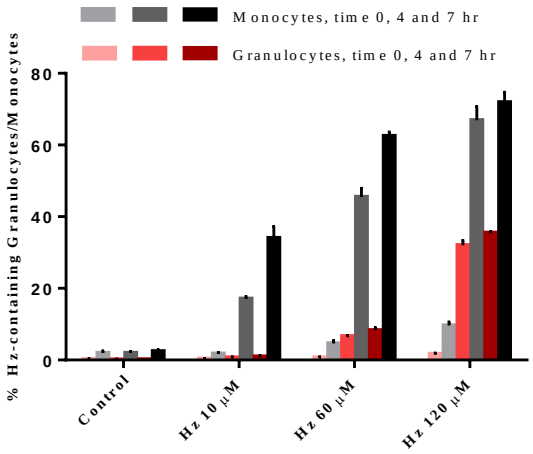

Figure 9. Hz phagocytosis *in-vitro* is dose and time dependant. Whole Blood from a healthy human volunteer was incubated with increasing sHz concentrations: no sHz (control), 10, 60 and 120 µM heme equivalents. The percentage of Hz-containing granulocytes and monocytes was determined at time zero, and after four and seven hours of incubation. Identification of leukocytes and depolarization was performed as described in the text and as shown in Figure 8. The results shown are the mean values of triplicates (± one SD) of one representative experiment.

Effect of different types of Hz in human PBMC

Hz detection was further investigated in human peripheral blood mononuclear cells (PBMC). Most *in vitro* studies use concentrations of Hz based on the assumption that an average adult infected with *P. falciparum*, with a 1% parasitaemia (relatively mild malaria), will release as much as 200 µmol of Hz at the end of each intra-erythrocytic cycle. This is based on reported estimates of haemoglobin degradation and conversion to Hz in *P. falciparum* infected cells, and on reference haematological values[262,308]. Although, these concentrations of Hz aim to be physiologically relevant, most experiments use amounts that when used *in vitro*, result in all phagocytes containing Hz, which is unlikely to represent the *in vivo* reality.

Using a similar strategy as that used for whole blood, Hz was detected in human PBMC isolated from buffy coats discarded from blood samples of healthy adults donors of both sexes, kindly provided by IPS (Instituto Português do Sangue). PBMC were stained with anti-CD14 and anti-CD16 antibodies and the monocyte population was defined as the population of cells expressing $CD14^{+}$. The percentage of Hz-containing monocytes following incubation with different Hz doses was then determined for a period of 24 hours. Using this strategy we determined that incubating human PBMC with 10-20 µM Hz resulted in a mixed population of non-Hz containing and Hz-

containing cells (Figure 10). The percentage of Hz-positive cells ranged from 29-55.8% for sHz and 17.3-31.4% for cHz.

Monocytes are often defined as expressing high levels of CD14 and low levels of CD16. However, in peripheral blood, differential expression of CD16 can subdivide the monocyte population into classical monocytes that are $CD14^{+}CD16^{-}$ and inflammatory monocytes that also express CD16 ($CD14^{+}CD16^{+}$). This population is known as inflammatory monocytes because it more closely resembles mature tissue macrophages[309,310]. Interestingly, when the geometric mean fluorescence intensity (gMFI) of CD16 in the monocyte population was investigated, it was observed that cHz-containing monocytes had significantly higher levels of CD16 gMFI (Figure 11). This supports the idea that Hz preparations may have different stimulatory activity depending on the presence/absence of adsorbed biomolecules on the Hz crystal faces.

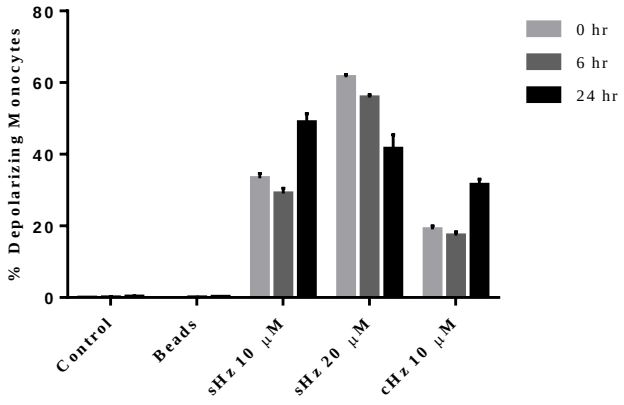

Figure 10. Hz detection in human peripheral blood mononuclear cells (PBMC). PBMC were isolated from buffy coats and incubated with sHz at 10 and 20 μM heme equivalents or with cHz at 10 μM heme equivalents. PBMC incubated with latex beads or left unexposed to Hz were used as controls. The percentage of Hz-containing monocytes was determined at time zero, and after six and 24 hours of incubation, by flow cytometry. The mean values of triplicates (± one SD) for one representative experiment are shown. Controls and beads had no depolarizing populations.

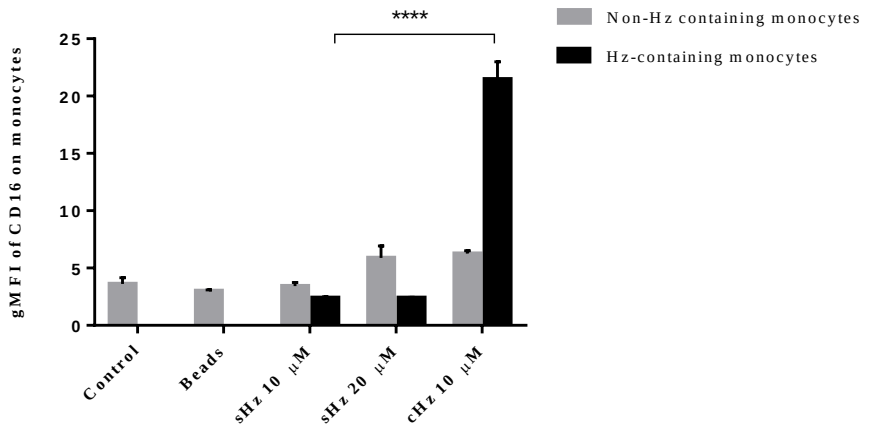

Figure 11. gMFI of CD16 on monocytes fed *in-vitro* with different types of Hz. PBMC were isolated from buffy coats and were incubated either with sHz at 10 and 20 μM heme equivalents or with crude Hz (cHz) at 10 μM heme equivalents. PBMCs incubated with latex beads or left unexposed to Hz were used as controls. Cells were incubated for 6 hours and then labelled with anti-CD14 and anti-CD16 antibodies. Geometric mean fluorescence intensity (gMFI) of CD16 was calculated for non-Hz containing monocytes (gray bars) and Hz-containing monocytes (black bars). Differences between sHZ and cHz were significant ($p < 0.0001$). Triplicate values (± one SD) for one representative experiment are shown. Controls and beads had no depolarizing populations.

Presence of Hz in leucocytes is correlated with disease severity in two models of experimental malaria.

Following successful detection of Hz using *in vitro* assays, where cells from healthy donors were incubated with sHz, fresh blood from two distinct mouse models of experimental malaria was investigated to see if Hz-containing cells could be detected and if a correlation with disease severity could be established. Mice infected with *P. berghei* ANKA (PbA) were sacrificed on day 5 when symptoms compatible with experimental cerebral malaria started to develop. Mice infected with *P. berghei* NK65 (PbNK65) were sacrificed on day 18 when they reached high parasitaemia and started showing signs of morbidity. Monocyte (inflammatory and resident) and granulocyte populations were identified based on their SSC-1 and on CD11b and Gr1 expression. CD11b is mainly expressed on monocytes and macrophages and at lower levels on granulocytes and NK cells whilst Gr1 is mainly expressed in mature granulocytes. Thus, using Petkova's gating strategy, granulocytes were defined as $CD11b^{+}SSC^{high}Gr1^{++}$, inflammatory monocytes as $CD11b^{+}SSC^{low}Gr1^{+}$ and resident monocytes as $CD11b^{+}SSC^{low}Gr1^{-}$[311]. Overall, results showed that the percentage of Hz-containing leukocytes increased when parasitaemia was higher (Figure 12). Interestingly, when mice infected with the two parasite strains were compared at a time-point at which their parasitaemias were similar, i.e. day 5 for PbA (5.7%) and day 12 for PbNK65 (7.7%),

PbA infected mice had significantly ($p<0.02$) higher percentages of Hz-containing inflammatory monocytes than PbNK65 infected mice (22.1% and 9.1%, respectively). Furthermore, at day 18 of infection, when PbNK65 mice were sick, the percentage of Hz-containing inflammatory monocytes was similar to that observed in PbA infected mice at day 5 of infection (14.2%). The levels of parasitaemia were, however, significantly higher in PbNK65-infected mice (28.5%) than in PbA-infected mice (5.7%). Taken together our data suggest that the percentage and type of Hz-containing phagocytes may be associated with disease severity.

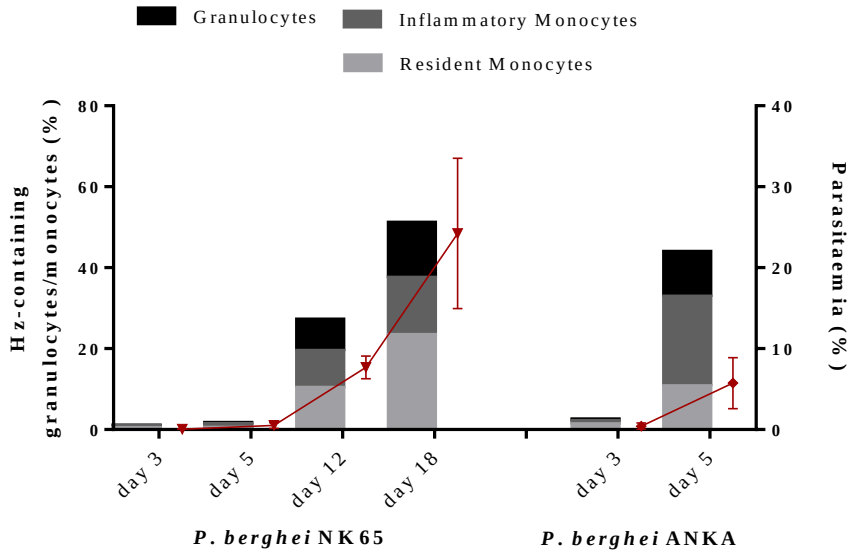

Figure 12. Hz containing leukocytes in two different mouse models of malaria. Groups of five C57BL/6 mice were infected with *P. berghei* ANKA (PbA) or with *P. berghei* NK65 (PbNK65). Blood was drawn on days 3, 5 12 and 18 and analysed after labelling with anti-CD11b and anti-Gr1. Mean percentages per group of Hz-containing monocytes and granulocytes, as well as parasitaemia (red line), are shown. Light grey bars: Hz-containing resident monocytes; dark grey bars: inflammatory monocytes and black bars: granulocytes. Uninfected controls had no Hz-containing leukocytes (data not shown). Mice infected with PbA were sacrificed on day 5.

Concluding remarks

The findings in this chapter showed that following the adaptation of the Cyflow® Blue laser cytometer for the detection of SSC-2 it was possible to detect Hz-containing cells in human whole blood and isolated PBMC. Using this detection method, it was shown that monocytes are the main population to phagocytose Hz in a dose- and time-dependant manner. It was also observed that cHz can induce different immunological effects, as shown by higher gMFI of CD16 on monocytes. This may be attributed to the presence of biomolecules on cHz, that are absent on sHz. Finally, our results using two different murine models of malaria infection suggest that detection of Hz in circulating granulocytes/monocites correlates with disease severity in mice.

2. Characterization of cellular functions impaired by ingestion of Hz

Introduction

Several studies suggest that monocytes and macrophages fed with Hz may have impaired cellular functions such as phagocytosis and generation of oxidative burst[208,237]. Impairment of these functions may be associated with reduced antibacterial and anti-tumour activities of monocytes in malaria patients[238]. Following the optimization of Hz detection using flow-cytometry, functional studies were carried out to characterize the immuno-modulatory properties of Hz at single-cell level. The aim was to investigate if Hz contributed to impairment of cellular functions (phagocytosis, oxidative burst and induction of TNF-α) only on Hz-containing cells or if the effects were propagated to non-Hz containing cells. Thus, Hz effects were assessed in the context of a mixed population of Hz-containing and non-Hz containing cells, which is most likely to reflect the *in vivo* scenario, where the median percentage of Hz-containing circulating monocytes has been reported to be 2-5%[312]. All functional studies performed in this section used synthetic Hz kindly supplied by Dr Cevayir Coban (referred to in Chapter I). As mentioned in Chapter I, sHz was favoured over cHz to avoid possible confounding factors from the presence of other biomoleucales (protein, DNA and possibly lipids) on cHz. The reason to use Coban's sHz instead of our own was due to the ease of access to larger batches of sHz, produced in a quality controlled manner, which allowed us to perform functional studies without inter -batch variability.

Results

Monocytes incubated with Hz have reduced phagocytic function

The effect of Hz ingestion on phagocytic function was investigated in PBMC isolated from buffy coats of healthy donors. Phagocytosis was quantified by flow cytometry using *E. coli* bioparticles conjugated with a pH sensitive dye (pHrodo™ dye), that only fluoresces inside the acidic phagosome. PBMC were fed with 10 and 50 µM sHz, for 6 hours and then assayed for phagocytic capacity. As shown in Figure 13, where the phagocytic capacity of unfed monocytes was compared to that of monocytes fed with either latex beads or sHz, there was a reduction in the phagocytic capacity of

sHz-fed monocytes, of approximately 90-95%. This occurred both in the Hz-containing and Hz-negative population in sHz-fed monocytes. Contrastingly, bead-fed monocytes showed no reduction in phagocytic capacity. Thus, our results suggest that while ingestion of latex beads does not impair a second round of phagocytosis, ingestion of sHz leads to impairment of further phagocytosis.

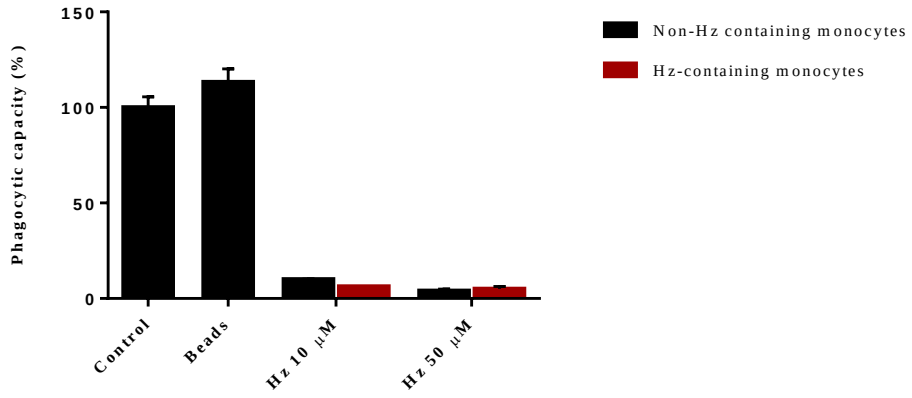

Figure 13. Phagocytic capacity of human PBMC fed with Hz. Peripheral blood mononuclear cells (PBMC) isolated from buffy coats of healthy donors were incubated for 6 hours in the presence of 10 or 50 µM sHz. Unfed PBMC and PBMC fed with latex beads were used as positive control (black bars). The phagocytic function was quantified by flow cytometry using *E. coli* bioparticles conjugated with a pH sensitive dye (pHrodo™ dye), which only fluoresces inside the acidic phagosome. The phagocytic capacity represents the percentage of monocytes with fluorescent bioparticles, normalized against the non-fed control.

Hz-containing monocytes have an impaired oxidative burst response

The oxidative burst response was evaluated in Hz-fed monocytes upon stimulation with phorbol myristate acetate (PMA) or following *M. bovis* BCG (BCG) infection. Thus, monocytes were fed with 10 or 50 µM sHz for 4 hours, and then either stimulated for 1 hour by the addition of PMA or by BCG infection. The 4 hour incubation period was sufficient to obtain similar amounts of Hz-containing cells to those obtained in the phagocytosis assay, where a 6-hour incubation period was used (not shown). Following stimulation/infection, the magnitude of oxidative burst was quantified by determining the gMFI of cleaved dihydrorhodamine 123 (DHR 123), a fluorogenic substrate which is converted to rhodamine 123 upon reaction with reactive oxygen species (ROS). Figures 14 and 15 show the reduced capacity of monocytes fed with sHz to produce ROS when stimulated with PMA or on BCG infection, respectively. This reduction in oxidative burst capacity was specific to monocytes that ingested Hz, since non-Hz

containing monocytes in the Hz-fed population had levels of ROS production identical to the non-fed positive control. The percentage of non-Hz containing monocytes in the Hz fed population was on average 30% for the lowest Hz concentration and 12% for the highest Hz concentration in the PMA experiments. Monocytes infected with BCG had percentages of non-Hz containing monocytes in the mixed population of 58% and 30% for the lowest and highest Hz concentrations, respectively.

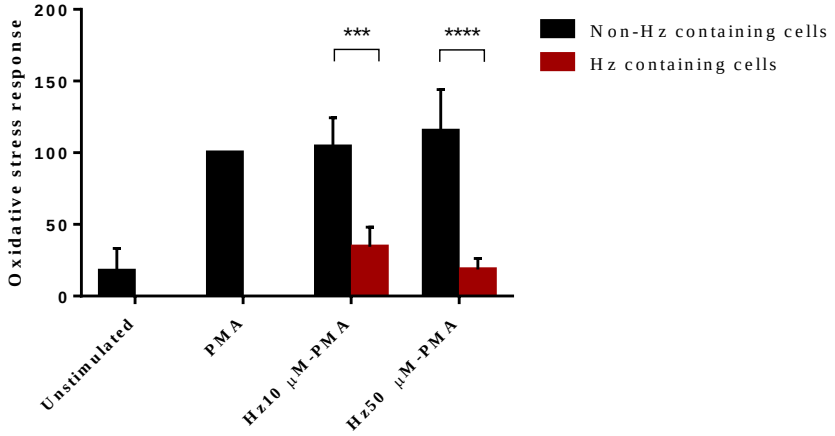

Figure 14. Oxidative capacity of Hz-fed PBMC post-PMA stimulation. Peripheral blood mononuclear cells (PBMC) isolated from buffy coats of healthy donors were incubated for 4 hours in the presence of 10 or 50 µM sHz. Following Hz ingestion, monocytes were stimulated with phorbol myristate acetate (PMA). Unfed, unstimulated PBMC and unfed PBMC stimulated with PMA were used as negative and positive controls, respectively. The magnitude of the oxidative burst was quantified by flow cytometry, via measurement of dihydrorhodamine 123 (DHR 123) oxidation. The gMFI of cleaved substrate of Hz-fed monocytes normalized against the unfed positive control, of five independent experiments is shown. Black bars: oxidative stress response in non-Hz containing monocytes; red bars: oxidative stress response in Hz-containing monocytes. Differences between Hz-containing and non-Hz containing monocytes were signinficant (***p=0.0002; ****p<0.0001).

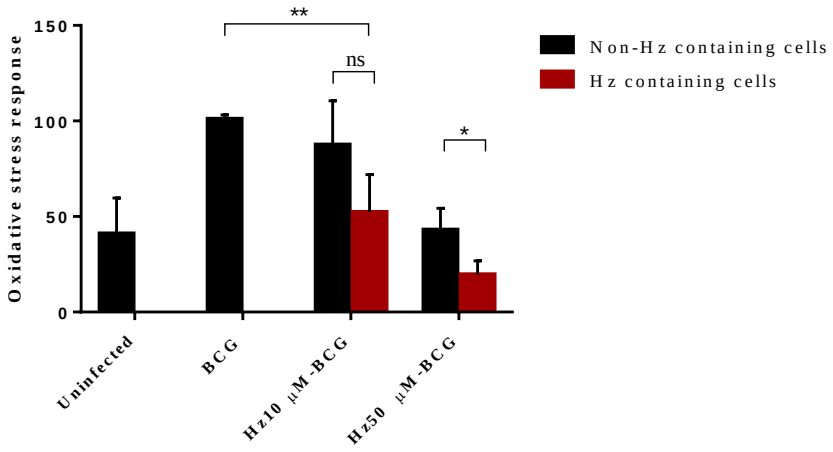

Figure 15. Oxidative capacity of Hz-fed PBMC following BCG infection. Peripheral blood mononuclear cells (PBMCs) isolated from buffy coats of healthy donors were incubated for 4 hours in the presence of 10 or 50 µM sHz. Following Hz ingestion, monocytes were infected with BCG for 1 hour. Unfed, uninfected PBMC and unfed PBMC infected with BCG were used as negative and positive controls, respectively. The oxidative stress response was quantified as described in Figure 14. Differences between Hz-containing and non-Hz containing monocytes were significant at the highest sHz concentration (p=0.0392) and between the Hz-containing population of the lower sHz concentration and the positive control (p=0.0026).

Production of TNF-α is decreased in Hz-fed PBMC

We were also interested in investigating whether Hz had a stimulatory effect on monocytes by inducing TNF-α production, as reported by others[257,313], or if its ingestion by monocytes could impair subsequent responses to other stimuli such as BCG infection. To assess whether Hz had stimulatory capacity, PBMC isolated from buffy coats of healthy donors were incubated with 10 µM sHz alone or in the presence of 2 µg/ml LPS. As shown in Figure 16, sHz by itself did not stimulate TNF-α production by PBMC, thus showing that Hz is not stimulatory. However, in the presence of LPS, Hz-fed PBMC produced TNF-α. There was a tendency for Hz-containing cells to produce lower amounts of TNF-α than non-Hz containing cells although this difference did not reach statistical significance (Figure 16).

Next, we investigated if levels of TNF-α induced by BCG infection of human PBMC were affected by sHz. For this, we used a *M. bovis* BCG strain that expresses GFP (green fluorescent protein) to identify infected cells. Thus, human PBMC were fed with 10 µM sHz and infected with BCG. The levels of TNF-α induced by BCG in the presence of sHz were compared to unfed PBMC infected with BCG. The results in

Figure 17 suggest that Hz exposure *per se* impaired TNF-α production in response to BCG infection, as both Hz-negative and Hz-containing PBMC had reduced levels of TNF-α production in response to BCG infection as compared to controls.

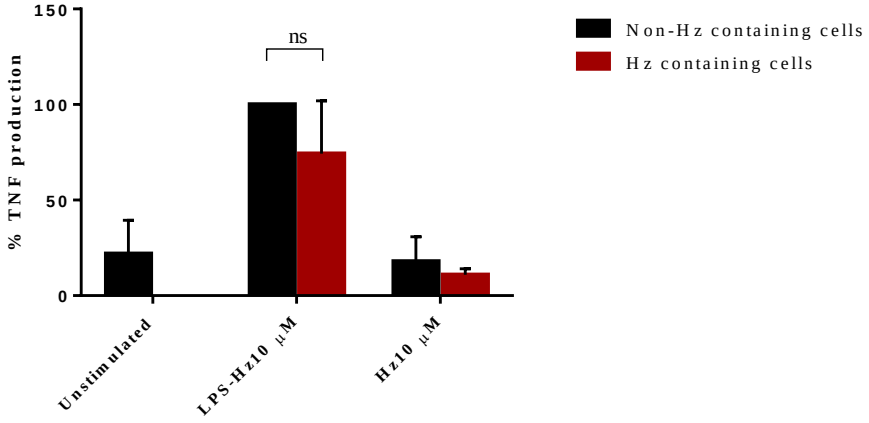

Figure 16. Ingestion of sHz by human PBMC does not induce TNF-α production. Peripheral blood mononuclear cells (PBMCs) isolated from buffy coats of healthy donors were fed with 10 µM sHz for 4 h. As a positive control for TNF-α production, PBMC were fed with 10 µM sHz in the presence of 2 µg/ml LPS. Unstimulated, unfed PBMC were included as a negative control. TNF- α production was determined by flow-cytometry, after intracellular staining. The gMFI, normalized against the non-Hz containing cells of the positive control, of four independent experiments, is shown.

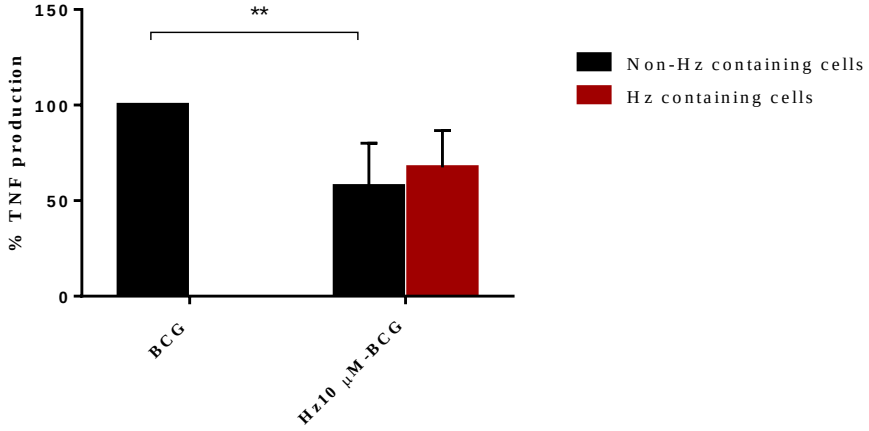

Figure 17. TNF-α production in BCG infected human PBMC, fed with sHz. Peripheral blood mononuclear cells (PBMCs) isolated from buffy coats of healthy donors were fed with 10 µM sHz for 4 h. PBMC were then infected with BCG (GFP-expressing strain) and TNF-α production determined by intracellular staining after 18 hours of infection. In parallel, unfed PBMC were infected with BCG as a positive control for TNF-α production. The gMFI, normalized against the positive control, of four independent experiments is shown. Production of TNF-α between positive control and non-Hz containing cells was significantly different (p=0.0092).

M. bovis BCG infection of Hz and non-Hz containing monocytes.

Given our results showing functional impairment of Hz-containing monocytes we went on to investigate the kinetics of BCG growth in Hz-fed and non Hz-fed monocytes. Bacterial growth was first determined by infecting PBMC, fed with either 10 µM sHz or latex beads, with BCG. Five days later, PBMC were lysed and serial dilutions of cell lysates were plated in solid media for determination of colony forming units (CFUs). Figure 18 compares the percentage of infection in unfed PBMC with PBMC fed with latex beads or sHz, prior to infection. Results showed that PBMC pre-fed with sHz had higher bacterial load than PBMC pre-fed with latex beads or unfed controls.

BCG growth was also investigated by cytometry and fluorescence microscopy as we wanted to investigate bacterial growth in the mixed population of Hz-containing and non-Hz containing cells. For this, the *M. bovis* BCG strain expressing GFP was used. Unfed/fed PBMC were infected with BCG-GFP strain for five days, and then analysed either by flow-cytometry (Figure 19) or by fluorescence microscopy (Figure 20). Flow-cytometry results showed no significant differences in bacterial growth between bead/sHz-fed PBMC and unfed controls. However, fluorescence microscopy results again suggested that Hz-fed PBMC have higher bacterial load than non-fed controls.

Overall these results suggest that ingestion of Hz by PBMC leads to functional impairment of these cells. This in turn results in a lower bactericidal capacity that contributes to higher BCG loads. This might mean that *in vivo*, accumulation of Hz might contribute to a lower capacity to control TB infection.

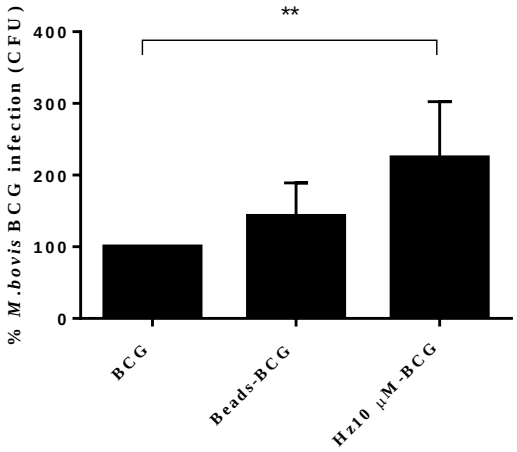

Figure 18. BCG infection of Hz-fed PBMC. Peripheral blood mononuclear cells (PBMCs) isolated from buffy coats of healthy donors were incubated for 4 hours with 10 µM sHz or with 0.001% latex beads. Following Hz/bead ingestion, monocytes were infected with BCG for 3 hours. Unfed PBMC were also infected with BCG in parallel, as a positive control. After five days, cells were lysed and serial dilutions plated to allow the determination of CFUs. Results shown are the mean percentage of infection (normalized to the positive control) of five independent experiments. Differences between positive control and Hz-fed PBMC were significant (p=0.0072).

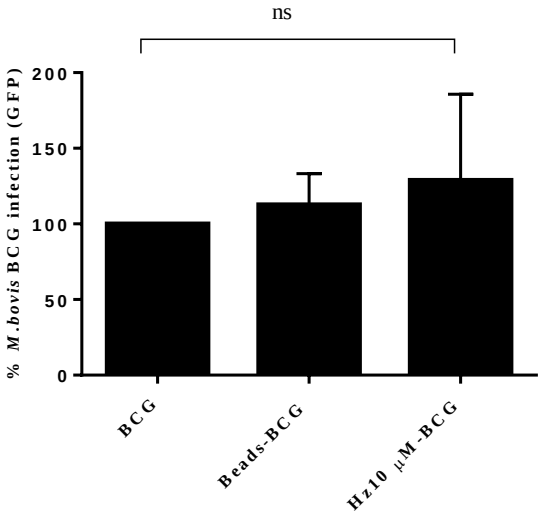

Figure 19. Assessment of BCG-GFP infection in Hz-containing monocytes. Peripheral blood mononuclear cells (PBMCs) isolated from buffy coats of healthy donors were incubated for 4 hours with 10 µM sHz or with 0.001% latex beads. Following Hz/bead ingestion, monocytes were infected with BCG-GFP strain for 3 hours. Unfed PBMC were also infected with BCG-GFP in parallel, as a positive control. After 5 days, cells were analysed using flow-cytometry to assess bacterial growth in Hz-containing monocytes. Results shown are the mean percentage of infection (gMFI of GFP positive cells, normalized to the positive control) of five independent experiments.

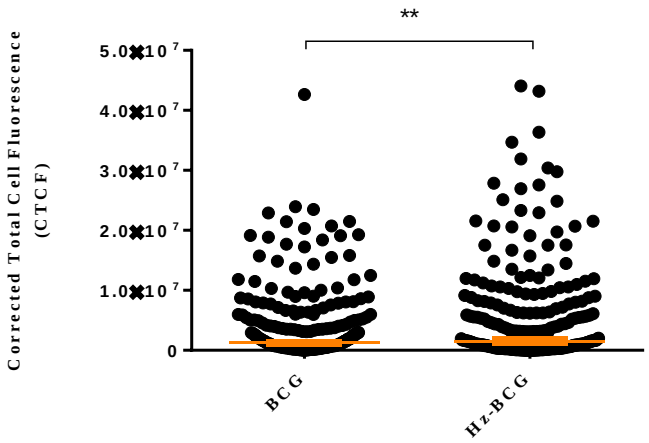

Figure 20. Assessment of BCG-GFP infection in Hz-containing monocytes by fluorescence microscopy. Peripheral blood mononuclear cells (PBMCs) isolated from buffy coats of healthy donors were incubated for 4 hours with 10 µM sHz. Following Hz ingestion, monocytes were infected with BCG-GFP strain for 3 hours. Unfed PBMC were also infected with BCG-GFP in parallel, as a positive control. After 5 days, cells were analysed by microscopy using a Zeiss Axiovert 200M microscope. An automatic programme was used to scan the cover slip and acquire 25 sequential photos. Images were then analysed using ImageJ 1.47v to measure the GFP integrated density (fluorescence). The geometric mean of the corrected total cell fluorescence (CTCF), of three independent experiments is shown (CTCF= fluorescence of the measured signal x area measured, corrected for the mean fluorescence of the background reading). Differences between unfed PBMC and Hz-fed PBMC were significant (p=0.0016).

Concluding Remarks

In this chapter the effects of Hz ingestion by human PBMC on cellular functions were investigated. Mainly, we investigated whether ingestion of Hz impaired phagocytosis, oxidative burst or the production of TNF-α. In contrast to previous studies, we aimed at finding possible Hz effects specifically on those cells that had ingested Hz, while investigating if these effects were propagated to non-Hz containing cells. To this end, we employed flow cytometry and the detection strategy described in the first part of this chapter. The results obtained suggested that cellular functions such as phagocytosis, oxidative burst and production of TNF-α following Hz ingestion were decreased when compared to non-fed control cells. Hz effects seemed to propagate to non-Hz containing cells in the case of phagocytosis and TNF-α production. However, in the case of the oxidative burst, significant differences were found between the responses of Hz-containing cells and non-Hz containing cells. While Hz-containing cells had decreased oxidative burst capacity, the non-Hz containing cells overall showed similar capacity to non-fed controls.

Next, we investigated whether the impairment of the aforementioned cellular functions would promote a poorer control of mycobacterial growth. Therefore, the growth of BCG was assessed in human PBMC following Hz ingestion. Growth was

monitored by first determining CFUs levels. Then, to investigate if bacterial growth was different in Hz-containing cells and non-Hz containing cells, a GFP-expressing strain of *M. bovis* BCG was used, to determine mycobacterial growth using flow-cytometry and fluorescence microscopy. CFUs determination and fluorescence microscopy showed that Hz-fed PBMC contained higher mycobacterial loads than non-fed controls, thus suggesting that Hz ingestion through impairment of cellular functions may contribute to loss of bactericidal function.

Materials and Methods

***M. bovis* BCG strains used**

When indicated PBMC were infected with *M. bovis* BCG-lux (BCG transformed with the plasmid pMV306G13-Lux (Addgene; Cambridge, MA, USA) kindly provided by Dr Brian Robertson (Imperial College, London, UK). Alternatively, PBMC were infected with *M. bovis* BCG-GFP (BCG transformed with a GFP expressing plasmid) which was a kind donation from Dr Bianca Schneider (Borstel Leibniz-Center for Medicine and Biosciences, Germany). Unless otherwise stated, all infections were performed with the BCG-lux strain.

Cultures of *M. bovis BCG-lux and M. bovis BCG-GFP* were grown in 7H9 broth (supplemented with 0.05% Tween-80 and 10% oleic-albumin-dextrose-catalase (OADC); BD Diagnostics, Franklin Lakes, NJ, USA). Cultures of BCG-GFP were additionally grown in the presence of kanamycin (20 µg/ml). Strains were grown for 7-10 days at 37°C, 5% CO_2 and used to prepare frozen vials in the presence of 25% glycerol.

Flow cytometer modification (depolarized Side Scatter detection)

The CyFlow® Blue laser (Partec, Münster, Germany) is a small, five parameter flow cytometer with blue laser (488 nm) excitation, and detectors for Forward Scatter (FSC), Side Scatter (SSC), green fluorescence (FL1), orange fluorescence (FL2) and red fluorescence (FL3). To allow for depolarized Side Scatter detection this set-up was changed, mainly by creating two SSC detectors, using a 50%/50% beam splitter. Then, a polarization filter was placed orthogonally (90º angle) to the polarization plane of the laser light, in front of one of these SSC detectors. Thus, allowing the detection of depolarized Side-Scatter. This and other necessary changes are indicated in Figure M1.

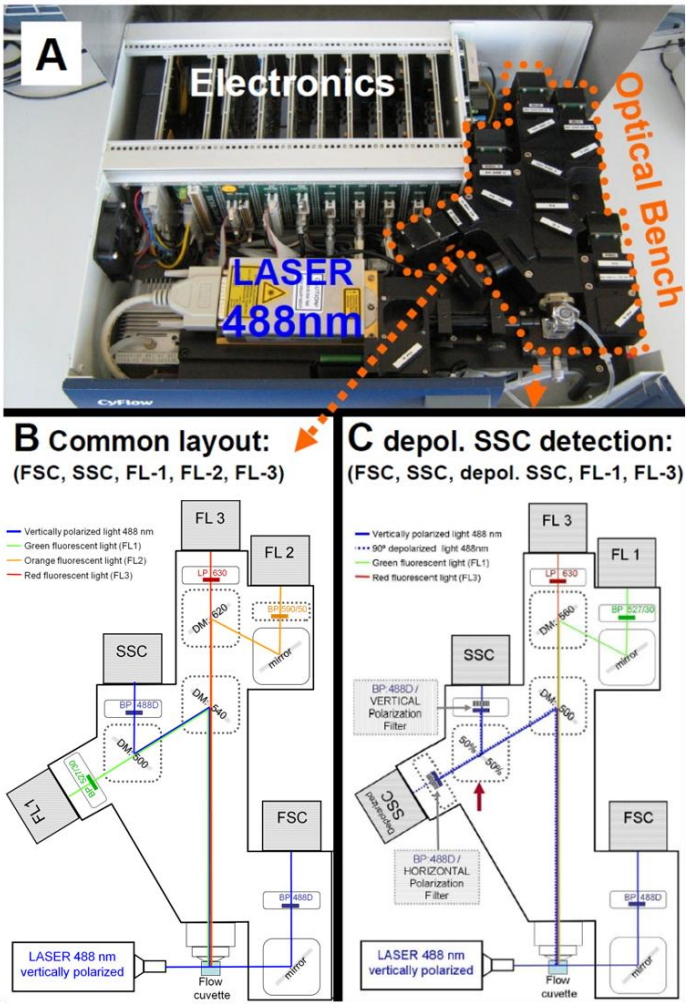

Figure M1. Alterations to the CyFLow® Blue laser flow cytometer to allow detection of depolarized side-scatter. A) The lid of the flow cytometer was removed to allow access to the optical bench of the cytometer. B) Light path in conventional filter set-up for detection of Forward Scatter (FSC), Side-Scatter (SSC), green (FL-1), orange (FL-2) and red (FL-3) fluorescence. C) Filter set-up that allows detection of depolarized Side-Scatter instead of FL-2 detection. Squares with broken line indicate dichroic mirrors that needed to be changed. Red arrow shows 50%/50% beam splitter. Other beam splitters which divert more light to the depolarized SSC are possible, such as 90%/10% or even 95%/5%. DM = Dichroic Mirror; BP = Bandpass filter, LP = Longpass filter; numbers indicate wavelength in nm.

In vitro incubation of human whole blood with sHz

Heparin-anticoagulated blood from healthy human donors was diluted 1:1 in RPMI 1640 (Gibco™) and distributed into a 24 well plate. Then, sHz was added at 10; 60 and 120 μM heme equivalent. The plate was incubated at 37°C in 5% CO_2. Leucocytes were analyzed in triplicates at the time points indicated.

In vitro incubation of human PBMCs with sHz and cHz

Human PBMC were isolated from 40 ml heparin-anticoagulated blood collected from healthy volunteers and after dilution 1:1 in RPMI 1640 was placed in a Ficoll gradient (Ficoll-Paque Plus, GE Healthcare; Uppsala, Sweden). Cells were centrifuged at 700 g for 20 min and the interface containing the PBMCs was collected. The PBMCs were washed, counted and resuspended at a concentration of 1×10^6 PBMC/ml in RPMI 1640 (supplemented with 2 mM L-glutamine, 10 mM Hepes, 0.05 mg/ml gentamicin and 10% fetal calf serum) and distributed into a 24 well plate. Then, sHz was added at 10 and 20 μM heme equivalent and cHz was added at 10 μM heme equivalent in triplicates. Polystyrene latex beads (0.1 μm) were diluted from stock at 10% (vol/vol) to a final concentration of 0.001% and used as control when indicated. The plate was incubated at 37°C in 5% CO_2 for the indicated times.

Flow cytometry analysis of human leucocytes

For the *in vitro* whole blood assay, 50 μl of blood suspension were incubated with anti-CD14 (fluorescein isothiocyanate, FITC) and anti-CD16 (phycoerythrin, PE) antibodies (Ebioscience, San Diego, CA, USA), following Hz incubation. RBC were lysed with BD FACS lysing solution (BD Biosciences; San Jose, CA, USA) for 5 minutes and washed before analysis. PBMCs were labelled as described for the whole blood assay, without RBC lysis. All *in vitro* samples were performed in triplicate.

Flow cytometric analysis of murine leukocytes

Groups of five C57BL/6 mice (7 weeks old from Charles River, Spain) were infected intraperitoneally (IP) with *Plasmodium berghei* ANKA (PbA) as model for experimental cerebral malaria or *P. berghei* NK65 (PbNK65) as model for hyperparasitaemia. Uninfected and PbNK65-infected mice were followed for 18 days. PbA-infected mice were sacrificed on day 5 when showing obvious signs of morbidity. Parasitaemia and flow cytometric analysis of blood was performed on days 3, 5, 12 and 18 post-infection. At each time point, approximately 25 μl of blood was collected from a tail vein, incubated with Fc-block and then labelled with anti-CD11b (FITC) and anti-Gr1 (PE) antibodies. After washing the cells, RBC were lysed with 125 μl of BD FACS lysing solution (BD Biosciences) for 5 min. The cells were washed again, resuspended in FACS buffer (1x PBS with 2% fetal calf serum) and analyzed by flow cytometry. Antibodies and Fc-block purchased from Ebioscience.

Isolation of human PBMC for functional assays

Human PBMC were isolated from buffy coats discarded from blood donations of healthy volunteers and kindly provided by Instituto Português do Sangue. Buffy coats were diluted 1:1 in RPMI 1640 and placed in a Histopaque gradient (Histopaque® 1077, Sigma-Aldrich). Cells were centrifuged at 600 g for 20 min (without centrifuge brake) and the interface containing the PBMC was collected. Then, PBMC were washed once in RPMI 1640, counted and resuspended at a concentration of 5×10^5 PBMC/ml in RPMI 1640. The PBMC suspension was distributed in 24-well plates and incubated for 1-2 h at 37ºC, in 5% CO_2 incubator, to promote cell adherence. At the end of the incubation time non-adherent cells were removed by aspirating the medium from the 24-well plates, and washing two times with warm 1x PBS. Warm RPMI 1640 (supplemented with 2 mM L-glutamine, 10 mM Hepes and 10% fetal calf serum) with or without Hz was added to the wells following the removal of adherent cells and incubated further at 37ºC, 5% CO_2.

Phagocytosis assay

The phagocytic capacity of human PBMC following Hz ingestion was evaluated using the pHrodo™ *E. coli* BioParticles® Phagocytosis Kit for flow cytometry (Molecular Probes, Invitrogen). *E. coli* bioparticles were opsonized with autologous serum before the phagocytic assay. Human PBMC from healthy donors were isolated as described above. Unfed-PBMC and PBMC fed with 10 and 50 μM Hz were incubated at 37C, 5% CO_2, for 6 hours. Then, the phagocytic assay was performed following manufacturer's instructions with the following modifications. Hz-fed PBMC and control PBMC were transferred to cytometry tubes and *E. coli* bioparticles added at a 20:1 (bioparticles:PBMC) ratio and incubated in a water bath at 37ºC for 180 min. At the end of the incubation time, tubes were kept on ice to terminate phagocytosis activity. Finally PBMC were stained with anti-CD14 (FITC) antibody for 20 min before acquisition on the cytometer.

Oxidative burst assay

The Phagoburst™ (Glycotope Biotechnology; Berlin, Germany) kit allows the detection of reactive oxygen species (ROS) by the addition and oxidation of the fluorogenic substrate dihydrorhodamine-123 (DHR-123). The gMFI of cells producing ROS can then be determined by flow cytometry using the green fluorescence channel

(FL1). Human PBMC from healthy donors were isolated as before. Hz at 10 and 50 μM was added to PBMC and incubated at 37ºC, 5% CO_2 for 4 h. Then, the oxidative burst assay was performed as per manufacturer's instructions with the following modifications. Following Hz incubation, Hz-fed and control unfed-PBMC were transferred to cytometry tubes. Then, phorbol 12-myristate 13-acetate (PMA) was used to stimulate ROS production. For this, PMA was added to unfed-PBMC and Hz-fed PBMC and cells incubated at 37ºC in a water bath for 1 h. Unfed-PBMC with no added PMA were included as a negative control. After stimulation with PMA, DHR-123 was added to cells and further incubated for 10 min at 37ºC. Finally, cells were stained with CD14 (PE) and incubated for 20 min on ice before flow cytometry analysis. Alternatively, PMA stimulation was replaced by one hour *M. bovis* BCG (BCG) infection (at a ratio of 10:1) to evaluate the oxidative response of Hz-containing PBMC to BCG infection.

TNF-α intracellular staining (with or without stimulation)

For quantification of TNF-α, isolated PBMC were fed with 10 μM Hz and incubated for 4 h at 37ºC, 5% CO_2. As a positive control for TNF-α production, Hz-fed PBMC were incubated in the presence of 2 μg/ml LPS. Brefeldin A (10 μg/ml; Sigma-Aldrich) was added to cells at the same time as Hz. Alternatively, isolated PBMC were fed with 10 μM Hz for 4 h and then infected with BCG-GFP strain for 18 h in the presence of 10 μg/ml Brefeldin A. Intracelular staining was performed by fixing cells by adding paraformaldehyde (PFA) to a final concentration of 2% and incubating for 20 min at room temperature (RT). Then, permeabilization buffer (0.5% saponin in 1x Facs buffer) was added to cells and further incubated for 10 min at RT. Finally, cells were washed 1x in permeabilization buffer and stained with TNF-α antibody (PE) for 20 min on ice before flow cytometry analysis.

Mycobacterial load determination of BCG-infected PBMC

Following PBMC isolation, 10 μM Hz was fed to PBMC for 4 h at 37ºC with 5% CO_2. Then Hz-fed and unfed-PBMC were infected with BCG-lux (at a multiplicity of infection (MOI) of 2), for 3 h at the end of which extracellular bacteria were removed by two washes in warm 1x PBS. RPMI 1640 (supplemented with 2 mM L-glutamine, 10 mM Hepes and 20% fetal calf serum) was added to cells and before incubation for 5 days at 37ºC, 5% CO_2. Mycobacterial burden determination by colony forming units

(CFUs) was performed as follows. After infection, PBMC were lysed by the addition of 1% saponin (0.1% final concentration) and serial dilutions of lysed PBMC were plated on 7H11 Agar (supplemented with OADC; BD Diagnostics). Plates were incubated at 37ºC, 5% CO_2, for 21 days before counting CFUs.

For quantification of mycobacterial growth by flow cytometry, isolated PBMC were fed with Hz (unfed PBMC were included as control). Then, Hz-fed and unfed PBMC were infected with BCG-GFP strain (MOI:10), as described above. Five days post-infection, cells were transferred to cytometry tubes, stained with CD14 (PE) and analysed by flow cytometry.

Quantification of mycobacterial growth by microscopy was performed by distributing isolated PBMC onto 10 mm microwell glass bottom dishes (MatTek Corporation; Homer Avenue, Ashland, MA, USA) pre-treated with poly-L-lysine (Sigma-Aldrich). Hz-fed and unfed PBMC were infected with BCG-GFP strain (MOI: 10), as before. Then, five days post-infection, cells were analysed by microscopy using a Zeiss Axiovert 200M microscope (Carl Zeiss, Göttingen, Germany) equipped with a cooled CCD camera (Roper Scientific Coolsnap HQ CCD).

Discussion

Hemozoin detection is normally restricted to microscopy. However, increasing interest in alternative methods of hemozoin detection and their applicability to new malaria diagnostic tests has driven research in recent years. Several methods have been proposed based on the paramagnetic and birefringent properties of hemozoin[314–316]. Although these methods seem promising, they present inherent limitations such as low sensitivity in the detection of *P. falciparum* malaria[317]. This is due to the fact that in *P. falciparum* malaria only immature forms are seen in peripheral blood circulation and these have lower hemozoin content. However, hemozoin based diagnostic tests might be useful in the diagnostic of other forms of malaria where mature forms with abundant hemozoin are also present in circulation.

Hemozoin detection by flow cytometry seems valuable as a rapid drug sensitivity assay or as a method to analyze Hz-containing and non-Hz containing leukocytes in the same sample, and to perform functional assays[305]. The first part of this chapter demonstrated how a conventional flow-cytometer could be modified, so that instead of the conventional layout, an additional SSC detector was included for the detection of depolarized side scatter. Following sHz incubation in whole blood, a gating strategy

was established to distinguish the cells that ingested hemozoin. This was achieved by comparing the conventional side scatter (SSC-1) with depolarized side scatter (SSC-2), and identifying cells with increased SSC-2. Monocytes could be distinguished from granulocytes by using a classical distinction in terms of their CD14 (monocytes) and CD16 (granulocytes) expression. However, it was observed that monocytes that ingested sHz also had increased SSC-1 and that their distribution overlapped with the granulocyte population. This is particularly important as some studies use a 'classical' monocyte gate strategy and may be excluding the Hz-containing monocytes from the analysis[318,319].

Ingestion of sHz both in whole blood or PBMC from healthy donors was time and dose dependant, and monocytes were the main cell population to phagocytose hemozoin. Classically, monocytes are considered to express CD14 while expressing low levels of CD16 ($CD14^{+}CD16^{-}$). However, it has been shown that during infection, other subclasses of monocytes emerge in circulation that express variable amounts of CD16[320]. During optimization studies, it was observed that whilst sHz did not seem to have an overall effect on the expression of CD16 on monocytes, cHz led to an increased expression of CD16. It is likely that cHz had increased stimulatory capacity than sHz, due to the presence of DNA and proteins. This highlights the importance of what was already discussed in the previous chapter, as to the necessity of careful hemozoin characterization.

Hemozoin detection was further investigated in leucocytes of two models of murine malaria. Infection of C57BL/6 mice with *P. berghei* ANKA is considered to be a model of experimental cerebral malaria (ECM) with shared characteristics with human cerebral malaria (HCM)[321], although this has been disputed by some[322]. Another model of murine malaria consists of *P. berghei* NK65 infection in C57BL/6 mice. This is a non-cerebral model, where mice usually die with hyperparasitaemia and is often used as a model for malaria-associated acute respiratory distress syndrome (MA-ARDS)[323]. The presence of hemozoin in circulating leucocytes has been suggested to correlate with disease severity[324,325], although a large scale study has challenged this by reporting no correlation[312]. However, these studies used microscopy and a leukocyte count based on a very low number of cells (100-200 monocytes/granulocytes). Also the reported number of patients with detectable Hz-containing monocytes and granulocytes was quite variable between study sites, which may account for the discrepant results between studies. Thus, using the two murine models described above it was investigated

if disease severity could be correlated with Hz-containing leukocytes in circulating blood. Results comparing the two models suggest that at similar parasitaemias, the percentage of Hz-containing inflammatory monocytes were a better predictor of disease severity. Similar findings were made in human malaria where inflammatory monocytes ($CD14^+$ monocytes which also express $CD16^+$) were positively correlated with severe malaria anaemia (SMA)[326]. However, in this study pigment content in circulating leukocytes was not evaluated.

It was also the aim of this chapter to establish a protocol for the analysis of Hz-containing and non-Hz containing cells, in the same sample. While most studies use Hz doses or times of incubation that result in the uptake of hemozoin by virtually every phagocyte, *in vivo*, only a proportion of phagocytes will contain hemozoin[327]. Moreover, analysis of Hz-containing and non-Hz containing cells in the same sample, allowed to access if impairment of cell functions was restricted to cells that ingested hemozoin, or if effects were propagated to non-Hz containing cells as well.

Phagocytosis, oxidative-stress response and TNF-α production were evaluated in isolated PBMC following sHz ingestion. Results obtained suggest that ingestion of sHz led to the impairment of all these important cell functions. The PBMC response to LPS stimulation in sHz-containing PBMC was also investigated. This was important to demonstrate that whilst sHz-containing PBMC produced TNF-α in response to LPS, sHz by itself had no stimulatory effect on PBMC. This suggests that the sHz used in our functional assays was free of LPS. Examination of Hz-containing PBMC and non-Hz containing PBMC populations showed that, while phagocytosis impairment seemed to be propagated to all cells exposed to sHz, impairment of ROS production seemed restricted to those cells that ingested sHz.

The mechanism by which hemozoin ingestion leads to impairment of phagocytosis is not known. However, inhibition of ROS production by hemozoin ingestion seems to be associated to production of lipid peroxidation derivatives, which promote oxidation and damage of essential components of the oxidative response, such as cytosolic subunits of NADPH oxidase (NOX) and protein kinase C (PKC)[237].

During *in vitro* experiments, sHz was often observed outside cells following the incubation period. Removal of this undigested hemozoin was resistant to PBS washes thus, it is possible that continued exposure to sHz promoted damage to cell membranes and possibly led to an impairment of phagocytosis, even in those cells that did not

ingest sHz. Furthermore, in our study the oxidative response impairment seemed to be limited to Hz-containing cells. This supports Schwarzer's investigation in which the inhibition mechanism of the oxidative response involves damage to cytosolic subunits[237]. Thus, it is reasonable to expect that only cells that have ingested hemozoin might become impaired in their oxidative response.

As important cellular functions were impaired by hemozoin we set out to investigate how these cells would be able to control intracellular growth of mycobacteria. Bacterial loads were investigated in sHz-containing PBMC, five days following infection with *M. bovis* BCG. Loads were first determined by CFUs, in which it was found that Hz-containing cells had higher levels of BCG than control unfed-PBMC. This correlated with previous data showing that hemozoin ingestion promoted lower microbicidal and anti-tumour activity[238]. A BCG strain expressing GFP was used to determine bacterial load by flow-cytometry and to assess differences in Hz-containing and non-Hz containing cells, on the same hemozoin exposed population. However, it was observed that after five days post infection virtually every cell contained hemozoin. Thus, the mycobacterial load was compared between infected-control and infected, sHz-fed PBMC. In this case, results obtained found no significant differences in bacterial loads. Use of flow-cytometry to detect small differences in mycobacterial loads might not be the best method to use, due to low sensitivity in detecting the GFP signal. Thus, microscopy was further employed to investigate bacterial burdens between unfed- and sHz-fed PBMC. Results obtained by microscopy corroborated results obtained by CFUs determination, in which higher bacterial burdens were observed in sHz-fed PBMC.

Thus, results in this chapter suggest that hemozoin impairs important cellular functions and more importantly, our assays suggest that hemozoin may not only impair functions of Hz-containing cells but also effects may be propagated to adjacent cells. It is tempting to speculate that, *in vivo*, functionally impaired cells will not only be restricted to pigment-containing leukocytes, but also to neighbouring cells with which they will interact.

CHAPTER III

Long term kinetics of hemozoin in mice organs

Introduction

The prolonged presence of Hz in tissues of individuals that had suffered from *Plasmodium* infections has been reported since the 18th century (reviewed in[222]) and, as already mentioned in the introduction to this thesis, it was, in fact, the presence of the pigment in host tissues that eventually aided in the discovery of the *Plasmodium* parasite and its mode of transmission[6]. However, little is known about the long-term kinetics of Hz *in vivo*.

Despite Hz being ingested by circulating granulocytes and monocytes, their median half-life in blood – 72 and 216 hours for Hz-containing granulocytes and Hz-containing monocytes, respectively – is relatively short[328]. Thus, the question remains as to what ultimately happens to Hz. Given the relatively short half-life of phagocytic cells in circulating blood it is likely that hemozoin is liberated and re-ingested by several generations of phagocytes, even when they are already located in host organs (tissue-resident phagocytes)[288]. Until now, only one study used a fluorometric method to try and address the issue of Hz elimination following an infection by the malaria parasite. This report showed that 70% of Hz disappeared from the liver over a period of 270 days after parasite clearance, whilst the amount of Hz in the spleen increased 8-fold during that period[329]. However, no other organs were investigated and no detailed investigation of what happens to Hz inside the aforementioned organs was performed. This chapter describes our investigation of Hz persistence and kinetics in the mammalian host.

Results

Hz quantification in murine tissues

As a first approach we decided to measure Hz in murine organs by a method similar to the one used by Levesque *et al*[329]. Two models of infection were used in these experiments: *P. berghei* NK65 (PbNK65), because of the substantial amount of Hz it produces during infection and *P. chabaudi* AS (PcAS), due to its similarities to the human malaria parasite, *P. falciparum.* These similarities include preferential infection of normocytes, although both can also infect reticulocytes; both can adhere to uninfected RBC (rosetting) and the fact *P. chabaudi* like *P. falciparum* sequester to endothelial cells, and as such, mature forms are almost never seen in peripheral blood circulation[330].

All mice infected with PbNK65 for 14 days developed infection achieving parasitaemias ranging from 9 to 40% (mean 26%). Starting at day 14 post-infection, mice were treated daily with chloroquine (CQ) until complete parasite clearance from peripheral blood (less than 1 parasite in 2000 red-blood cells), eight days later. Mice infected with PcAS developed parasitaemias of 20 to 43% (mean 30%). PcAS infection is a self-limiting infection with infected mice able to self-cure. Clearance of peripheral blood parasitaemia was confirmed 20 days post-infection. Then, at the indicated time points, mice were sacrificed and Hz in homogenized liver and spleen quantified as heme equivalents, as described. Results are shown in Figure 21 for mice infected with PbNK65 and Figure 22 for mice infected with PcAS. Overall Hz levels in both models seemed constant over time, with a slight tendency to increase in the liver.

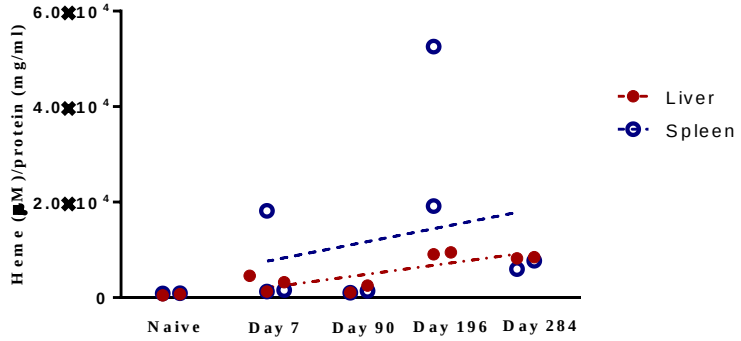

Figure 21. Colorimetric Hz quantification in liver and spleen of PbNK65-infected mice post-malaria clearance. Hz in livers and spleens of *P. berghei* NK65-infected mice was quantified after parasite clearance by a colorimetric assay (QuantiChrom Heme Assay Kit) and expressed in heme equivalents (normalized to protein content). Overall Hz content remained quite stable over time. Liver and spleen of uninfected control mice had negligible amounts of detectable heme (468 and 890 μM heme/protein (mg/ml), respectively) most likely due to the presence of erythrocytes in these tissues.

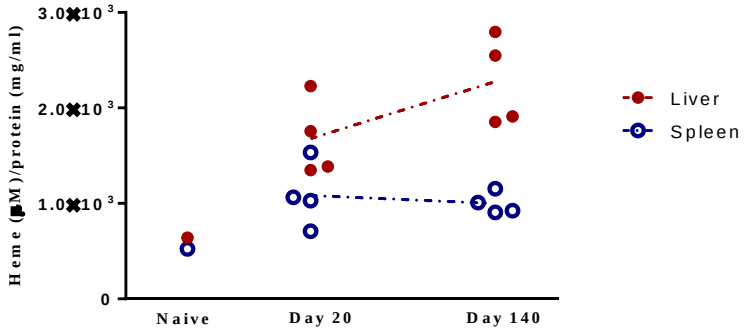

Figure 22. Colorimetric Hz quantification in liver and spleen of PcAS-infected mice post-malaria infection. Hz quantification in livers and spleens of PcAS infected mice was quantified at the indicated time points, as in Figure 21. Overall Hz content remained quite stable over time. Liver and spleen of uninfected control mice had negligible amounts of detectable heme (640 and 523.2 μM heme/protein (mg/ml), respectively), most likely due to the presence of erythrocytes in these tissues.

Hz kinetics in host tissues

Since a simple quantification of Hz inside the host tissues provides no information about the location of Hz inside the different organs studied, we next investigated what happens to Hz after parasite clearance, using histological cuts of liver, spleen and bone marrow. Analyses of these sections revealed that Hz deposition in liver, spleen, and bone marrow of PbNK65-infected mice showed an initially sparse distribution of smaller-sized extracellular particles, as shown by the white arrows in Figure 23. Immediately after parasite clearance, Hz seemed to present a higher density in the liver than in the other organs analyzed. With time, Hz tended to accumulate in larger-sized intracellular particles (black arrows). This was accompanied by a redistribution of Hz from the liver to the hematopoietic organs (spleen and bone marrow). In the spleen, Hz deposition seemed to localize preferentially to the red pulp, as reported by others[331].

Organs of PcAS-infected mice were observed 20 days post-infection, at a time when parasites were no longer observed in circulation. The second time point was analyzed 140 days post-infection. Figure 24 illustrates the kinetics of Hz for liver, spleen and bone marrow. It was similar to that which we had already observed for PbNK65-infected mice, with Hz distribution initially sparse and consisting of smaller-sized extracellular particles. Observation of organ sections at day 140 indicated that, over time, Hz was also redistributed from the liver to the hematopoietic organs. Hz deposition in the spleen also seemed to localize preferentially to the red pulp. Interestingly, PcAS-infected mice had smaller Hz aggregates when compared to the larger aggregates observed in the organs of their PbNK65-infected counterparts. This might reflect different rates of Hz production/tissue accumulation.

Table 2 summarises the histopathological findings of Hz distribution for PbNK65- and PcAS-infected mice.

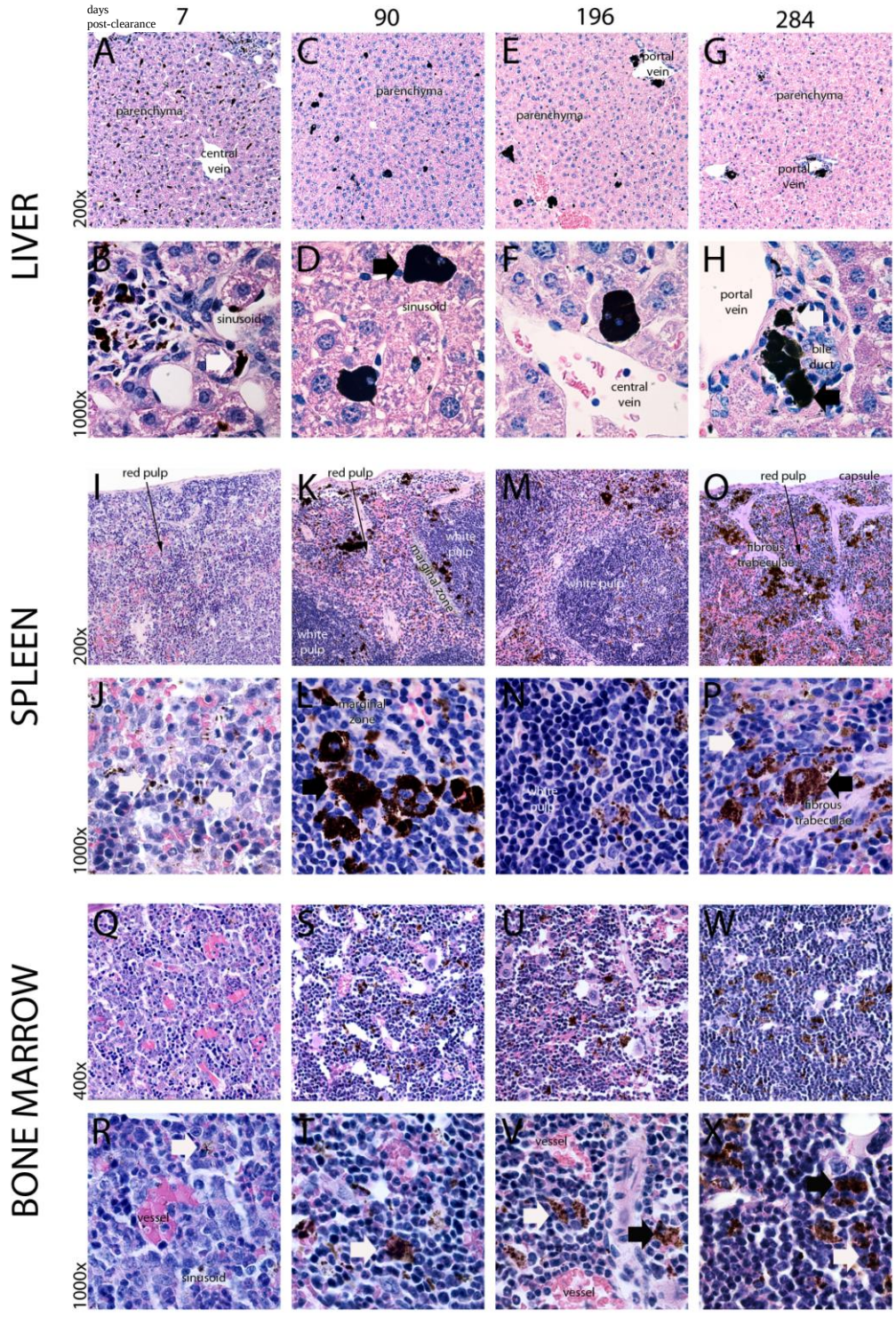

Figure 23. Kinetics of Hz distribution in liver, spleen, and bone marrow of PbNK65 infected mice. Mice were infected with *P. berghei NK65*, and at the indicated time points, organs were extracted for histology. Hz kinetics for liver, spleen, and bone marrow showed an initially sparse distribution of small-sized extracellular particles (white arrows) with increased density in the liver (A, B). This progressed to medium- and large-sized intracellular particles (C–H) (black arrows) with a decrease in density in the liver (E–H) and increase in spleen (M–P) and bone marrow (U–X). This redistribution was accompanied by a distinct organ-specific topographic localization of Hz, which appeared to encompass migration, first to liver (B) and then to the hematopoietic organs (spleen and bone marrow). See Table 1 for a detailed characterization of size, location, organ specific topography, and distribution pattern of Hz in these organs.

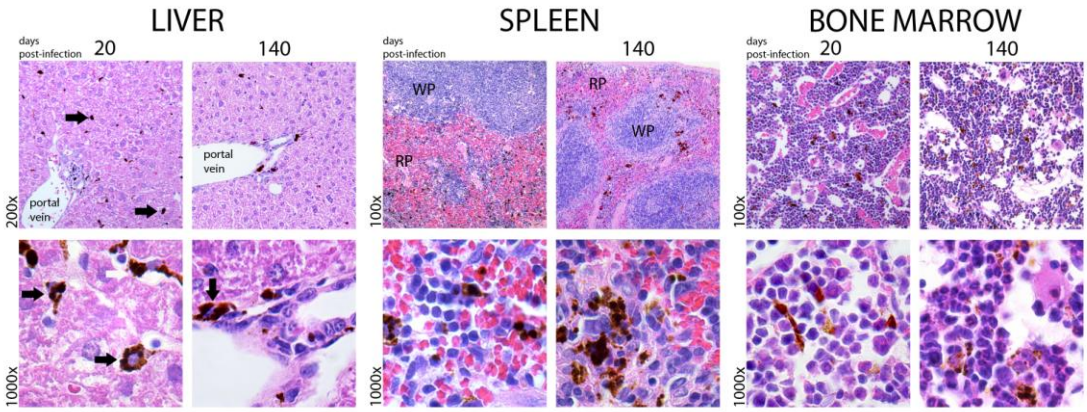

Figure 24. Kinetics of Hz distribution in liver, spleen, and bone marrow of PcAS-infected mice. Mice were infected with *P. chabaudi*, and at the indicated time points organs were extracted for histology. Hz kinetics for liver, spleen, and bone marrow were similar to PbNK65-infected mice: an initially sparse distribution of small-sized extracellular particles with increased density in the liver. This progressed to similar-sized intracellular particles (black arrows) with a decrease in density in the liver and increase in spleen and bone marrow. This redistribution was also accompanied by a distinct organ-specific topographic localization of Hz, which appeared to encompass migration, first to liver and then to the hematopoietic organs (spleen and bone marrow). See Table 1 for a detailed characterization of size, location, organ specific topography, and distribution pattern of Hz in these organs.

organ	Days PC or PI	*Modifiers* particle size[a]	location		topography (organ-specific)	distribution[b]	severity[c]
LIVER	7	S	extracellular	-	sinusoidal	Diffuse	moderate
	20*	S-M	extra and intracellular	endothelial/kupffer cells	sinusoidal	Difffuse	moderate
	90	M-L	intracellular	kupffer cells	sinusoidal	Multifocal	moderate
	140*	L	intracellular	kupffer cells	sinusoidal and perivascular (periportal/perivenular)	Multifocal	moderate
	196	L	intracellular	kupffer cells	perivascular (periportal/perivenular)	Multifocal	mild
	284	L	extra and intracellular	kupffer cells	periportal, acinar	Multifocal	mild
SPLEEN	7	S	extracellular	-	red pulp	Diffuse	minimal
	20*	S-M	extra and intracellular	phagocytic mononuclear cells	red pulp	Diffuse	moderate
	90	M-L	intracellular	phagocytic mononuclear cells	red pulp; marginal zone	Multifocal	moderate
	140*	M-L	intracellular	phagocytic mononuclear cells	red pulp; marginal zone	Multifocal	moderate
	196	L	intracellular	phagocytic mononuclear cells	red pulp; white pulp	Multifocal	moderate
	284	L	extra and intracellular	phagocytic mononuclear cells	red pulp (subcapsular; fibrous trabeculae)	Multifocal	moderate
BONE MARROW	7	S	extracellular	-	sinusoidal	Multifocal	minimal
	20*	S-M	extracellular	-	stromal	Multifocal	mild
	90	M	extracellular	-	stromal	Multifocal	mild
	140*	M	extra and intracellular	phagocytic mononuclear cells	stromal	Multifocal	moderate
	196	L	extra and intracellular	stromal/phagocytic mononuclear cells	stromal	Multifocal	moderate
	284	L	extra and intracellular	stromal/phagocytic mononuclear cells	stromal	multifocal to diffuse	moderate

**P. chabaudi AS* (all other time-points refer to *P. berghei* NK65)

Table 2. Histopathological characterization of hemozoin: size, distribution, and organ-specific topography. Mice were infected with PbNK65 or PcAS, and at the indicated time points (PC – post-malaria clearance and PI – post-malaria infection, for PbNK65 and PcAS, respectively), organs were extracted for histology. aParticle size: S, small; M, medium; L, large. bDistribution: diffuse, affects the majority of the section examined; multifocal, more than one focus. cSeverity: minimal, amount of change barely exceeds normal limits; mild, easily identified but of limited severity; moderate, the change is prominent but with potential to increase.

Hz resides inside phagocytic cells

As an alternative approach to Hz quantification by a colorimetric assay, we further investigated its kinetics by flow cytometry. Hz detection was investigated in $CD11b^+$ phagocytic cells present in whole blood and single cell suspensions of liver, spleen, and bone marrow. As mentioned in the previous chapter, CD11b is expressed in monocytes, mature macrophages, neutrophils, and NK cells. In all infected mice Hz accumulation could be detected irrespective of the strain used and is shown in Figure 25 (PbNK65) and Figure 26 (PcAS). Uninfected mice were negative for depolarizing cells. Overall, in both infection models, high numbers of Hz-containing phagocytic cells could be detected (7 days after the end of CQ treatment for PbNK65 model and 20 days post-infection for PcAS model), when single-cell suspensions were investigated just immediately after parasite clearance. In whole-blood, Hz-containing cells were below background levels after the first time point, which is consistent with the clearance kinetics of pigmented cells from peripheral blood reported by White *et al*[328]. Interestingly, in PbNK65-infected mice, pigmented cells were again observable 280 days after parasite clearance. In livers and spleens of these mice a marked decrease in Hz-containing phagocytes occurred after the first time point. However, levels of Hz-containing phagocytes remained stable over the remaining time points investigated (medians of 18.9 and 18.2% for liver and spleen, respectively). In the bone marrow, Hz-containing phagocytes were low overall, and remained at median levels of 2%.

In PcAS-infected mice, only two time points were investigated, but a larger number of mice were included per group. Levels of Hz-containing phagocytes from liver and spleen 20 days post-infection were quiet variable (with medians of 26.2 and 13.5, respectively). This was probably a reflection of individual mouse parasitaemia (ie higher parasitaemia leading to increased Hz accumulation) as this ranged between 20.3%-43.2%. However, when Hz-containing phagocytes were investigated 140 days post-infection, inter-individual levels were identical. Contrary to what was seen in the PbNK65 model, where levels of Hz-containing phagocytes were stable with time, levels of Hz-containing phagocytes in PcAS-infected mice tended to decrease in the liver and increase in the spleen (19% and 21.8%, respectively).

Although the latest time point investigated was 280 days after parasite clearance (for mice infected with PbNK65), the findings presented suggest that Hz may persist for even longer periods of time. Considering that the mean lifespan of C57BL/6 mice is

approximately 850 days[332] this represents a substantial amount of time during which Hz may contribute to the modulation of the immune system.

Results in this chapter suggest that, rather than being eliminated from the host, Hz is redistributed in host organs. Initially, Hz deposition in organs occurred in the form of small-sized extracellular particles. Later, Hz tended to accumulate in larger-sized intracellular particles. Accumulation of Hz occurred mainly in the liver at earlier time points but seemed to shift to the hematopoietic organs (spleen and bone marrow) at later time points.

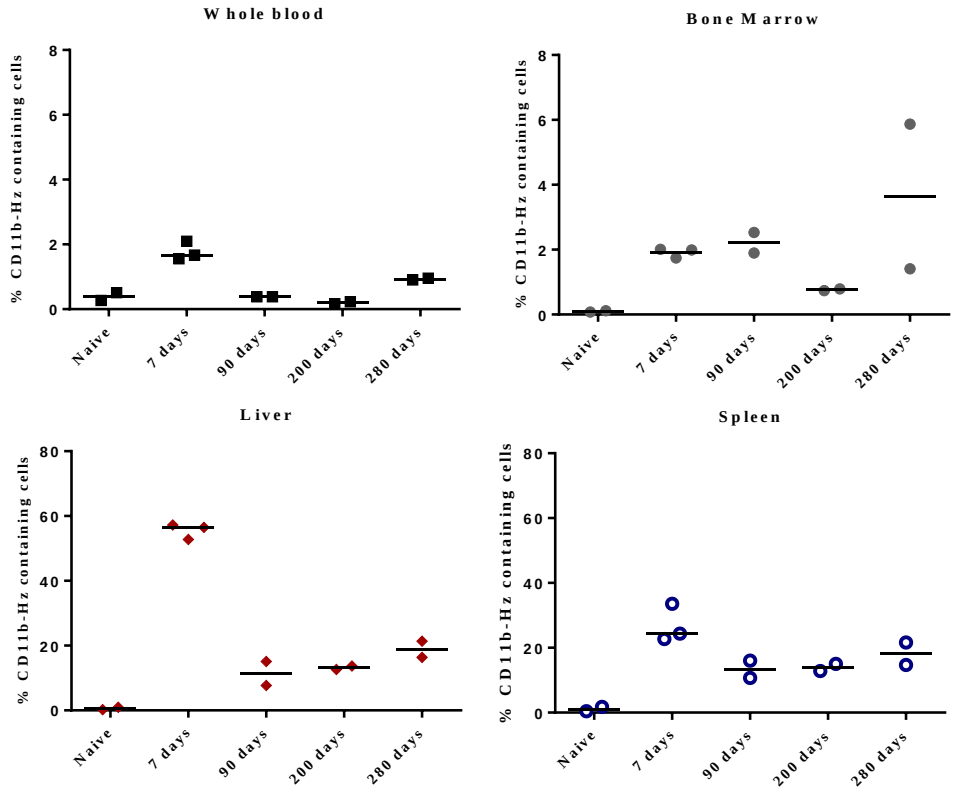

Figure 25. Detection of Hz by flow-cytometry in the cells of PbNK65-infected mice. Hz was detected in phagocytic cells obtained from *P. berghei* NK65-infected mice, post-parasite clearance, at different times, based on SSC-2. Hz could be detected in $CD11b^+$ phagocytic cells in all infected mice, whilst uninfected mice were negative for depolarizing cells. High numbers of Hz-containing phagocytic cells could be detected at the first time point (7 days after the end of CQ treatment) in livers and spleens with median levels of 56.5% and 24.4%, respectively. However, there was a marked decrease at later time points which seemed to stabilize between 90, and 196 days after CQ treatment finished. In bone marrow, the frequency of Hz-containing phagocytes was low overall (remaining at median levels of 2%)., levels of Hz-containing phagocytes in blood decreased to levels considered to be negative, with the exception of the last time point, where Hz-containing phagocytes were again detected.

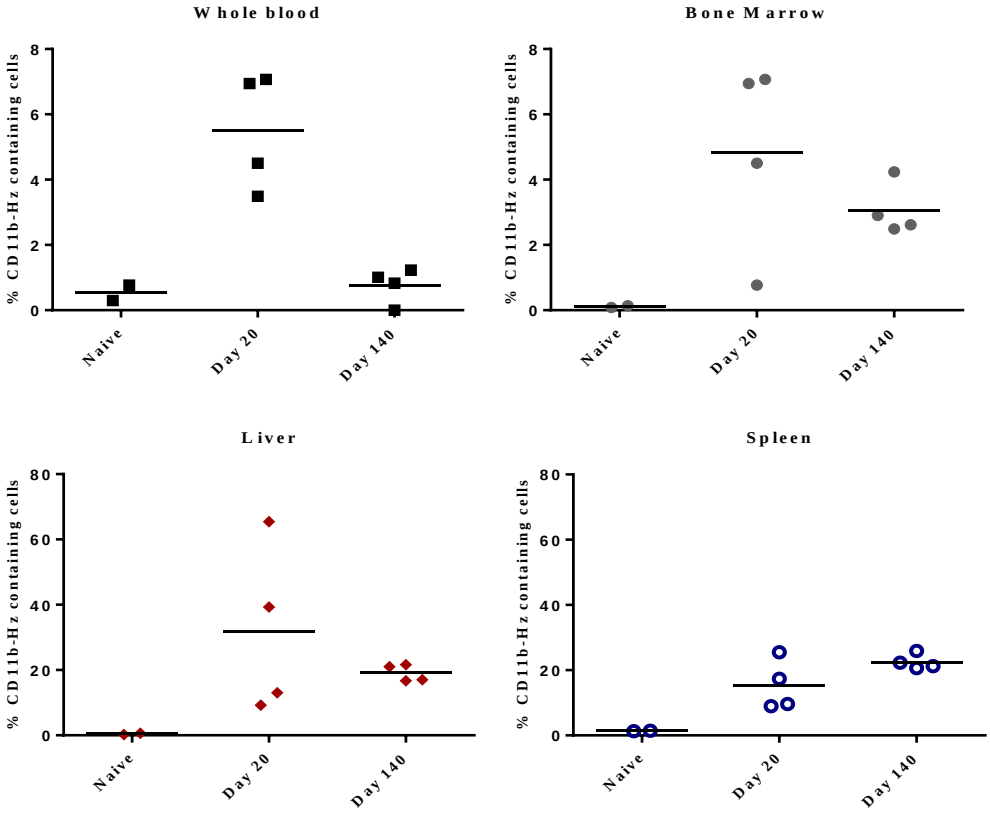

Figure 26. Detection of Hz by flow cytometry in the cells of PcAS-infected mice. Hz was detected in phagocytic cells obtained from PcAS-infected mice, at 20 and 140 days post-infection, based on SSC-2. As for the PbNK65 model, presence of Hz was investigated in $CD11b^+$ phagocytic cells of whole-blood and single cell suspensions of liver, spleen, and bone marrow. Hz was detected in phagocytic cells of all infected mice whilst uninfected mice had no detectable depolarizing cells. At the first time point median levels of Hz-containing phagocytic cells in livers and spleens were 26.2 and 13.5%, respectively. At the second time point measured, the median level of Hz-containing phagocytes decreased in the liver (19%) but increased in the spleen (21.8%). Hz-containing phagocytes in bone marrow were low overall (3%) and blood levels decreased over time to background levels.

Concluding Remarks

Evidence for Hz accumulation in host tissues following malaria was previously demonstrated. However, further investigation about what eventually happens to Hz inside those tissues was lacking. Therefore, the aim of this chapter was to investigate the kinetics of Hz inside tissue organs using two models of murine malaria. Following malaria parasite clearance Hz deposition was investigated in liver, spleen and bone marrow. At all the time points investigated Hz could be detected in the aforementioned organs. Overall, histological observations suggest that initial Hz deposition in organs was in the form of small-sized extracellular particles. At later time points, Hz tended to accumulate in the form of larger-sized intracellular particles. This seemed to be accompanied by a shift in distribution from the liver to the hematopoietic organs (spleen and bone marrow). It was also observed that in the spleen Hz deposition seemed to occur preferentially in the red pulp.

Single-cell suspensions of the organs were also analysed by flow-cytometry to investigate Hz deposition inside phagocytic cells. In whole blood, Hz was only detected in the earliest time point following parasite clearance. However, for the other tissues investigated Hz could be detected in all time points investigated. Hz deposition was overall low in the bone marrow and was more pronounced in liver and spleen. While in PbNK65 levels of Hz seemed quite stable in liver and spleen at the later time points evaluated, in PcAS the levels of Hz tended to decrease over time in liver and increase in the spleen.

Materials and Methods

Mice and Parasites

C57BL/6 mice (7 weeks old) were purchased from Charles River (Spain). Infected red blood cells (iRBC) from *P. berghei* NK65 (PbNK65) and *P. chabaudi* AS (PcAS) for infections were obtained from donor mice previously infected from frozen vials for each of the strains. Blood was collected by cardiac puncture and the parasitaemia was determined by counting the number of iRBC per 2000 RBC on Giemsa-stained blood smears.

Mice infection

C57BL/6 mice were infected IP with 1×10^6 PbNK65- or PcAS-iRBC. The PbNK65 infection was allowed to progress for 14 days during which mice reached high parasitaemias (ranging from 9–49%, average of 26%). Then, starting at day 14 after infection, mice were treated daily for 8 days with 100 µl IP injections of 7 mg/ml Chloroquine (CQ). Mice infected with PcAS reached peak parasitaemias by day 8 post-infection (ranging from 20-43%, mean of 30%) and cleared the infection by day 20 post-infection. Absence of parasites in circulating peripheral blood was confirmed on Giemsa stained blood smears at the end treatment/clearance period. Then, at the indicated time points mice were sacrificed with CO_2 narcosis and whole-blood and selected organs (liver, spleen, and bone marrow) were extracted and aliquoted for subsequent Hz determinations.

Quantification of Hz in murine tissues

A portion of liver, spleen, or bone marrow were mashed and resuspended in 1x PBS. After filtering through a 40 µm cell strainer, lysis buffer (50 mM tris-HCL in 1% Triton® X-100) was added to this extract. After lysis, 2 µl were used to measure protein content by the Bradford method following the manufacturer's instructions (Bio-Rad); 50 µl were converted to heme by dissolution in 2 mM NaOH and used to determine the amount of Hz, using the QuantiChrom assay kit as described previously.

Histopathology

Harvested organs (liver, spleen and bone marrow) were fixed in 4% vol/vol PFA and embedded in paraffin. Serial sections (3 µm) were stained with hematoxylin and eosin (H&E) and analyzed in a Leica DM2500 microscope, coupled with a Leica MC170 HD microscope camera. Tissue sections were examined by a pathologist blinded to experimental groups.

Hz analysis by flow cytometry

Liver portions were treated with DNase and then mashed through a 100 µm cell strainer. The resulting cell suspension was diluted in RPMI medium with 2% fetal calf serum to a final volume of 30 ml, washed and the pellet put on a 35% Percoll gradient (in RPMI). The obtained cells were washed again and then labeled for analysis. The spleen was mashed through a 100 µm cell strainer and resuspended in PBS. The bone

marrow was flushed from a femur bone into PBS using an insulin hypodermic needle and resuspended several times with the help of the needle to generate a single cell suspension. Whole blood was obtained by cardiac puncture in the presence of heparin, and washed with PBS. Whole blood and single cell suspensions from liver, spleen, and bone marrow were incubated with Fc-block and labelled with anti-CD11b (FITC) antibody. Erythrocytes were then lysed with 125 µl of BD FACS lysing solution (BD Biosciences) prior to analysis. The cells were washed again and resuspended in Facs buffer before flow cytometry analysis.

Discussion

The hemozoin accumulation in liver and spleen in a model of murine malaria was previously investigated by Levesque *et al*[329]. This study measured hemozoin concentration over a period of 9 months using a fluoromeric method, which was previously established by Sullivan *et al*[333]. Findings by Levesque propose that over time hemozoin concentration in the liver seemed to decrease, while it increased in the spleen, which suggested that overall hemozoin concentration in the murine host remained unchanged. In humans, evidence for hemozoin accumulation in host organs exists from autopsies of individuals that died of malaria since a time before the malaria parasite was discovered, as already mentioned (reviewed in[222]). Further evidence is provided by studies showing that hemozoin accumulates preferentially in brain, liver, spleen and lungs (reviewed in[334]). However, information on hemozoin dynamics following malaria clearance is limited. First, in many African countries autopsies are not routinely performed, either because of lack of certified personnel but mainly because of cultural reasons, especially in children[335]. Second, autopsies made to individuals dying of malaria would not be useful, since it would be impossible to distinguish hemozoin deposition from recent malaria episodes (including the one leading to death), from older malaria infections. The most useful information would possibly be obtained from autopsies of individuals dying from malaria un-related causes but with a recorded history of malaria. These individuals might either be immigrants of malaria endemic areas that moved to malaria free regions, those living in malaria regions that have meanwhile become malaria free or cases of imported malaria where individuals survived infection. It is very likely that autopsies of individuals with these characteristics have been performed. However, the importance of such findings are probably disregarded by the pathologist performing the autopsy, and in developed

countries it might even be the case that the “black pigment deposits” might not be recognized for what they are.

Therefore, although evidence suggests that hemozoin may concentrate in tissue organs for very long periods of time after the last malaria episode, not much is really known as to what really happens to hemozoin over time in humans. We set out to further the knowledge on hemozoin dynamics in two models of murine malaria, *P. berghei NK65* (PbNK65) and *P. chabaudi* AS (PcAS). As mentioned, the choice of strain was based on the high amount of hemozoin produced by PbNK65 and due to the similarities of a PcAS infection to *P. falciparum*. Also, as infection by PcAS is self resolving and the peak parasitaemia occurs around day 8 post infection, it is likely that the amount of hemozoin produced during infection is lower than during an infection with PbNK65. The first approach was to investigate hemozoin accumulation using a similar method than Levesque *et al*. Both are based on harvesting organs of *Plasmodium* infected mice, and determining hemozoin concentration in those organs at several time points, following infection clearance. We determined hemozoin concentration in liver, spleen and bone marrow using a colorimetric method (QuantiChrom Heme Assay kit).

Overall our results correlate to those obtained by Levesque, in which hemozoin was detected in all organs investigated, up to 9 months after infection clearance. However, in our study hemozoin concentration either remained fairly stable throughout the time points analysed, or tended to increase in the case of the liver for both infection models. These differences might be explained by individual mice developing different parasitaemias, which may contribute to variable levels of hemozoin deposition. Moreover, in our study C57BL/6 mice were used, while Levesque used ICR mice, where different parasite loads or different hemozoin dynamics may occur. The limitation of this study was that in only provided information as to the overall content of hemozoin, without giving any information as to the localization of hemozoin within organs and to its dynamics over time.

Thus, we also investigated hemozoin distribution in histological sections of liver, spleen and bone marrow. Observation of histological preparations of the aforementioned organs, suggested that hemozoin distribution following malaria clearance was initially sparse and that over time, hemozoin accumulated in larger sized

intracellular (Kupffer cells) aggregates. Hemozoin also seemed to have an early preferential accumulation in the liver that tended to shift to the spleen. This suggests that hemozoin deposition in the organs is not static, which can have several implications. Hemozoin accumulation inside Kupffer cells and the increase in size of aggregates suggests that hemozoin is likely re-ingested several times, as macrophages reach the end of their life time. Re-ingestion of hemozoin by several generations of phagocytes is likely to change the biomolecules attached to hemozoin, which may contribute to the production of different biological effects, caused by hemozoin[288]. Finally, Hz-ladden macrophages might participate in the response to other infections in the organs in which they reside, and contribute to an impaired/dysregulated immune response.

Flow cytometry might also be a useful method for the quantification of hemozoin inside several organs. Our results suggested that shortly after malaria clearance while parasites are no longer seen in circulation (not shown), hemozoin is still detected inside phagocytes in circulating blood. This is consistent with evidence showing that following malaria clearance, Hz-containing leukocytes persist for median times of 72 and 216 hours (up to 9 days) in granulocytes and monocytes, respectively[328]. At later time points this was no longer observed with one exception (last time point in the PbNK65 model). The appearance of Hz-containing phagocytes in the last time point probably consists of recent immigrants from the bone marrow. Hemozoin was detected in the bone marrow of both models studied throughout all the time points analysed. This is in line with findings by Casals-Pascual *et al*, in which post-mortem analysis of bone marrow of children dying of malaria, were found to contain Hz-containing myeloid cells, with associated abnormal erythropoiesis[336].

Considering that the average life span of a mouse is around 850 days[332], it is impressive that hemozoin could still be detected in mouse organs 280 and 140 days, following parasite clearance for PbNK65 and PcAS, respectively. This represents approximately a quarter of the life span of a mouse. Assuming that the same happens in humans and considering that in malaria endemic regions, such as sub-Saharan Africa, the same individual is likely to get infected several times throughout life[189], then it is likely that the amount of hemozoin accumulated in organs is enormous. If intracellular hemozoin in these organs consistently contributes to impairment of functions of these cells, then affected individuals will potentially have a proportion of immune cells that respond to other pathogens at suboptimal levels.

CHAPTER IV

In vivo Malaria and Tuberculosis co-infection in a murine model.

Introduction

The next question we wanted to address regarded the interplay between malaria and tuberculosis *in vivo*. Our *in vitro* data suggested that Hz ingestion by phagocytic cells leads to their functional impairment and thus may have contributed to the increased mycobacterial burden observed. Therefore, we wanted to investigate whether Hz deposition inside phagocytic cells during an infection by the malaria parasite could aggravate a subsequent tuberculosis infection *in vivo*. We first assessed the outcome of tuberculosis co-infection during acute malaria. Then we investigated tuberculosis disease during chronic malaria, to compare how the tuberculosis disease will progress when malaria parasites were no longer detected in circulation. We hypothesized that this would be a good model to test how the long term deposition of Hz in host organs would affect the ability of the host to control tuberculosis infection.

The murine model chosen was the *P. chabaudi* AS (PcAS) strain for the malaria infection and the *M. bovis* BCG (BCG) strain for the tuberculosis infection. Our choice was based on the fact that PcAS infection in mice resembles the human infection with *P. falciparum*. As mentioned in the previous chapter, this includes preferential infection of normocytes, adherence to uninfected RBC and sequestration to endothelial cells, so that mature forms are almost never seen in peripheral blood circulation[330]. The choice of BCG and the use of intraperitoneal route of infection were due to the fact that this model of infection more closely resembles the course of infection in humans. Although it might not be a good model to investigate pulmonary tuberculosis, it is a well established model for the study of cellular immunity and granuloma formation[337]. Following infection, mycobacteria are disseminated mainly to the liver and spleen and granulomas are usually visible two weeks post-infection. Eventually, replication of mycobacteria is controlled by the adaptive immune response, a process normally occurring three weeks post-infection. However, viable bacilli continue to persist at low numbers in infected organs[337]. Thus, using the model of BCG infection/intraperitoneal

route allows for the investigation of both active tuberculosis as well as latent tuberculosis infection.

1. Tuberculosis co-infection during acute malaria.

Results

M. bovis co-infection in malaria infected mice leads to decreased survival.

C57BL/6 mice were first infected with PcAS, and four days later, with BCG. Single-infections with PcAS and BCG were used as controls. Co-infected mice exhibited reduced survival compared to the single-infected control mice. Figure 27 shows the Kaplan Meier survival of mice from 4 independent experiments. Out of a total of 19 mice per group, 7 (37%) died in the co-infected group between days 6-7 post-BCG infection. Co-infected mice still alive at day 7, were extremely sick and thus we decided to terminate the experiment at this time. All mice in control groups survived.

Clinically relevant manifestations of PcAS single-infected mice were characteristic of malaria disease such as ruffled fur, moderate weight loss and lethargy. However, these symptoms were aggravated in the co-infected group, where all mice developed progressive cachexia, until death or sacrifice. BCG single-infected mice did not show any clinical manifestations of disease. Figure 28 shows the degree of weight change in infected mice (three independent experiments); PcAS single-infected animals featured moderate weight loss, whereas in co-infected animals, weight loss was more severe. The clinical manifestations, summarized in Table 3 established a clinical scale of disease severity. Using this scale we set the humane endpoint at stage IV, which usually occurred between days 6-7 post BCG infection (10 to 11 days post PcAS infection).

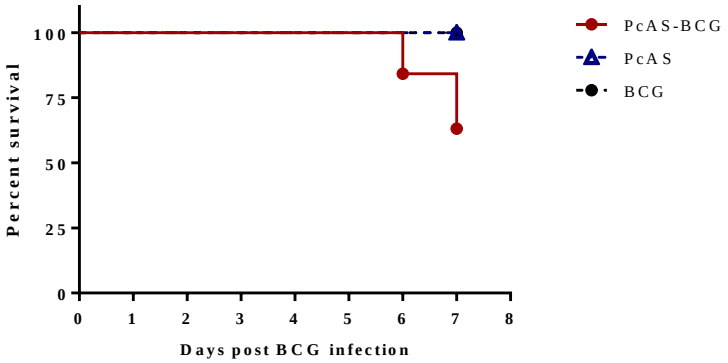

Figure 27. Co-infection with BCG decreases survival of PcAS infected mice. C57BL/6 mice were infected with PcAS and after 4 days co-infected with BCG. Mice single-infected with PcAS or BCG were included as controls. The survival of mice from 4 independent experiments is shown. All mice in the single-infected groups survived, featuring either mild symptoms (PCAS) or no signs of disease (BCG). In the co-infected group 7 out of 19 mice died (37%), with surviving mice exhibiting severe signs of disease.

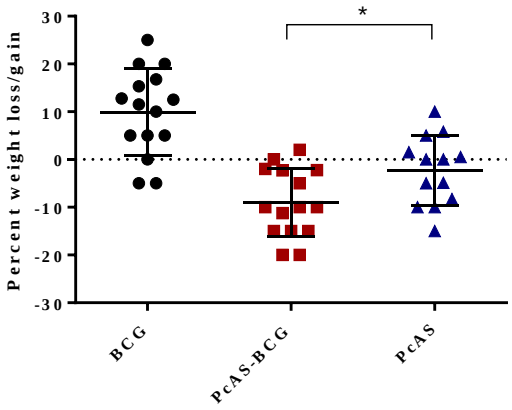

Figure 28. Co-infected mice had more pronounced weight loss than PcAS mice. Weight change of infected animals was monitored from the time they were infected with PcAS. The percentage of weight change of the mice by the end of the experiment, in the different groups, is shown. Results are from 3 independent experiments. Mild weight loss was observable in the PcAS single-infected group whereas in the co-infected group weight loss was more severe. Contrastingly, BCG single-infected mice actually gained weight.

Clinical Manifestations
I. no signs II. ruffled fur and/or abnormal posture and/or minor weight loss (<15%) III. lethargy, mild hypothermia and/or moderate weight loss (≥ 20%) IV.* reduced response to stimulation, severe hypothermia (shivers) and/or respiratory distress/hyperventilation V. prostration and/or severe weight loss (>25%) VI. Death
*The humane endpoint was defined as mice reaching stage 4

Table 3. Clinical scale of disease severity. The table describes symptoms developed during the course of infection in co-infected and PcAS single-infected mice. The more prominent manifestations of disease were weight loss, hypothermia and reduced response to stimulation, that ultimately resulted in death. The more severe manifestations (stages IV-VI) were only observed in co-infected mice, whereas PcAS single-infected mice did not progress beyond stage III. BCG single-infected mice showed none of the clinical manifestations described above. Table was adapted from Cunnington *et al*[338].

Malaria parasitaemia and mycobacterial burden was not exacerbated in co-infected animals.

To determine if the decreased survival of co-infected animals was due to an exacerbation of the malaria disease or from increased tuberculosis disease, we investigated parasitaemia levels and mycobacterial burden. Parasitaemia levels, determined by counting parasitized RBC in peripheral blood smears, were similar in co-infected and PcAS single-infected animals, as show in Figure 29. Both co-infected and PcAS single-infected mice reached peak parasitaemia at day 7 post-PcAS infection (average levels for one representative experiment were 30 and 25%, respectively).

The mycobacterial load was first determined by luminescence. The BCG strain we used expresses the full luciferase operon which renders the mycobacteria auto-luminescent. This allowed us to investigate the total mycobacterial burden of infected mice at the beginning of infection, as well as at the end of the experiment. As illustrated in Figure 30, the mycobacterial burden 7 days post BCG infection was similar between co-infected and BCG single-infected mice. Interestingly, at day 3 post BCG infection, co-infected mice appeared to have a lower infection level than the BCG single-infected mice. We next quantified colony forming units (CFUs) in livers and spleens of infected mice. Mice were sacrificed at day seven post-BCG infection, or earlier (day 6) if they had already reached stage IV of the clinical scale. Dilutions of homogenized organs were plated on 7H11 agar and CFUs counted 3 weeks later. As shown in Figure 31,

higher mycobacterial counts could be found in the spleens of infected mice than in the livers. However, no differences were found in mycobacterial counts of livers and spleens between co-infected and BCG single-infected mice.

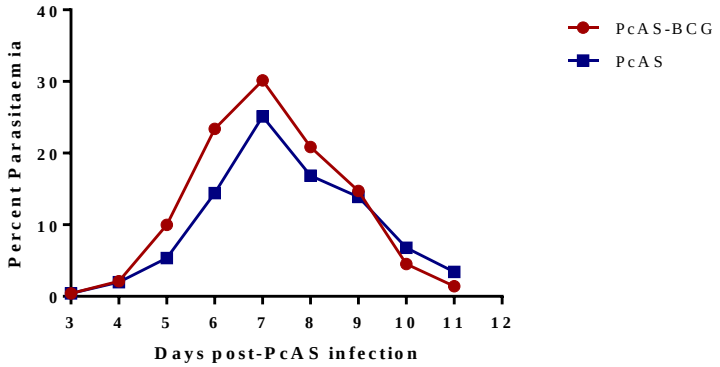

Figure 29. Parasitaemia levels of co-infected and PcAS single-infected mice. Parasitaemia was monitored starting three days post-PcAS infection. Blood was collected daily and the percentage of infected RBC determined in Giemsa stained blood smears. Both co-infected and PcAS single-infected mice reached peak parasitaemia at 7 days post-infection, with an average parasitaemia of 30 and 25%, respectively. The result of a single representative experiment is shown.

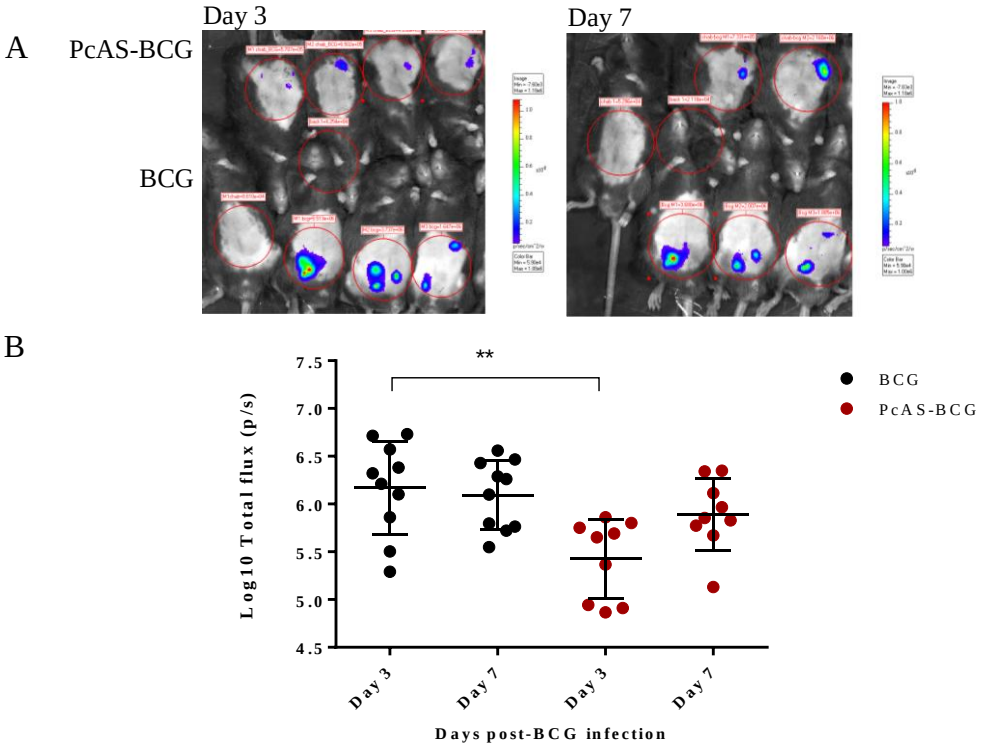

Figure 30. Mycobacterial burden of co-infected and BCG single-infected mice. Mycobacterial burden following BCG infection was determined at 3 and 7 days post infection. A – The upper panel is an example of acquired images using the IVIS® Imaging system. Variations in colour represent the relative levels of bioluminescence ranging from low (blue), to medium (green) and high (yellow/red). B – The graph represents the $\log_{10}$ of the quantified luminescence (photons/sec) as measured using the region of interest tool (ROI) in the Living Image software program, after background normalization. At day 7 post-infection no differences could be found between the co-infected and BCG single-infected group. However, at day 3 post-infection the mycobacterial load in the co-infected group was significantly lower than in the BCG single-infected group (p= 0.0025). The results for two independent experiments are shown.

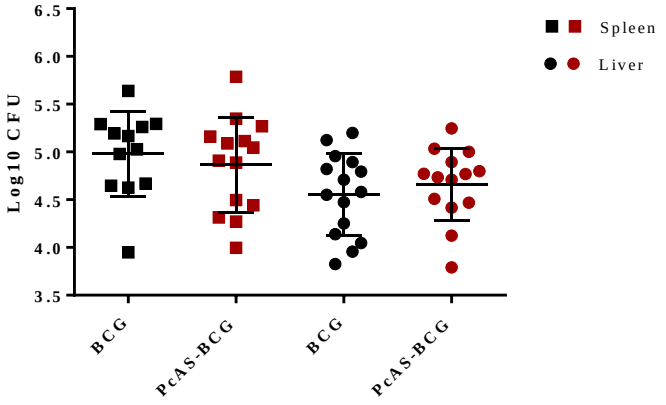

Figure 31. Mycobacterial burden in liver and spleens of co-infected and BCG single-infected mice. Infected mice were sacrificed at day seven post-BCG infection, or earlier (day 6) if they had already reached stage IV of the clinical scale of disease severity (Table 3). Liver and spleens were homogenized and dilutions plated on 7H11 agar. CFUs were counted 3 weeks later. The $\log_{10}$ of the CFUs count for mice from 3 independent experiments is shown. Whilst the spleen had higher bacterial loads than the liver, the mycobacterial load in co-infected mice as compared to BCG single-infected control mice was similar.

Malaria-induced anaemia is more severe in co-infected animals

Mice infected with PcAS develop anaemia due to destruction of infected erythrocytes (RBC) and removal of uninfected RBC, together with suppression of erythropoiesis and occurrence of dyserythropoiesis. Anaemia is negatively correlated with parasitaemia and normal levels are recovered after the peak of parasitaemia. We investigated the levels of anaemia in co-infected and single-infected mice using a hematology analyzer to determine the number of erythrocytes (RBC) and hemoglobin (HGB) levels. As shown in Figure 32, co-infected animals had significantly lower levels of RBC and HGB than single-infected animals, indicating an aggravated anaemia of PcAS-infected animals in the presence of BCG. Other parameters measured, such as hematocrit (HCT) were also lower in co-infected animals whilst mean corpuscular volume (MCV), mean corpuscular hemoglobin (MCH) and mean corpuscular hemoglobin concentration (MCHC) were not significantly different between the co-infected and PcAS single-infected groups, although they were consistent with anaemia (not shown).

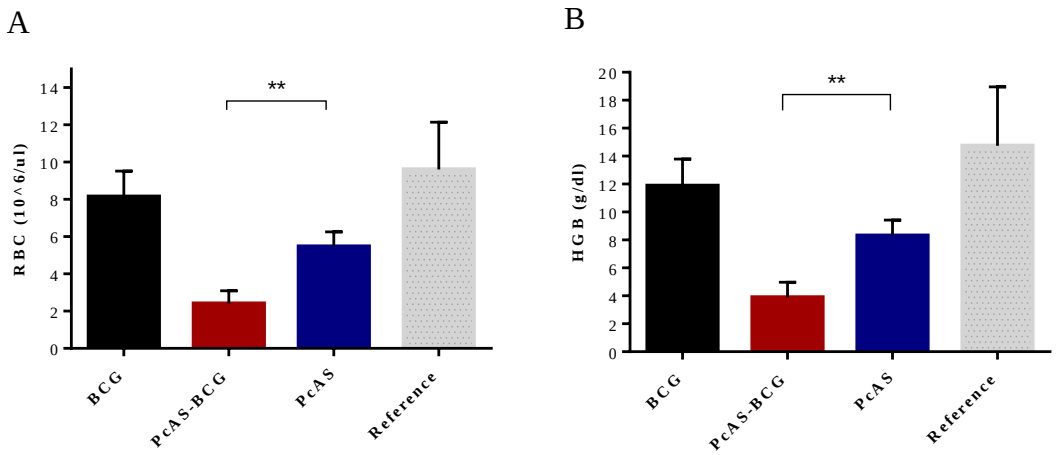

Figure 32. Hematology measurements of co-infected and single-infected mice. When mice were sacrificed (6-7 days after BCG infection) blood was collected from the orbital sinus and a full blood count was determined in a hematology analyzer. The erythrocyte count (RBC, A) and hemoglobin concentration (HGB, B) are shown. PcAS single-infected mice were anaemic, as indicated by the lower values of RBC and HGB. Co-infected mice had significantly lower levels of RBC (p=0.0014) and HGB (p=0.0017). BCG single-infected mice had normal levels of RBC and HGB when compared to reference values (reference values provided by Charles River for male C57BL/6 mice, 8-10 weeks of age).

Co-infection increased inflammatory tissue responses in liver

To further characterize pathology in infected animals, serial sections of liver, lung, spleen, bone marrow and kidney were stained with hematoxylin and eosin. The liver was the organ that displayed the most important pathological changes (Figure 33). Livers of co-infected mice showed features of both PcAS and BCG single-infections, with the presence of lymphocyte-rich inflammatory foci (seen in PcAS single-infection) interspersed with macrophage-rich foci (seen in BCG single-infection). Inflammatory-cell infiltration in co-infected mice was multifocal to diffuse, and of mild to moderate severity. In the single-infection controls these changes were mostly mild. Mild, multifocal hepatocellular necrosis was spatially associated with macrophage-rich foci and only present in co-infected mice and BCG single-infected mice. The severity of pathological findings are summarized in Figure 33B) and tended to be more severe in PcAS-BCG co-infected mice.

For the other organs, severe red pulp hyperplasia, characteristic of *Plasmodium* blood stage infection, was seen for co-infected and PcAS single-infected mice, while BCG single-infected mice showed no changes. The same was observed for bone marrow, with mild to moderate myeloid hyperplasia (not shown). No significant changes were seen in kidney and lung in any of the experimental groups.

A

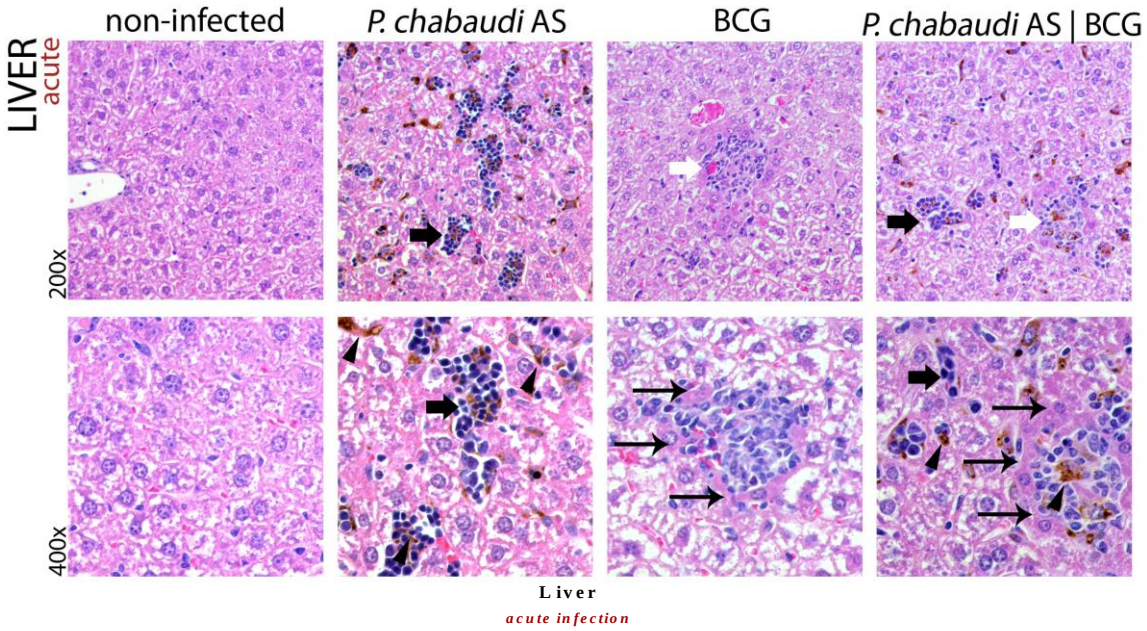

B

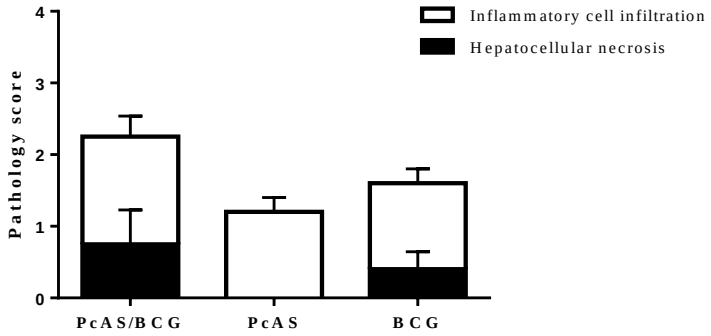

Figure 33. Liver lesions in co-infected mice during acute malaria. A – PcAS single-infected mice displayed inflammatory cell infiltration, mainly lymphocytic (black arrows), multifocal to diffuse and of mild to moderate severity; scattered hemozoin-laden Kupffer cells/macrophages were also seen. BCG single-infected mice also showed inflammatory cell infiltration, multifocal to diffuse, of mild to moderate severity, but inflammatory cells were mainly myeloid (macrophages, white arrows). The liver of co-infected mice showed both myeloid cell-rich and lymphocyte-rich inflammatory foci, multifocal to diffuse in distribution and of mild to moderate severity. Hepatocellular necrosis (black thin arrows) was only seen in BCG single-infected and co-infected mice, being associated with inflammatory foci and of mild severity. B – Severity in the form of inflammatory cell infiltration and/or necrosis is represented for the different experimental groups to summarize pathological findings in the liver.
Hemozoin (black arrowheads); lymphocyte-rich inflammatory foci (black block arrows); myeloid cell-rich inflammatory foci (white block arrows); hepatocellular necrosis (black thin arrows).

2. Tuberculosis co-infection during chronic malaria.

Results

BCG co-infection during chronic malaria leads to mild decrease in survival.

To assess the long term effects of Hz deposition in host organs on subsequent control of tuberculosis disease, mice were infected with PcAS and the infection allowed to progress for 20 days, before BCG co-infection. PcAS is a self-limited infection and, as such, by day 20 post-infection, no parasites could be detected in peripheral blood smears. However, mice remain chronically infected, as parasites can persist at subpatent levels, with occasional detectable recrudescence for up to 2-3 months[330,339].

Figure 34 shows the survival of mice in 2 independent experiments. Of a total of 10 mice, 3 (30%) died in the chronic PcAS-BCG infected group. All mice in the control groups survived (n=9 for BCG single-infected group, and n=4 for PcAS single-infected group). Clinically relevant manifestations, as described in Table 3, were only observed during PcAS-infection, and corresponded to moderate manifestations of weight loss, ruffled fur and lethargy. None of the mice in the two experiments reached stage IV of the clinical scale of disease severity. By the time malaria parasites were cleared from circulation, mice had recovered their initial weight. Following BCG infection, mice weights across all groups either remained unchanged or tended to increase (Figure 35).

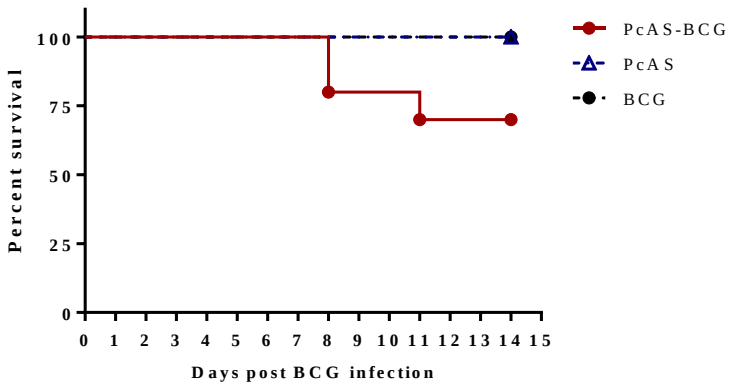

Figure 34. BCG co-infection in chronic PcAS-infected mice leads to moderate survival impairment. C57BL/6 mice were infected with PcAS for 20 days until parasite clearance and establishment of chronic infection. Mice were then co-infected with BCG. Control groups included BCG single-infected mice and PcAS chronic mice. The survival of mice in 2 independent experiments is shown. All mice in the single-infected groups survived, whilst in the co-infected group 3 out of 10 mice died (30%).

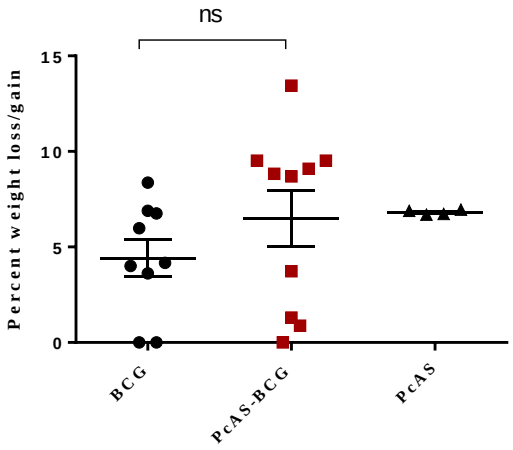

Figure 35. BCG co-infection in chronic PcAS-infected mice does not lead to weight loss. Weight change of infected animals was monitored from the time mice were infected with PcAS. The percentage of weight change of mice at the end of the experiment, relative to their weight at the time of BCG infection is shown. Results are shown for 2 independent experiments. Whilst mice infected with PcAS lost weight during malaria infection (not shown), from the time chronic infection was established mice in the different groups either maintained or increased their weight.

Mycobacterial burden is similar in chronic PcAS-BCG and BCG single-infected animals.

Next, the mycobacterial burdens in chronic PcAS-BCG and BCG single-infected mice were investigated. Compared to mice in the acute co-infection, survival of chronic PcAS-BCG infected mice seemed to be increased since they survived longer, while only displaying moderate manifestations of disease and without reaching stage IV of the clinical scale of disease severity. Thus, CFUs levels were determined later (14 days post-BCG infection) than during acute co-infection. This allowed us to investigate mycobacterial burdens at a later time, which could help determine whether there are any differences in the ability of mice to control BCG growth, and to investigate granuloma formation. In the first experiment, mycobacterial load was also determined by luminescence. As shown in Figure 36, the mycobacterial burden in both groups appeared to decrease from day 3 to day 14 post-BCG infection. Although not significant, the decrease in mycobacterial load seemed faster in the BCG single-infected group than in the PcAS-BCG group.

Determination of CFUs levels revealed that mycobacterial burden in spleens and livers of chronic PcAS-BCG as compared to BCG single-infected mice was not significantly different. However, there were less BCG single-infected mice with detectable CFUs in the spleen than chronic PcAS-BCG infected mice (Figure 37).

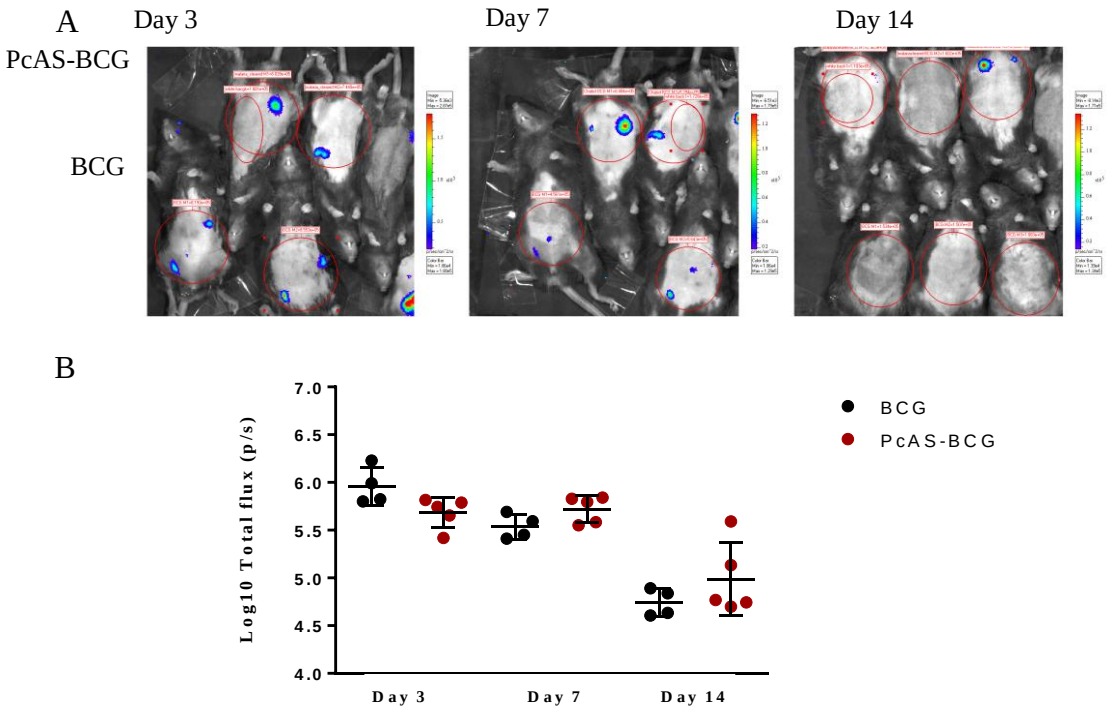

Figure 36. Mycobacterial burden of chronic PcAS-BCG and BCG single-infected mice. Mycobacterial burden following BCG infection was determined at 3, 7 and 14 days post-infection. A - The upper panel is an example of acquired images using the IVIS® Imaging system. B – The graph depicts the $\log_{10}$ quantified luminescence (photons/sec) as measured using the region of interest tool (ROI) in the Living Image software program, after background normalization. No differences could be found between the chronic PcAS-BCG and BCG single-infected groups at any time-point. However, mycobacterial levels decreased from day 7 to day 14 post-BCG infection. The result for a single experiment is shown.

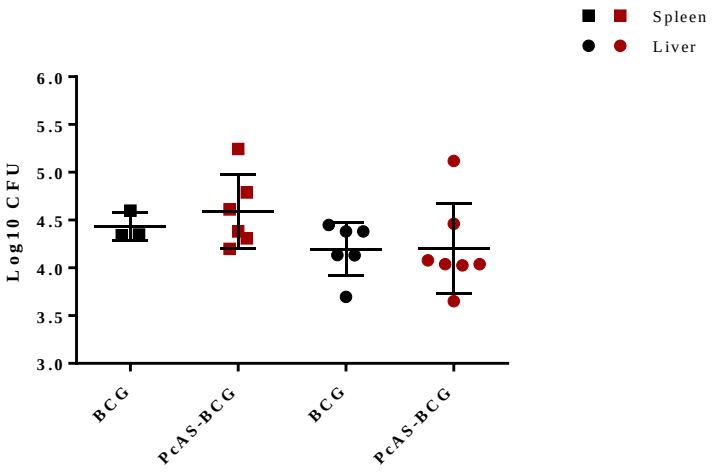

Figure 37. Mycobacterial burden in liver and spleens of chronic PcAS-BCG and BCG single-infected mice. Infected mice were sacrificed at day 14 post-BCG infection. CFUs were also performed for mice that died at day 11, but not at day 8, post-BCG infection. Liver and spleens were homogenized and dilutions plated on 7H11 agar. CFUs were counted 3 weeks later. The $\log_{10}$ of the CFUs count for mice from 2 independent experiments is shown. Whilst the mycobacterial load was similar in chronic PcAS-BCG and BCG single-infected controls, fewer BCG single-infected mice had detectable CFUs in the spleen than chronic PcAS-BCG infected mice (3/9 mice vs. 6/10 mice, respectively).

Malaria-induced anaemia is still present in chronic PcAS-BCG infected mice

Hematological analysis was performed at the time of sacrifice in chronic PcAS-BCG and single-infected controls. As shown in Figure 38, chronic PcAS single-infected mice had levels of RBC and HGB identical to BCG single-infected mice, suggesting that these mice had recovered from anaemia. However, chronic PcAS-BCG infected mice still had significantly lower levels of RBC and HGB than single-infected animals, suggesting that BCG infection may impair the recovery of PcAS-infected mice from anaemia. Likewise, HCT was also lower in chronic PcAS-BCG infected animals whilst MCV, MCH and MCHC did not significantly differ from chronic PcAS single-infection (not shown).

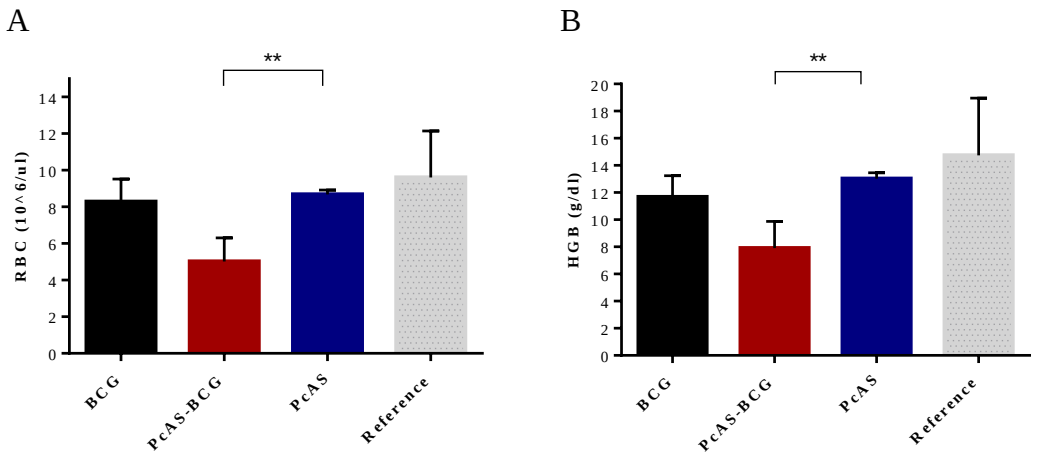

Figure 38. Hematology measurements of chronic PcAS-BCG and single-infected mice. Blood was collected from the orbital sinus, on the day mice were sacrificed and a full blood count was determined. The erythrocyte count (RBC, A) and the hemoglobin concentration (HGB, B) are shown. PcAS and BCG single-infected mice had RBC and HGB values similar to reference values. However, chronic PcAS-BCG infected mice still presented significantly lower values of RBC (p=0.0033) and HGB (p=0.005) than PcAS single-infected mice. Reference values as provided by Charles River for male C57BL/6 mice, 8-10 weeks of age.

Inflammatory tissue responses in chronic PcAS-BCG infection.

The inflammatory tissue response in chronic PcAS-BCG co-infection was also investigated in serial sections of liver, lung, spleen, bone marrow and kidney, stained with hematoxylin and eosin. As already seen for co-infection during acute malaria the liver was the organ that displayed the most important pathological changes (Figure 39). Significant hepatic lesions were only observed in BCG single-infected and in chronic PcAS-BCG co-infected mice, corresponding to inflammatory cells, mainly

macrophages and neutrophils, multifocal and of moderate severity, which were similar in both groups. However, the livers of PcAS single-infected mice revealed the presence of Hz-laden Kupffer cells, diffuse and of mild severity, with minimal inflammatory cell infiltration; whilst in PcAS-BCG co-infected mice, Hz was mainly found inside macrophages, associated with granulomas, with multifocal distribution (Figure 39C). Findings for the other organs were similar to the ones already described during acute malaria infection.

Overall these results show that malaria-tuberculosis co-infection results in severe disease. In the acute model, only 37% of mice died however, remaining co-infected animals developed progressive cachexia and had to be sacrificed. Although we did not observe increased parasitaemia nor increased bacterial loads in these mice, we did observe that malaria-induced anaemia was aggravated. Severe disease was not observed when mice were infected with tuberculosis during chronic malaria. However, at the end of the experiment co-infected mice still showed evidence of malaria-induced anaemia, whilst the PcAS-single infected mice had already recovered. Histological findings revealed that in the acute model, co-infected animals had increased inflammation and necrosis, which was no longer observed in co-infected animals in the chronic model. On the other hand, the chronic model revealed granuloma-like structures, which in the case of co-infected animals had an increased accumulation of Hz-containing Kupffer cells.

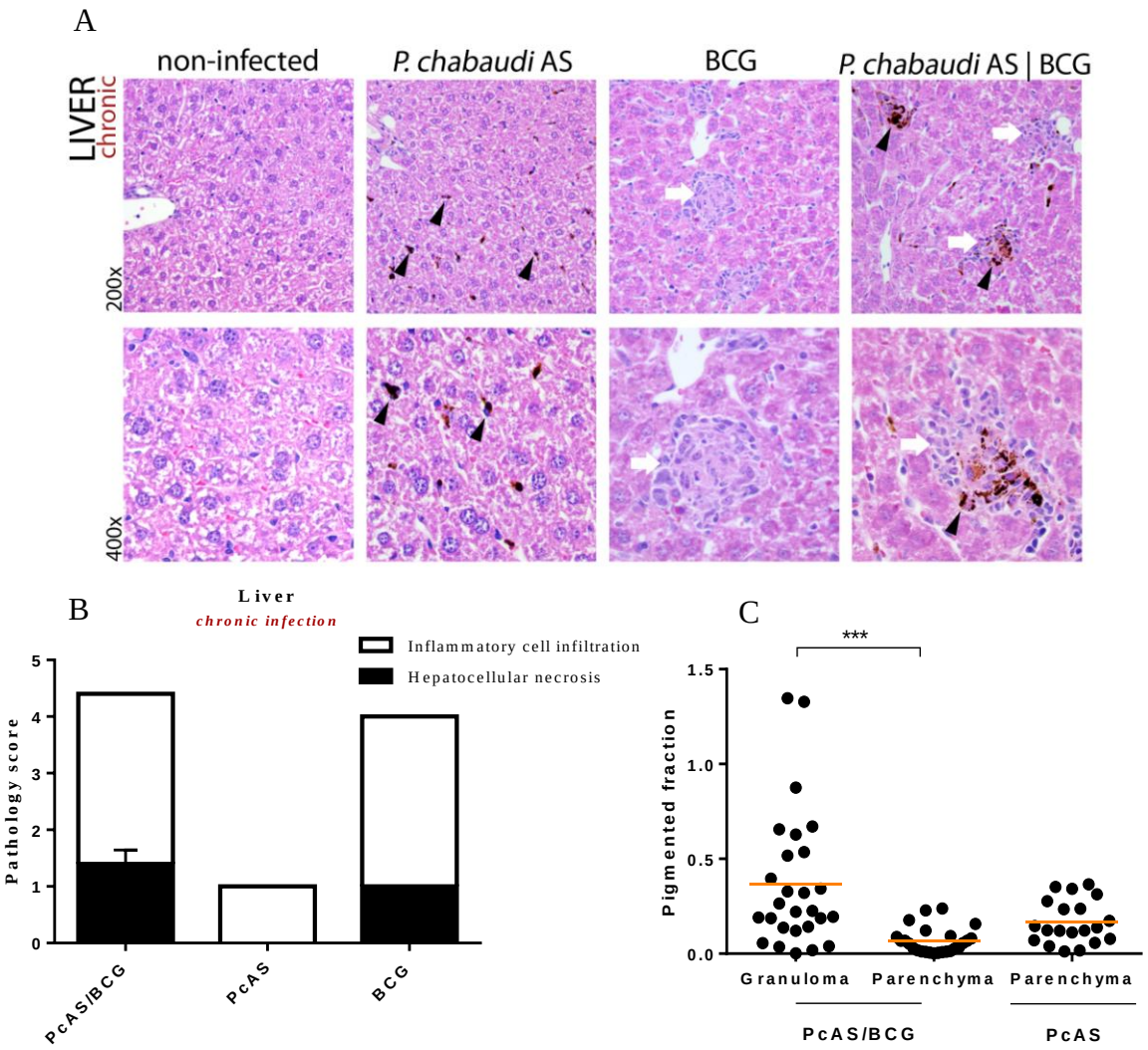

Figure 39. Liver lesions in co-infected mice during chronic malaria infection. A – Livers of PcAS single-infected mice displayed only minimal inflammatory cell infiltration and scattered hemozoin-laden Kupffer cells. BCG single-infected mice showed inflammatory cell infiltration, multifocal and of moderate severity, composed of foci (granulomas) of macrophages and neutrophils (white arrows), surrounding cell debris. The liver lesions of chronic PcAS-BCG infected mice were very similar to those seen for BCG single-infected mice (white block arrows), with further accumulation of hemozoin-laden phagocytic cells in the granulomas (arrowheads). B – Shown is the summary of the pathology severity (inflammatory cell infiltration and/or necrosis) found in the liver. C – Hz deposition in granulomas and surrounding parenchyma of co-infected animals was quantified and compared to Hz deposition in the parenchyma of PcAS single-infected animals. As shown, in co-infected animals Hz deposition occurs preferencially in granulomas. Quantification was performed using image analysis and expressed as the proportion of pixels occupied by Hz to the total pixel area.

Concluding Remarks

This chapter concerned the investigation of *in vivo* interactions of malaria-tuberculosis co-infection. PcAS infection resembles the human *P. falciparum* infection and was used to model acute malaria as wells as chronic infection. BCG infection was used to investigate the control of mycobacterial growth in the context of a malaria co-infection. The findings presented suggest that tuberculosis co-infection during acute malaria severely impairs the disease outcome of co-infected mice. Although parasitaemia and bacterial loads in C57BL/6 mice were not significantly different from those of control animals, 37% of co-infected animals died quickly after BCG co-infection, and all surviving mice showed signs of severe disease. The course of infection was characterized by increased weight loss and severe anaemia. Histological examination revealed increased leukocyte infiltration and necrosis in livers of co-infected animals.

Chronic malaria-infected animals had a mortality of 30%. However, they survived longer than acute malaria-infected animals and surviving animals only exhibited mild symptoms of disease. At the time mice were sacrificed, PcAS single-infected mice had recovered from anaemia, whilst PcAS-BCG co-infected mice still exhibited lower levels of RBC and HGB. Histology examination showed that liver lesions of chronic PcAS-BCG infected mice and BCG single-infected mice were very similar. However, in PcAS-BCG co-infected mice there was a preferential accumulation of Hz in association with granulomas when compared to PcAS single-infected mice, in which Hz accumulated in Kupffer cells and presented a scattered distribution throughout the parenchyma.

Materials and Methods

Mice infection

C57BL/6 mice (6 weeks from Charles River, Spain) were infected IP with 1×10^6 PcAS-iRBC. Then, for the acute infection mice were infected with 1×10^7 BCG CFUs (from frozen vials) by IP injection four days post-malaria infection. For the chronic malaria infection, mice were infected with 1×10^7 BCG CFUs 20 days post-malaria infection. Absence of parasites in circulating peripheral blood of mice 20 days post-infection was confirmed on Giemsa stained blood smears. At the indicated time points or when mice reached stage IV of the clinical scale of disease severity, mice were

sacrificed with CO_2 narcosis. When under anesthesia mice were sacrificed by cervical dislocation.

Assessment of mycobacterial load by bioluminescence

Assessment of bioluminescence was performed using a Xenogen IVIS® Lumina imaging system (PerkinElmer, Massachusetts, USA). At the indicated time points, mice were anesthetized IP with a mixture of ketamine (Imalgene 1000, 75 mg/Kg body weight; Merial, Duluth, GA, USA) and medetomidine (Domitor, 1 mg/Kg body weight; Pfizer, New York, NY, USA) in 1x PBS. Mice were contained in a large airtight box for safety reasons, and placed inside the imaging chamber of the IVIS® imaging system, with the stage heated to 37°C. Quantification of emitted photons was performed over 5 min using the Living Image software version 3.0. Bioluminescence within specific regions of individual mice was quantified using the ROI tool in the Living Image software program (given as photons/s).

Mycobacterial burden in murine organs

Mice were sacrificed by cervical dislocation, while still under anesthesia and liver and spleen harvested for CFUs determination. Harvested organs were weighted before removing a portion for histology analysis (see below). Organs were then placed in 1 ml 1x PBS and homogenized. Homogenized organs were serial diluted before plating on 7H11 agar plates. Plates were incubated at 37ºC, 5% CO_2 for 21 days before counting CFUs.

Histopathology

A portion of selected organs (liver, lung, spleen, bone marrow and kidney) was harvested, fixed in formalin and embedded in paraffin. Serial sections (3 μm) were stained with hematoxylin and eosin (H&E) and analyzed in a Leica DM2500 microscope, coupled with Leica MC170 HD microscope camera.

Analysis was performed by a pathologist blinded to experimental groups and the scoring system for liver lesions was as follows: for severity of hepatocellular damage or inflammatory cell infiltration the lesion was classified as absent (0), minimal (< 5%; 1), mild (5-25%; 2), moderate (25-50%; 3), severe (> 50%; 4). Additional modifiers, like the distribution (focal, multifocal, multifocal to diffuse, diffuse), the predominant

inflammatory cell type (neutrophils, macrophages and kupffer cells, lymphocytes) and the hemozoin distribution pattern were also assessed.

Hematological analysis

Blood was collected from the orbital sinus while animals were under anesthesia into micro collection tubes (containing 0.78 mg K2-EDTA; CAPIJECT®, Terumo; Somerset, NJ, USA). Blood was analyzed using an impedance hematology analyzer (PocH-100iV, Sysmex; Kobe, Japan).

Granuloma association with Hz

Images acquired for histopathology analysis were used to quantify Hz deposition in granulomas and surrounding parenchyma in liver sections. ImageJ software 1.47v was used to determine the proportion of pixels occupied by Hz in granulomas or in the parenchyma and expressed as the proportion occupied by Hz to the total pixel area measured.

Discussion

Malaria, especially in sub-Saharan Africa, is endemic with many other diseases and co-infections between different agents are likely to occur. Malaria co-infection with HIV[126] is well documented, as well as co-infections with helminths[129], and the common occurrence of malaria with bacteremia[106]. However, not much is known about malaria-tuberculosis co-infections and how the two diseases may interact, as well as the likely outcome of such co-infections. Reasons for this lack of knowledge might be because malaria is mainly a disease occurring in young children, whilst tuberculosis normally occurs in adults[296]. Another probable cause might be that while malaria and tuberculosis endemic regions overlap, spatial variations may occur as malaria is more frequent in rural areas, whilst tuberculosis is more frequent in overpopulated urban areas[159,160]. However, unplanned expansion of urban areas and rural practices in peri-urban regions may lead to increased malaria transmission[36], creating a setting which may also be prone for the transmission of tuberculosis. This may explain findings in ancient Lower Egypt, where evidence for malaria-tuberculosis co-infection was revealed by investigation of malaria and tuberculosis ancient DNA[158]. Modern studies are limited but suggest that malaria-tuberculosis co-infections might be overlooked[161,163] and probably promote more severe disease and mortality[164].

As our findings suggested that monocyte functions are impaired *in vitro*, and may promote increased mycobacterial burdens, as well as that hemozoin may persist in the host for a long time after malaria clearance, we wanted to investigate how malaria and tuberculosis may interact *in vivo*. Particularly, we were interested in investigating what would be the effect of hemozoin accumulation in tissue organs, on the susceptibility to tuberculosis infection. For this, the murine model was used, using two experimental approaches. The first model investigated acute infection, where mice were co-infected with BCG while malaria infection by PcAS was still ongoing. The second approach investigated BCG infection following clearance of PcAS infection (20 days post infection). In this model recrudescence might still occur for the following 10 days and at lower levels for up to 3 months[339]. This model of infection likely resembles individuals in malaria endemic countries, probably suffering from several malaria episodes until semi-immunity is developed. Such individuals may harbor asymptomatic parasitaemia (with low levels of circulating parasites), and likely have hemozoin accumulated in their organs.

Results from both studies suggested that tuberculosis infection following malaria decreased the survival of co-infected mice. This was more striking in the acute model of infection where co-infected mice developed progressive cachexia and died or became extremely sick. These findings are similar to a study by Leisewitz *et al* where malaria-tuberculosis co-infection also exhibited decreased survival, although in this study mice were infected first with tuberculosis and then with the malaria parasite[173]. Another study by Hawkes *et al*[174] used a similar model of infection to Leisewitz *et al*, and although co-infection increased mycobacterial loads in organs, no decrease in mice survival was reported. In fact, most if not all murine studies on malaria-tuberculosis co-infection are performed by first infecting mice with tuberculosis, and then with a malaria parasite strain. This follows the assumption that infection by a malaria parasite will disrupt latent tuberculosis infection, and promote active disease[171,174]. However, when an individual first comes in contact with tuberculosis, it is likely that that individual already had malaria during childhood. Therefore, infection of mice with a malaria parasite strain first, and then with tuberculosis, might mimic better what would happen in a human setting.

The lower survival of mice due to co-infection is likely associated to an exacerbated Th1 inflammatory response. A review on co-infections has suggested that upon co-infection, the second infectious agent is likely to: exacerbate pathology

associated to the first infectious agent; have no effect or the first agent confers protection towards the second[340]. Studies have shown that tuberculosis infection can confer protection towards an otherwise lethal infection of malaria[170,172,173]. Lethality by *P. yoelii* or *P. chabaudi* in these studies is correlated to a weaker immune response, which also depends on the combination of parasite/mouse genotype used. Thus, mice that normally mount weaker immune responses to malaria become protected if they are previously infected with tuberculosis, since it will likely prime the immune response to a subsequent infection by the *Plasmodium* parasite. However, when co-infection occurs in a scenario where both infections induce strong immune responses, tuberculosis induced protection is no longer observed, and the co-infection likely becomes lethal. This is further supported by our results, where co-infected mice during acute disease quickly succumbed to disease and associated pathology (leukocyte infiltration, necrosis and malaria anaemia) was more severe in co-infected mice. Although we did not assess the production of inflammatory cytokines, it has been shown in other studies that increased inflammatory response is associated to increased pathology[171,175]. Interestingly, investigation of mycobacterial load by luminescence suggested that, at the beginning of infection, BCG load was lower in co-infected animals, which might be indicative of an ongoing immune response. Nonetheless, at the end of the experiment mycobacterial loads were similar between animals, suggesting that while in the BCG-single infected group mycobacterial growth was controlled, in the co-infected group there was an increased mycobacterial survival, probably due to a lower bactericidal capacity.

In the chronic model, although co-infected mice also succumbed to disease, mice did not become as ill as co-infected mice, in the acute model. Histopathological investigation of organs of co-infected mice revealed that, pathology observed was not significantly different from mice in the BCG-single infected group. Mycobacterial loads were also similar between the two groups. The data suggests that, impairment of phagocyte functions by ingestion of hemozoin seems to have little effect on the overall outcome of tuberculosis infection. However, histological findings of tuberculosis infection in mice with chronic malaria, suggest that Hz-containing macrophages have a preferential localization within granulomas. Hz-containing macrophages were also observed in PcAS-single infected mice however, distribution was dispersed throughout the liver parenchyma. The study by Hawkes *et al* did a similar observation[174]. However,

whilst increased mycobacterial loads were observed in livers and spleens of co-infected animals in this study, we did not observe significant differences between groups. This might be explained by slight differences in virulence between the strains of BCG used. Several reports suggest that the peak of BCG infection in mice occurs at 14 days post infection, and chronic infection is thought to be established three weeks post-infection[337]. However, in our hands mycobacterial loads already seemed lower than initial levels following 14 days post infection, which might be indicative that our strain was more attenuated. On the other hand, reported differences in bacterial loads are usually small (usually less than 1 log difference)[174]. Only when virulent strains are used, such as *M. tuberculosis* H37Rv, more significant differences are observed (approximately 1 log)[175]. In fact, it has been shown that granuloma formation and mycobacterial dissemination by macrophages might differ between virulent strains, and strains lacking the Region of Difference-1 (RD1), such as BCG, which might contribute to different mycobacterial burdens[85]. Thus, it might be that in humans Hz-loaded macrophages, by participating in granuloma formation, will contribute to higher mycobacterial loads and increased dissemination, and may even promote progression to active tuberculosis disease, rather than establishing latency.

In both acute and chronic models, co-infected animals seemed more anaemic than PcAS-single infected animals. In fact, following malaria clearance, PcAS-single infected animals recovered from malaria induced anaemia, which did not seem to occur in mice infected with BCG following PcAS infection. Similar findings have been observed in humans, in that co-occurrence of bacteremia with malaria, or following a recent episode of malaria, seem to contribute to more severe anaemia[146].

Thus, *in vivo* findings suggest that malaria-tuberculosis co-infection is detrimental and co-infected hosts will likely have a poor outcome, when compared to single infections. Although hemozoin contribution did not appear to have an important role in the overall immune response to tuberculosis, it was observed that hemozoin was significantly present in granulomas of co-infected animals. Therefore, as discussed above it might be that the relevance of hemozoin presence within granulomas might only become apparent in a model where virulent strains are used, such as the ones that would be found in human infections.

Conclusions and Future Perspectives

The aims of this project were to investigate malaria-tuberculosis co-infection, with particular interest on the possible role of hemozoin phagocytosis by immune cells, and its deposition in host organs following infection. We wanted to first investigate the functional properties of hemozoin containing cells. Ideally, samples from malaria infected patients would have been analyzed. However, these samples were not readily available and more importantly, blood samples from human malaria patients usually have relatively low frequency of Hz-containing leukocytes. Thus, *in vitro* assays were performed in which hemozoin was added to PBMC, isolated from healthy donors.

The methods available for the production of hemozoin are quiet diverse. This can range from synthetically produced hemozoin, to hemozoin isolated from cultures. The source of hemozoin, and/or the protocol employed to obtain it, is particularly important as some discrepant results have been attributed to differences in size of hemozoin crystals[277], or the presence of certain molecules on the crystal surface[282]. Early studies on hemozoin in general did not characterized hemozoin at all, while more recent studies have performed some kind of characterization, and very few studies performed a thorough analysis of the hemozoin produced, with SEM and X-ray analysis. Thus, the beginning of this thesis' project started with the development of standard methods for hemozoin production. Obtained hemozoin was then characterized to define crystal morphology and size, and also assessed for the presence of DNA, protein and heme contamination.

Following hemozoin production, the next step was to establish hemozoin detection using flow-cytometry. Most methods available for the detection of hemozoin are based on microscopy[341,342]. However, there is an increased interest in improving these methods of detection, for the rapid diagnostic of malaria. This includes automation of microscopy and the exploitation of the magnetic properties of hemozoin[315]. Yet, cases where mature forms of the parasite (the ones with higher hemozoin content) are absent from blood circulation, such as in *P. falciparum* infection, might be a limiting factor for such methods[317]. We established a method for hemozoin detection using flow cytometry, which is based on the detection of depolarized side scatter[305]. This method is promising both for the phenotypic and functional characterization of hemozoin containing cells, as well as a drug sensitivity test. Using

this method we were able for the first time to investigate the functional properties of phagocytes, following Hz ingestion, at the single cell level. Although impairment of cell functions by Hz was demonstrated previously, our investigation provided further information by suggesting that exposure to hemozoin can impair functions in cells that have not ingested hemozoin (such as phagocytosis). Whilst in other cases, such as the oxidative response, impairment was only observed in cells that had ingested hemozoin. We propose that this likely reflects hemozoin induced damage to different cell components, essential for these cellular functions that might only be located intracellularly, or might also be exposed to the extracellular environment. Because phagocytosis and the oxidative response were impaired upon hemozoin ingestion, we investigated how well these cells would control mycobacterial growth. Results obtained by us, suggest that PBMC infected with *M. bovis* BCG (BCG) following hemozoin ingestion, have higher mycobacterial loads than unfed controls, infected with BCG. The limitation of this study was that we were unable to compare Hz-containing and non-Hz containing cells, within the Hz-fed PBMC sample. This was because five days post-infection virtually every PBMC contained hemozoin.

We then investigated the kinetics of hemozoin using a murine model. Our hypothesis was that if hemozoin impairs important cell functions, and its presence in host tissues is long lasting and cumulative with each infection, then continuous malaria episodes and hemozoin deposition in host organs could have a major negative impact on host immunity. However, even though hemozoin presence in host organs has been recognized in several autopsies from individuals dying of malaria, it is not known what happens to hemozoin in these organs once an individual is no longer exposed to malaria. The challenge in answering such a question relies on the difficulty in accessing autopsy data from individuals dying from malaria un-related causes, but with a recorded history of malaria. Therefore, we decided to use the murine model to investigate hemozoin dynamics in host organs following malaria clearance. Using two models of murine malaria, it was observed that Hz accumulates in organs for long periods of time, and that there is a tendency for Hz to shift to larger agglomerates of intracellular localization, in livers and spleens. In the spleen, Hz showed a preferential localization within the red-pulp[343]. Our results suggested that while hemozoin seems to be recycled by repeated phagocytosis, and may shift both within and between different organs (liver to spleen), evidence for hemozoin elimination was not clear. Hemozoin accumulation in the bone

marrow was also found, which might have important implications if the same occurs in humans. This accumulation in the bone marrow may contribute to inhibition of erythropoiesis, as already suggested by some, and contribute to severe malaria anaemia[336]. If Hz is not eliminated, or elimination only occurs at very slow rates, then inhibition of erythropoiesis and contribution of hemozoin to malaria associated anaemia might go far beyond malaria clearance/infection cure.

The *in vivo* susceptibility of mice to a tuberculosis infection was also investigated. We first wanted to determined how these two diseases would interact, as published data using murine models suggested that tuberculosis infection could confer protection against malaria, whilst others suggested that tuberculosis infection would be exacerbated by malaria. Of note, all of the published studies on malaria co-infection found in the literature used tuberculosis infection first, followed by malaria. This was based on the hypothesis that BCG vaccination or a tuberculosis infection would protect against malaria. Alternatively, latency of tuberculosis infection would be disrupted by malaria and lead to tuberculosis reactivation, increased pathology and bacterial load. However, this might not be the more natural occurrence in the human setting. As malaria is typically a disease affecting very young children and tuberculosis normally affects adults, we assumed that tuberculosis would occur following a malaria episode, or the two might occur at the same time. We were also interested in investigating if hemozoin accumulation in host organs would increase tuberculosis disease, by increasing bacterial loads. Results obtained suggested that malaria co-occurrence with tuberculosis greatly decreased mice survival. This was likely due to an aggravated inflammatory response, because neither increased parasitaemia nor mycobacterial load was observed in co-infected animals, relative to control groups. Nonetheless, livers of co-infected mice tended to have more inflammatory leukocyte infiltrations and more necrosis. Mice chronically infected with malaria parasites did not succumb to disease upon BCG infection, as did mice during acute malaria. The model of chronic *Plasmodium* infection allowed the investigation of the contribution of hemozoin to tuberculosis infection. Results seem to suggest that hemozoin deposition in organs does not seem to increase tuberculosis related pathology. However, we did observe that hemozoin deposition occurred preferentially in granulomas. Thus, using a model of infection where virulent strains of tuberculosis are used, such as *M. tuberculosis* H37Rv, might reveal differences in terms of mycobacterial load, which was not observed here.

This is supported by studies showing that virulent strains of tuberculosis use granulomas to disseminate mycobacterial infection, and that virulence factors encoded within the RD1 region, which is absent in BCG, play an essential role in this granuloma manipulation[85].

Thus, although *in vitro* results suggest that hemozoin might have an important role in the modulation of phagocytic cell function, and may impair responses to other infections; *in vivo* hemozoin did not seem to play a very significant role. However, the contribution of hemozoin might be more apparent *in vivo*, in the context of an infection with a virulent strain, such as *M. tuberculosis* H37Rv. Hence, it would be interesting to investigate malaria-tuberculosis co-infection in C57Bl/6 mice using the *P. chabaudi* AS and *M. tuberculosis* H37Rv strains. It might also be important to use the natural route of infection, for each of the infectious agents (i.e mosquito bite for *P. chabaudi* and aerosol infection for *M. tuberculosis*), which might reveal further interactions, not addressed in our study. Another relevant approach would be to characterize Hz-containing macrophages *ex vivo*. These macrophages could be obtained from livers or spleens of *Plasmodium* infected mice and then assessed for their functional capacity by flow-cytometry. This might provide further information as to the effects of hemozoin deposition in host organs. Moreover, as hemozoin would be acquired naturally as a result of the *Plasmodium* infection, doubts regarding the source of hemozoin, and confounding factors arising from the use of synthetic/isolated hemozoin, would not be in question here. Finally, our novel flow-cytometry method could also be used to study functional differences between hemozoin-containing and non-hemozoin containing leukocytes, from human malarious patients. Normally, these cells are present at low levels in malarious patients, which make functional analysis difficult. However, as our flow-cytometric method allows the detection of those cells which contain hemozoin, analysis of these cells might be possible, at significant levels, even when they are present at lower numbers.

References

1. Cox, F. E. G. History of human parasitology. *Clin. Microbiol. Rev.* **15,** 595–612 (2002).

2. Pappas, G., Kiriaze, I. J. & Falagas, M. E. Insights into infectious disease in the era of Hippocrates. *Int. J. Infect. Dis.* **12,** 347–50 (2008).

3. Nerlich, A. G., Schraut, B., Dittrich, S., Jelinek, T. & Zink, A. R. *Plasmodium falciparum* in ancient Egypt. *Emerg. Infect. Dis.* **14,** 1317–9 (2008).

4. Sallares, R., Bouwman, A. & Anderung, C. The spread of malaria to Southern Europe in antiquity: new approaches to old problems. *Med. Hist.* **48,** 311–28 (2004).

5. Reiter, P. From Shakespeare to Defoe: malaria in England in the Little Ice Age. *Emerg. Infect. Dis.* **6,** 1–11

6. Cox, F. E. History of the discovery of the malaria parasites and their vectors. *Parasit. Vectors* **3,** 5 (2010).

7. Laveran, A. Un nouveau parasite trouvé dans le sang de malades atteints de fièvre palustre. Origine parasitaire des accidents de l'impaludisme. *Bull. Mem. Soc. Med. Hop. Paris* **17,** 158–164 (1880).

8. Franchini, G. Su di un plasmodio pigmentato di una scimmia. *Arch. Ital. di Sci. Mediche Colon.* **8,** 187–190 (1927).

9. Singh, B. *et al.* A large focus of naturally acquired *Plasmodium knowlesi* infections in human beings. *Lancet* **363,** 1017–1024 (2004).

10. Antinori, S., Galimberti, L., Milazzo, L. & Corbellino, M. *Plasmodium knowlesi*: the emerging zoonotic malaria parasite. *Acta Trop.* **125,** 191–201 (2013).

11. MacCallum, W. G. On the haematozoan infections of birds. *J. Exp. Med.* **3,** 117–36 (1898).

12. Ross, R. The rôle of the mosquito in the evolution of the malarial parasite. *Lancet* **152,** 488–490 (1898).

13. James, S. P. & Tate, P. Exo-erythrocytic schizogony in *Plasmodium gallinaceum* Brumpt, 1935. *Parasitology* **30,** 128–139 (1938).

14. Shortt, H. H. E., Fairley, N. H., Covell, G., Shute, P. G. & Garnham, P. C. C. The pre-erythrocytic stage of *Plasmodium falciparum*. *Trans. R. Soc. Trop. Med. Hyg.* **44,** 405–419 (1951).

15. Shortt, H. E. & Garnham, P. C. C. The pre-erythrocytic stage of human malaria, *Plasmodium vivax*. *Br. Med. J.* **1,** 547 (1948).

16. Garnham, P. C. *et al.* Pre-erythrocytic Stages of Human Malaria: *Plasmodium Ovale*. *Br. Med. J.* **1,** 257 (1954).

17. Amino, R. *et al.* Quantitative imaging of *Plasmodium* transmission from mosquito to mammal. *Nat. Med.* **12,** 220–4 (2006).

18. Ménard, R. *et al.* Looking under the skin: the first steps in malarial infection and immunity. *Nat. Rev. Microbiol.* **11,** 701–712 (2013).

19. Tavares, J. *et al.* Role of host cell traversal by the malaria sporozoite during liver infection. *J. Exp. Med.* **210,** 905–15 (2013).

20. Mota, M. M. *et al.* Migration of *Plasmodium* sporozoites through cells before infection. *Science* **291,** 141–4 (2001).

21. Coppens, I., Sullivan, D. J. & Prigge, S. T. An update on the rapid advances in malaria parasite cell biology. *Trends Parasitol.* **26,** 305–10 (2010).

22. Sturm, A. *et al.* Manipulation of host hepatocytes by the malaria parasite for delivery into liver sinusoids. *Science* **313,** 1287–90 (2006).

23. Baer, K., Klotz, C., Kappe, S. H. I., Schnieder, T. & Frevert, U. Release of hepatic *Plasmodium yoelii* merozoites into the pulmonary microvasculature. *PLoS Pathog.* **3,** e171 (2007).

24. Greenwood, B. M. *et al.* Malaria: progress, perils, and prospects for eradication. *J. Clin. Invest.* **118,** 1266–76 (2008).

25. Wipasa, J., Elliott, S., Xu, H. & Good, M. F. Immunity to asexual blood stage malaria and vaccine approaches. *Immunol. Cell Biol.* **80,** 401–14 (2002).

26. Cowman, A. F. & Crabb, B. S. Invasion of red blood cells by malaria parasites. *Cell* **124,** 755–66 (2006).

27. Hay, S. I., Guerra, C. A., Tatem, A. J., Noor, A. M. & Snow, R. W. The global distribution and population at risk of malaria: past, present, and future. *Lancet Infect. Dis.* **4,** 327–36 (2004).

28. Majori, G. Short history of malaria and its eradication in Italy with short notes on the fight against the infection in the mediterranean basin. *Mediterr. J. Hematol. Infect. Dis.* **4,** e2012016 (2012).

29. Mendis, K. *et al.* From malaria control to eradication: The WHO perspective. *Trop. Med. Int. Heal. TM IH* **14,** 802–9 (2009).

30. Brown, G. in *Health.* 65–83 (Future Leaders, 2011).

31. Nájera, J. A., González-Silva, M. & Alonso, P. L. Some lessons for the future from the Global Malaria Eradication Programme (1955-1969). *PLoS Med.* **8,** e1000412 (2011).

32. Alonso, P. L. *et al.* A research agenda to underpin malaria eradication. *PLoS Med.* **8,** e1000406 (2011).

33. Knudsen, A. B. & Slooff, R. Vector-borne disease problems in rapid urbanization: new approaches to vector control. *Bull. World Health Organ.* **70,** 1–6 (1992).

34. Gallup, J. L. & Sachs, J. D. The economic burden of malaria. *Am. J. Trop. Med. Hyg.* **64,** 85–96 (2001).

35. Sachs, J. & Malaney, P. The economic and social burden of malaria. *Nature* **415,** 680–5 (2002).

36. De Silva, P. M. & Marshall, J. M. Factors contributing to urban malaria transmission in sub-saharan Africa: a systematic review. *J. Trop. Med.* **2012,** 819563 (2012).

37. Crubézy, E. *et al.* Identification of Mycobacterium DNA in an Egyptian Pott's disease of 5,400 years old. *C. R. Acad. Sci. III.* **321,** 941–51 (1998).

38. Zink, A., Haas, C. J., Reischl, U., Szeimies, U. & Nerlich, A. G. Molecular analysis of skeletal tuberculosis in an ancient Egyptian population. *J. Med. Microbiol.* **50,** 355–66 (2001).

39. Gagneux, S. Host-pathogen coevolution in human tuberculosis. *Philos. Trans. R. Soc. Lond. B. Biol. Sci.* **367,** 850–9 (2012).

40. Murray, J. F. A century of tuberculosis. *Am. J. Respir. Crit. Care Med.* **169,** 1181–6 (2004).

41. Murray, J. F. The white plague: down and out, or up and coming? J. Burns Amberson lecture. *Am. Rev. Respir. Dis.* **140,** 1788–95 (1989).

42. Koch, R. Die aetiologie der tuberculose. *Berliner Klin. wochenschrift* **15,** 221–30 (1882).

43. Kaufmann, S. H. E. & Schaible, U. E. 100th anniversary of Robert Koch's Nobel Prize for the discovery of the tubercle bacillus. *Trends Microbiol.* **13,** 469–475 (2005).

44. Daniel, T. M. The history of tuberculosis. *Respir. Med.* **100,** 1862–70 (2006).

45. Schatz, A., Bugle, E. & Waksman, S. A. Streptomycin, a Substance Exhibiting Antibiotic Activity Against Gram-Positive and Gram-Negative Bacteria. *Exp. Biol. Med.* **55,** 66–69 (1944).

46. Weitzman, D., de Wend Cayley, F. & Wingfield, A. Streptomycin in the treatment of pulmonary tuberculosis. *Br. J. Tuberc. Dis. Chest* **44,** 98–104 (1950).

47. Tempel, C. W., Hughes, F. J., Mardis, R. E., Towbin, M. N. & Dye, W. E. Combined intermittent regimens employing streptomycin and para-aminosalicylic acid in the treatment of pulmonary tuberculosis; a comparison with daily and intermittent dosage schedules. *Br. Med. J.* **63,** 295–311 (1951).

48. Dunner, E. & Brown, W. Streptomycin Para-Aminosalicylate in the Treatment of Pulmonary Tuberculosis. *Dis. Chest* **19,** 438 (1951).

49. Bernstein, J., Lott, W. A., Steinberg, B. A. & Yale, H. L. Chemotherapy of experimental tuberculosis. V. Isonicotinic acid hydrazide (nydrazid) and related compounds. *Am. Rev. Tuberc.* **65,** 357–64 (1952).

50. Fox, H. H. The chemical approach to the control of tuberculosis. *Science* **116,** 129–34 (1952).

51. World Health Organization, WHO, Global tuberculosis report 2012. *Geneva, Switz. WHO. 2012 ISBN 978 92 4 156450 2* at <http://www.who.int/tb/publications/>

52. Frieden, T. R., Sterling, T. R., Munsiff, S. S., Watt, C. J. & Dye, C. Tuberculosis. *Lancet* **362,** 887–899 (2003).

53. Sutherland, I. Recent studies in the epidemiology of tuberculosis, based on the risk of being infected with tubercle bacilli. *Adv. Tuberc. Res.* **19,** 1–63 (1976).

54. Vynnycky, E. Lifetime Risks, Incubation Period, and Serial Interval of Tuberculosis. *Am. J. Epidemiol.* **152,** 247–263 (2000).

55. O'Garra, A. *et al.* The immune response in tuberculosis. *Annu. Rev. Immunol.* **31,** 475–527 (2013).

56. Brändli, O. The Clinical Presentation of Tuberculosis. *Respiration* **65,** 97–105 (1998).

57. Schlesinger, L. S. Entry of *Mycobacterium tuberculosis* into mononuclear phagocytes. *Curr. Top. Microbiol. Immunol.* **215,** 71–96 (1996).

58. Eruslanov, E. B. *et al.* Neutrophil responses to *Mycobacterium tuberculosis* infection in genetically susceptible and resistant mice. *Infect. Immun.* **73,** 1744–53 (2005).

59. Eum, S.-Y. *et al.* Neutrophils are the predominant infected phagocytic cells in the airways of patients with active pulmonary TB. *Chest* **137,** 122–8 (2010).

60. Wolf, A. J. *et al.* Mycobacterium tuberculosis infects dendritic cells with high frequency and impairs their function *in vivo*. *J. Immunol.* **179,** 2509–19 (2007).

61. Lowe, D. M., Redford, P. S., Wilkinson, R. J., O'Garra, A. & Martineau, A. R. Neutrophils in tuberculosis: friend or foe? *Trends Immunol.* **33,** 14–25 (2012).

62. Kleinnijenhuis, J., Oosting, M., Joosten, L. A. B., Netea, M. G. & Van Crevel, R. Innate immune recognition of *Mycobacterium tuberculosis*. *Clin. Dev. Immunol.* **2011,** 405310 (2011).

63. Kleinnijenhuis, J., Oosting, M., Joosten, L. A. B., Netea, M. G. & Van Crevel, R. Apoptosis is an innate defense function of macrophages against *Mycobacterium tuberculosis*. *Mucosal Immunol.* **4,** 279–87 (2011).

64. Seiler, P. *et al.* Early granuloma formation after aerosol *Mycobacterium tuberculosis* infection is regulated by neutrophils via CXCR3-signaling chemokines. *Eur. J. Immunol.* **33,** 2676–86 (2003).

65. Seiler, P. *et al.* Lung neutrophils facilitate activation of naive antigen-specific CD4+ T cells during *Mycobacterium tuberculosis* infection. *J. Immunol.* **186,** 7110–9 (2011).

66. Barnes, P. F. *et al.* Predictors of short-term prognosis in patients with pulmonary tuberculosis. *J. Infect. Dis.* **158,** 366–71 (1988).

67. Keller, C. *et al.* Genetically determined susceptibility to tuberculosis in mice causally involves accelerated and enhanced recruitment of granulocytes. *Infect. Immun.* **74,** 4295–309 (2006).

68. Blomgran, R., Desvignes, L., Briken, V. & Ernst, J. D. *Mycobacterium tuberculosis* inhibits neutrophil apoptosis, leading to delayed activation of naive CD4 T cells. *Cell Host Microbe* **11,** 81–90 (2012).

69. Flesch, I. E. & Kaufmann, S. H. Mechanisms involved in mycobacterial growth inhibition by gamma interferon-activated bone marrow macrophages: role of reactive nitrogen intermediates. *Infect. Immun.* **59,** 3213–8 (1991).

70. Chan, J., Xing, Y., Magliozzo, R. S. & Bloom, B. R. Killing of virulent *Mycobacterium tuberculosis* by reactive nitrogen intermediates produced by activated murine macrophages. *J. Gen. Microbiol.* **175,** 1111–22 (1992).

71. Jackett, P. S., Aber, V. R. & Lowrie, D. B. Virulence and resistance to superoxide, low pH and hydrogen peroxide among strains of *Mycobacterium tuberculosis*. *J. Gen. Microbiol.* **104,** 37–45 (1978).

72. Pacheco, S. A., Powers, K. M., Engelmann, F., Messaoudi, I. & Purdy, G. E. Autophagic Killing Effects against *Mycobacterium tuberculosis* by Alveolar Macrophages from Young and Aged Rhesus Macaques. *PLoS One* **8,** e66985 (2013).

73. Gutierrez, M. G. *et al.* Autophagy Is a Defense Mechanism Inhibiting BCG and *Mycobacterium tuberculosis* Survival in Infected Macrophages. *Cell* **119,** 753–766 (2004).

74. Gordon, A. H., Hart, P. D. & Young, M. R. Ammonia inhibits phagosome-lysosome fusion in macrophages. *Nature* **286,** 79–80 (1980).

75. Goren, M. B., D'Arcy Hart, P., Young, M. R. & Armstrong, J. A. Prevention of phagosome-lysosome fusion in cultured macrophages by sulfatides of *Mycobacterium tuberculosis*. *Proc. Natl. Acad. Sci. U. S. A.* **73,** 2510–4 (1976).

76. McDonough, K. A., Kress, Y. & Bloom, B. R. Pathogenesis of tuberculosis: interaction of *Mycobacterium tuberculosis* with macrophages. *Infect. Immun.* **61,** 2763–73 (1993).

77. Moreira, A. L. *et al.* Sequestration of Mycobacterium tuberculosis in tight vacuoles *in vivo* in lung macrophages of mice infected by the respiratory route. *Infect. Immun.* **65,** 305–8 (1997).

78. Wayne, L. G. Dormancy of *Mycobacterium tuberculosis* and latency of disease. *Eur. J. Clin. Microbiol. Infect. Dis.* **13,** 908–14 (1994).

79. Keane, J. *et al.* Tuberculosis associated with infliximab, a tumor necrosis factor alpha-neutralizing agent. *N. Engl. J. Med.* **345,** 1098–104 (2001).

80. Harris, J. & Keane, J. How tumour necrosis factor blockers interfere with tuberculosis immunity. *Clin. Exp. Immunol.* **161,** 1–9 (2010).

81. Flynn, J. L. *et al.* Tumor necrosis factor-alpha is required in the protective immune response against *Mycobacterium tuberculosis* in mice. *Immunity* **2,** 561–72 (1995).

82. Lin, P. L. *et al.* Tumor necrosis factor neutralization results in disseminated disease in acute and latent *Mycobacterium tuberculosis* infection with normal granuloma structure in a cynomolgus macaque model. *Arthritis Rheum.* **62,** 340–50 (2010).

83. Rom, W. N. *et al.* Human host response to *Mycobacterium tuberculosis*. *Schweiz. Med. Wochenschr.* **125,** 2178–85 (1995).

84. Boros, D. L. *Granulomatous infections and inflammations cellular and molecular mechanisms.* (ASM Press, 2003).

85. Ramakrishnan, L. Revisiting the role of the granuloma in tuberculosis. *Nat. Rev. Immunol.* **12,** 352–66 (2012).

86. Feldman, W. H. & Baggenstoss, A. H. The residual infectivity of the primary complex of tuberculosis. *Am. J. Pathol.* **14,** 473–490.3 (1938).

87. Aronson, J. D. & Whitney, C. E. The types of tubercle bacilli found in tuberculous lesions and in nontuberculous tissue in man. *J. Infect. Dis.* **47,** 30–55 (1930).

88. Aronson, J. D. & Whitney, C. E. Structural deficiencies in granuloma formation in TNF gene-targeted mice underlie the heightened susceptibility to aerosol *Mycobacterium tuberculosis* infection, which is not compensated for by lymphotoxin. *J. Immunol.* **162,** 3504–11 (1999).

89. Chakravarty, S. D. *et al.* Tumor necrosis factor blockade in chronic murine tuberculosis enhances granulomatous inflammation and disorganizes granulomas in the lungs. *Infect. Immun.* **76,** 916–26 (2008).

90. Stenger, S. Immunological control of tuberculosis: role of tumour necrosis factor and more. *Ann. Rheum. Dis.* **64 Suppl 4,** iv24–8 (2005).

91. Roach, D. R. *et al.* TNF regulates chemokine induction essential for cell recruitment, granuloma formation, and clearance of mycobacterial infection. *J. Immunol.* **168,** 4620–7 (2002).

92. Ramakrishnan, L. Looking within the zebrafish to understand the tuberculous granuloma. *Adv. Exp. Med. Biol.* **783,** 251–66 (2013).

93. Davis, J. M. *et al.* Real-Time Visualization of Mycobacterium-Macrophage Interactions Leading to Initiation of Granuloma Formation in Zebrafish Embryos. *Immunity* **17,** 693–702 (2002).

94. Davis, J. M. & Ramakrishnan, L. The role of the granuloma in expansion and dissemination of early tuberculous infection. *Cell* **136,** 37–49 (2009).

95. Wolf, A. J. *et al.* Initiation of the adaptive immune response to *Mycobacterium tuberculosis* depends on antigen production in the local lymph node, not the lungs. *J. Exp. Med.* **205,** 105–15 (2008).

96. Chackerian, A. A., Alt, J. M., Perera, T. V., Dascher, C. C. & Behar, S. M. Dissemination of *Mycobacterium tuberculosis* Is Influenced by Host Factors and Precedes the Initiation of T-Cell Immunity. *Infect. Immun.* **70,** 4501–4509 (2002).

97. Khader, S. A. *et al.* IL-23 and IL-17 in the establishment of protective pulmonary CD4+ T cell responses after vaccination and during *Mycobacterium tuberculosis* challenge. *Nat. Immunol.* **8,** 369–77 (2007).

98. Shafiani, S., Tucker-Heard, G., Kariyone, A., Takatsu, K. & Urdahl, K. B. Pathogen-specific regulatory T cells delay the arrival of effector T cells in the lung during early tuberculosis. *J. Exp. Med.* **207,** 1409–20 (2010).

99. Gallegos, A. M., Pamer, E. G. & Glickman, M. S. Delayed protection by ESAT-6-specific effector CD4+ T cells after airborne *M. tuberculosis* infection. *J. Exp. Med.* **205,** 2359–68 (2008).

100. Shi, L., Jung, Y.-J., Tyagi, S., Gennaro, M. L. & North, R. J. Expression of Th1-mediated immunity in mouse lungs induces a *Mycobacterium tuberculosis*

transcription pattern characteristic of nonreplicating persistence. *Proc. Natl. Acad. Sci. U. S. A.* **100,** 241–6 (2003).

101. Urdahl, K. B., Shafiani, S. & Ernst, J. D. Initiation and regulation of T-cell responses in tuberculosis. *Mucosal Immunol.* **4,** 288–93 (2011).

102. Reiley, W. W. *et al.* Distinct functions of antigen-specific CD4 T cells during murine *Mycobacterium tuberculosis* infection. *Proc. Natl. Acad. Sci. U. S. A.* **107,** 19408–13 (2010).

103. Barber, D. L. *et al.* Restoring function in exhausted CD8 T cells during chronic viral infection. *Nature* **439,** 682–7 (2006).

104. Vitoria, M. *et al.* The global fight against HIV/AIDS, tuberculosis, and malaria: current status and future perspectives. *Am. J. Clin. Pathol.* **131,** 844–8 (2009).

105. Troye-Blomberg, M. & Berzins, K. Immune interactions in malaria co-infections with other endemic infectious diseases: implications for the development of improved disease interventions. *Microbes Infect.* **10,** 948–52 (2008).

106. Were, T. *et al.* Bacteremia in Kenyan children presenting with malaria. *J. Clin. Microbiol.* **49,** 671–6 (2011).

107. Molyneux, D. H., Hotez, P. J. & Fenwick, A. "Rapid-impact interventions": how a policy of integrated control for Africa's neglected tropical diseases could benefit the poor. *PLoS Med.* **2,** e336 (2005).

108. Graham, S. M., Walsh, A. L., Molyneux, E. M., Phiri, A. J. & Molyneux, M. E. Clinical presentation of non-typhoidal *Salmonella* bacteraemia in Malawian children. *Trans. R. Soc. Trop. Med. Hyg.* **94,** 310–4 (2000).

109. Mackenzie, G. *et al.* A decline in the incidence of invasive non-typhoidal *Salmonella* infection in The Gambia temporally associated with a decline in malaria infection. *PLoS One* **5,** e10568 (2010).

110. Berkley, J., Mwarumba, S., Bramham, K., Lowe, B. & Marsh, K. Bacteraemia complicating severe malaria in children. *Trans. R. Soc. Trop. Med. Hyg.* **93,** 283–286 (1999).

111. Raso, G. *et al.* Multiple parasite infections and their relationship to self-reported morbidity in a community of rural Côte d'Ivoire. *Int. J. Epidemiol.* **33,** 1092–102 (2004).

112. Lustigman, S. *et al.* A research agenda for helminth diseases of humans: the problem of helminthiases. *PLoS Negl. Trop. Dis.* **6,** e1582 (2012).

113. Hotez, P. J. *et al.* Incorporating a rapid-impact package for neglected tropical diseases with programs for HIV/AIDS, tuberculosis, and malaria. *PLoS Med.* **3,** e102 (2006).

114. Hotez, P. Enlarging the "Audacious Goal": elimination of the world's high prevalence neglected tropical diseases. *Vaccine* **29 Suppl 4,** D104–10 (2011).

115. Pisell, T. L. *et al.* Immune activation and induction of HIV-1 replication within CD14 macrophages during acute *Plasmodium falciparum* malaria coinfection. *AIDS* **16,** 1503–9 (2002).

116. Kublin, J. G. *et al.* Effect of *Plasmodium falciparum* malaria on concentration of HIV-1-RNA in the blood of adults in rural Malawi: a prospective cohort study. *Lancet* **365,** 233–40 (2005).

117. Rénia, L. & Potter, S. M. Co-infection of malaria with HIV: an immunological perspective. *Parasite Immunol.* **28,** 589–95 (2006).

118. Xiao, L., Owen, S. M., Rudolph, D. L., Lal, R. B. & Lal, A. A. *Plasmodium falciparum* antigen-induced human immunodeficiency virus type 1 replication is mediated through induction of tumor necrosis factor-alpha. *J. Infect. Dis.* **177,** 437–45 (1998).

119. Cuadros, D. F., Branscum, A. J. & Crowley, P. H. HIV-malaria co-infection: effects of malaria on the prevalence of HIV in East sub-Saharan Africa. *Int. J. Epidemiol.* **40,** 931–9 (2011).

120. Cuadros, D. F., Branscum, A. J. & García-Ramos, G. No evidence of association between HIV-1 and malaria in populations with low HIV-1 prevalence. *PLoS One* **6,** e23458 (2011).

121. Laar, A. K. *et al.* Predictors of fetal anemia and cord blood malaria parasitemia among newborns of HIV-positive mothers. *BMC Res. Notes* **6,** 350 (2013).

122. Bloland, P. B. *et al.* Maternal HIV infection and infant mortality in Malawi: evidence for increased mortality due to placental malaria infection. *AIDS* **9,** 721–6 (1995).

123. Ter Kuile, F. O. *et al.* The burden of co-infection with human immunodeficiency virus type 1 and malaria in pregnant women in sub-saharan Africa. *Am. J. Trop. Med. Hyg.* **71,** 41–54 (2004).

124. Chalwe, V. *et al.* Increased risk for severe malaria in HIV-1-infected adults, Zambia. *Emerg. Infect. Dis.* **15,** 749; quiz 858 (2009).

125. Cohen, C. *et al.* Increased prevalence of severe malaria in HIV-infected adults in South Africa. *Clin. Infect. Dis.* **41,** 1631–7 (2005).

126. González, R., Ataíde, R., Naniche, D., Menéndez, C. & Mayor, A. HIV and malaria interactions: where do we stand? *Expert Rev. Anti. Infect. Ther.* **10,** 153–65 (2012).

127. Mermin, J., Lule, J. R. & Ekwaru, J. P. Association between malaria and CD4 cell count decline among persons with HIV. *J. Acquir. Immune Defic. Syndr.* **41,** 129–30 (2006).

128. Diou, J., Tardif, M. R., Barat, C. & Tremblay, M. J. Dendritic cells derived from hemozoin-loaded monocytes display a partial maturation phenotype that promotes HIV-1 trans-infection of CD4+ T cells and virus replication. *J. Immunol.* **184,** 2899–907 (2010).

129. Nacher, M. Interactions between worms and malaria: good worms or bad worms? *Malar. J.* **10,** 259 (2011).

130. Melo, G. C. *et al.* Concurrent helminthic infection protects schoolchildren with *Plasmodium vivax* from anemia. *PLoS One* **5,** e11206 (2010).

131. Brutus, L. *et al.* Parasitic co-infections: does *Ascaris lumbricoides* protect against *Plasmodium falciparum* infection? *Am. J. Trop. Med. Hyg.* **75,** 194–8 (2006).

132. Degarege, A., Animut, A., Legesse, M. & Erko, B. Malaria severity status in patients with soil-transmitted helminth infections. *Acta Trop.* **112,** 8–11 (2009).

133. Nacher, M. *et al.* Intestinal helminth infections are associated with increased incidence of *Plasmodium falciparum* malaria in Thailand. *J. Parasitol.* **88,** 55–8 (2002).

134. Spiegel, A., Tall, A., Raphenon, G., Trape, J. F. & Druilhe, P. Increased frequency of malaria attacks in subjects co-infected by intestinal worms and *Plasmodium falciparum* malaria. *Trans. R. Soc. Trop. Med. Hyg.* **97,** 198–9 (2003).

135. Nacher, M. *et al.* Helminth infections are associated with protection from cerebral malaria and increased nitrogen derivatives concentrations in Thailand. *Am. J. Trop. Med. Hyg.* **66,** 304–9 (2002).

136. Nacher, M. *et al.* Helminth infections are associated with protection from malaria-related acute renal failure and jaundice in Thailand. *Am. J. Trop. Med. Hyg.* **65,** 834–6 (2001).

137. Boel, M. *et al.* Complex interactions between soil-transmitted helminths and malaria in pregnant women on the Thai-Burmese border. *PLoS Negl. Trop. Dis.* **4,** e887 (2010).

138. Midzi, N. *et al.* The burden of polyparasitism among primary schoolchildren in rural and farming areas in Zimbabwe. *Trans. R. Soc. Trop. Med. Hyg.* **102,** 1039–45 (2008).

139. Pullan, R. L., Kabatereine, N. B., Bukirwa, H., Staedke, S. G. & Brooker, S. Heterogeneities and consequences of *Plasmodium* species and hookworm coinfection: a population based study in Uganda. *J. Infect. Dis.* **203,** 406–17 (2011).

140. Nacher, M. Worms and malaria: noisy nuisances and silent benefits. *Parasite Immunol.* **24,** 391–3 (2002).

141. Hartgers, F. C. *et al.* Responses to malarial antigens are altered in helminth-infected children. *J. Infect. Dis.* **199,** 1528–35 (2009).

142. Wammes, L. J. *et al.* Regulatory T cells in human geohelminth infection suppress immune responses to BCG and *Plasmodium falciparum*. *Eur. J. Immunol.* **40,** 437–42 (2010).

143. Druilhe, P., Tall, A. & Sokhna, C. Worms can worsen malaria: towards a new means to roll back malaria? *Trends Parasitol.* **21,** 359–62 (2005).

144. Giglioli, G. Paratyphoid C an Endemic Disease of British Guiana: A Clinical and Pathological Outline. *Proc. R. Soc. Med.* **23,** 165–77 (1929).

145. Hayasaka, C. Im Verlauf einer Malariakur durch *Bacillus enteritidis* Gärtner entstandene Meningitis und Sepsis. *Tohoku J. Exp. Med.* **21,** 466–504 (1933).

146. Mabey, D. C., Brown, A. & Greenwood, B. M. *Plasmodium falciparum* malaria and Salmonella infections in Gambian children. *J. Infect. Dis.* **155,** 1319–21 (1987).

147. Bygbjerg, I. C. & Lanng, C. Septicaemia as a complication of falciparum malaria. *Trans. R. Soc. Trop. Med. Hyg.* **76,** 705 (1982).

148. Commey, J., Quarm-Goka, B. & Agyepong, I. Persistent fever in severe malaria in children. *Cent. Afr. J. Med.* **40,** 257–60 (1994).

149. Kharazmi, A., Høiby, N. & Theander, T. G. *Pseudomonas aeruginosa* septicaemia in a patient with severe *Plasmodium falciparum*. *Trans. R. Soc. Trop. Med. Hyg.* **81,** 49–50 (1987).

150. Prada, J. Bacterial strains isolated from blood cultures of Nigerian children with cerebral malaria. *Lancet* **342,** 1114 (1993).

151. Gopinath, R., Keystone, J. & Kain, K. Concurrent falciparum malaria and *Salmonella* bacteremia in travelers: report of two cases. *Clin. Infect. Dis.* **20,** 706–708 (1995).

152. Brent, A. *et al. Salmonella* bacteremia in Kenyan children. *Pediatr. Infect. Dis. J.* **25,** 230–6 (2006).

153. Mtove, G. *et al.* Invasive salmonellosis among children admitted to a rural Tanzanian hospital and a comparison with previous studies. *PLoS One* **5,** e9244 (2010).

154. Scott, J. A. G. *et al.* Relation between falciparum malaria and bacteraemia in Kenyan children: a population-based, case-control study and a longitudinal study. *Lancet* **378,** 1316–23 (2011).

155. Nielsen, M. V. *et al.* Incidence and characteristics of bacteremia among children in rural Ghana. *PLoS One* **7,** e44063 (2012).

156. Bassat, Q. *et al.* Severe malaria and concomitant bacteraemia in children admitted to a rural Mozambican hospital. *Trop. Med. Int. Health* **14,** 1011–9 (2009).

157. Graham, S. M. *et al.* Nontyphoidal *Salmonella* infections of children in tropical Africa. *Pediatr. Infect. Dis. J.* **19,** 1189–96 (2000).

158. Lalremruata, A. *et al.* Molecular identification of falciparum malaria and human tuberculosis co-infections in mummies from the Fayum depression (Lower Egypt). *PLoS One* **8,** e60307 (2013).

159. Pond, B. S. Malaria indicator surveys demonstrate a markedly lower prevalence of malaria in large cities of sub-Saharan Africa | MalariaWorld. *Malar. J.* **12,** 313 (2013).

160. Banerjee, A., Harries, A. D. & Salaniponi, F. M. Differences in tuberculosis incidence rates in township and in rural populations in Ntcheu District, Malawi. *Trans. R. Soc. Trop. Med. Hyg.* **93,** 392–3 (1999).

161. Li, X.-X. & Zhou, X.-N. Co-infection of tuberculosis and parasitic diseases in humans: a systematic review. *Parasit. Vectors* **6,** 79 (2013).

162. Range, N. *et al.* HIV and parasitic co-infections in tuberculosis patients: a cross-sectional study in Mwanza, Tanzania. *Ann. Trop. Med. Parasitol.* **101,** 343–51 (2007).

163. Valadas, E. *et al.* Tuberculosis with malaria or HIV co-infection in a large hospital in Luanda, Angola. *J. Infect. Dev. Ctries.* **7,** 269–72 (2013).

164. Colombatti, R. *et al.* Malaria prevention reduces in-hospital mortality among severely ill tuberculosis patients: a three-step intervention in Bissau, Guinea-Bissau. *BMC Infect. Dis.* **11,** 57 (2011).

165. Bazaz-Malik, G. Increased resistance to malaria after *Mycobacterium tuberculosis* infection. *Indian J. Med. Res.* **61,** 1014–24 (1973).

166. Singh, J., Ray, A. P. & Nair, C. P. Relationship of tuberculosis on the course and intensity of plasmodial infections in *M. mulatta*. *Indian J. Malariol.* **10,** 3–10 (1956).

167. Clark, I. A., Allison, A. C. & Cox, F. E. Protection of mice against Babesia, and *Plasmodium* with BCG. *Nature* **259,** 309–311 (1976).

168. Stevenson, M., Lemieux, S. & Skamene, E. Genetic control of resistance to murine malaria. *J. Cell. Biochem.* **24,** 91–102 (1984).

169. Murphy, J. R. Host defenses in murine malaria: nonspecific resistance to *Plasmodium berghei* generated in response to *Mycobacterium bovis* infection or *Corynebacterium parvum* stimulation. *Infect. Immun.* **33,** 199–211 (1981).

170. Matsumoto, S. *et al. Mycobacterium bovis* bacillus calmette-guérin induces protective immunity against infection by *Plasmodium yoelii* at blood-stage depending on shifting immunity toward Th1 type and inducing protective IgG2a after the parasite infection. *Vaccine* **19,** 779–87 (2000).

171. Scott, C. P., Kumar, N., Bishai, W. R. & Manabe, Y. C. Short report: modulation of Mycobacterium tuberculosis infection by *Plasmodium* in the murine model. *Am. J. Trop. Med. Hyg.* **70,** 144–8 (2004).

172. Page, K. R. *et al. Mycobacterium*-Induced Potentiation of Type 1 Immune Responses and Protection against Malaria Are Host Specific. **73,** 8369–8380 (2005).

173. Leisewitz, A. L., Rockett, K. & Kwiatkowski, D. BCG-malaria co-Infection has paradoxical effects on C57BL/6 and A/J mouse strains. *Parasite Immunol.* **30,** 1–12 (2008).

174. Hawkes, M. *et al.* Malaria exacerbates experimental mycobacterial infection *in vitro* and *in vivo*. *Microbes Infect.* **12,** 864–74 (2010).

175. Mueller, A.-K. *et al.* Natural transmission of *Plasmodium berghei* exacerbates chronic tuberculosis in an experimental co-infection model. *PLoS One* **7,** e48110 (2012).

176. Smrkovski, L. L. & Strickland, G. T. Rodent malaria: BCG-induced protection and immunosuppression. *J. Immunol.* **121,** 1257–61 (1978).

177. Parra, M. *et al.* Malaria infections do not compromise vaccine-induced immunity against tuberculosis in mice. *PLoS One* **6,** e28164 (2011).

178. Miller, L. H., Ackerman, H. C., Su, X. & Wellems, T. E. Malaria biology and disease pathogenesis: insights for new treatments. *Nat. Med.* **19,** 156–67 (2013).

179. Miller, L. H., Good, M. F. & Milon, G. Malaria pathogenesis. *Science* **264,** 1878–83 (1994).

180. Maitland, K. & Newton, C. R. J. C. Acidosis of severe falciparum malaria: heading for a shock? *Trends Parasitol.* **21,** 11–16 (2005).

181. Chakravarty, S. *et al.* CD8+ T lymphocytes protective against malaria liver stages are primed in skin-draining lymph nodes. *Nat. Med.* **13,** 1035–41 (2007).

182. Torgler, R. *et al.* Sporozoite-mediated hepatocyte wounding limits *Plasmodium* parasite development via MyD88-mediated NF-kappa B activation and inducible NO synthase expression. *J. Immunol.* **180,** 3990–9 (2008).

183. Khan, Z. M. & Vanderberg, J. P. Role of host cellular response in differential susceptibility of nonimmunized BALB/c mice to *Plasmodium berghei* and *Plasmodium yoelii* sporozoites. *Infect. Immun.* **59,** 2529–34 (1991).

184. Van de Sand, C. *et al.* The liver stage of *Plasmodium berghei* inhibits host cell apoptosis. *Mol. Microbiol.* **58,** 731–42 (2005).

185. Epiphanio, S. *et al.* Heme oxygenase-1 is an anti-inflammatory host factor that promotes murine plasmodium liver infection. *Cell Host Microbe* **3,** 331–8 (2008).

186. Liehl, P. & Mota, M. M. Innate recognition of malarial parasites by mammalian hosts. *Int. J. Parasitol.* **42,** 557–566 (2012).

187. Singh, A. P. *et al. Plasmodium* circumsporozoite protein promotes the development of the liver stages of the parasite. *Cell* **131,** 492–504 (2007).

188. Graewe, S. *et al.* Hostile takeover by *Plasmodium*: reorganization of parasite and host cell membranes during liver stage egress. *PLoS Pathog.* **7,** e1002224 (2011).

189. Artavanis-Tsakonas, K., Tongren, J. E. & Riley, E. M. The war between the malaria parasite and the immune system: immunity, immunoregulation and immunopathology. *Clin. Exp. Immunol.* **133,** 145–52 (2003).

190. Favre, N., Ryffel, B., Bordmann, G. & Rudin, W. The course of *Plasmodium chabaudi chabaudi* infections in interferon-gamma receptor deficient mice. *Parasite Immunol.* **19,** 375–83 (1997).

191. Stevenson, M. M., Tam, M. F., Wolf, S. F. & Sher, A. IL-12-induced protection against blood-stage *Plasmodium chabaudi* AS requires IFN-gamma and TNF-alpha and occurs via a nitric oxide-dependent mechanism. *J. Immunol.* **155,** 2545–56 (1995).

192. Deloron, P., Chougnet, C., Lepers, J. P., Tallet, S. & Coulanges, P. Protective value of elevated levels of gamma interferon in serum against exoerythrocytic stages of *Plasmodium falciparum*. *J. Clin. Microbiol.* **29,** 1757–60 (1991).

193. Luty, A. J. *et al.* Interferon-gamma responses are associated with resistance to reinfection with *Plasmodium falciparum* in young African children. *J. Infect. Dis.* **179,** 980–8 (1999).

194. Artavanis-Tsakonas, K. & Riley, E. M. Innate immune response to malaria: rapid induction of IFN-gamma from human NK cells by live *Plasmodium falciparum*-infected erythrocytes. *J. Immunol.* **169,** 2956–63 (2002).

195. Artavanis-Tsakonas, K. *et al.* Activation of a subset of human NK cells upon contact with *Plasmodium falciparum*-infected erythrocytes. *J. Immunol.* **171,** 5396–405 (2003).

196. Su, Z., Fortin, A., Gros, P. & Stevenson, M. M. Opsonin-independent phagocytosis: an effector mechanism against acute blood-stage *Plasmodium chabaudi* AS infection. *J. Infect. Dis.* **186,** 1321–9 (2002).

197. Malaguarnera, L. & Musumeci, S. The immune response to *Plasmodium falciparum* malaria. *Lancet Infect. Dis.* **2,** 472–8 (2002).

198. Urban, B. C., Ing, R. & Stevenson, M. M. Early interactions between blood-stage plasmodium parasites and the immune system. *Curr. Top. Microbiol. Immunol.* **297,** 25–70 (2005).

199. Troye-Blomberg, M. *et al.* Human gamma delta T cells that inhibit the *in vitro* growth of the asexual blood stages of the Plasmodium falciparum parasite express cytolytic and proinflammatory molecules. *Scand. J. Immunol.* **50,** 642–50 (1999).

200. Stevenson, M. M. & Riley, E. M. Innate immunity to malaria. *Nat. Rev. Immunol.* **4,** 169–80 (2004).

201. Engwerda, C. R. *et al.* Locally up-regulated lymphotoxin alpha, not systemic tumor necrosis factor alpha, is the principle mediator of murine cerebral malaria. *J. Exp. Med.* **195,** 1371–7 (2002).

202. Yoshimoto, T. *et al.* A pathogenic role of IL-12 in blood-stage murine malaria lethal strain *Plasmodium berghei* NK65 infection. *J. Immunol.* **160,** 5500–5 (1998).

203. Newbold, C. I., Pinches, R., Roberts, D. J. & Marsh, K. *Plasmodium falciparum*: the human agglutinating antibody response to the infected red cell surface is predominantly variant specific. *Exp. Parasitol.* **75,** 281–92 (1992).

204. Sherman, I. W., Eda, S. & Winograd, E. Cytoadherence and sequestration in *Plasmodium falciparum*: defining the ties that bind. *Microbes Infect.* **5,** 897–909 (2003).

205. Saul, A. The role of variant surface antigens on malaria-infected red blood cells. *Parasitol. Today* **15,** 455–7 (1999).

206. Mackintosh, C. L., Beeson, J. G. & Marsh, K. Clinical features and pathogenesis of severe malaria. *Trends Parasitol.* **20,** 597–603 (2004).

207. Serghides, L., Smith, T. G., Patel, S. N. & Kain, K. C. CD36 and malaria: friends or foes? *Trends Parasitol.* **19,** 461–469 (2003).

208. Schwarzer, E. *et al.* Impairment of macrophage functions after ingestion of *Plasmodium falciparum*-infected erythrocytes or isolated malarial pigment. *J. Exp. Med.* **176,** 1033–41 (1992).

209. Urban, B. C. *et al. Plasmodium falciparum*-infected erythrocytes modulate the maturation of dendritic cells. *Nature* **400,** 73–7 (1999).

210. Urban, B. C., Willcox, N. & Roberts, D. J. A role for CD36 in the regulation of dendritic cell function. *Proc. Natl. Acad. Sci. U. S. A.* **98,** 8750–5 (2001).

211. Urban, B. C. Peripheral blood dendritic cells in children with acute *Plasmodium falciparum* malaria. *Blood* **98,** 2859–2861 (2001).

212. Struik, S. S. & Riley, E. M. Does malaria suffer from lack of memory? *Immunol. Rev.* **201,** 268–90 (2004).

213. McGregor, I. A. & Barr, M. Antibody response to tetanus toxoid inoculation in malarious and non-malarious Gambian children. *Trans. R. Soc. Trop. Med. Hyg.* **56 ,** 364–367 (1962).

214. Barr, M. & McGregor, I. A. Diphtheria antitoxin levels in the serum of Gambian Africans. *Trans. R. Soc. Trop. Med. Hyg.* **56,** 368–70 (1962).

215. Greenwood, B. M., Palit, A., Bradley-Moore, A. & Bryceson, A. D. M. Immunosuppression in children with malaria. *Lancet* **299,** 169–172 (1972).

216. Williamson, W. A. & Greenwood, B. M. Impairment of the immune response to vaccination after acute malaria. *Lancet* **311,** 1328–1329 (1978).

217. Greenwood, B. M. *et al.* The immune response to a meningococcal polysaccharide vaccine in an African village. *Trans. R. Soc. Trop. Med. Hyg.* **74,** 340–6 (1980).

218. Usen, S., Milligan, P., Ethevenaux, C., Greenwood, B. & Mulholland, K. Effect of fever on the serum antibody response of Gambian children to *Haemophilus influenzae* type b conjugate vaccine. *Pediatr. Infect. Dis. J.* **19,** 444–9 (2000).

219. Burkitt, D. P. Etiology of Burkitt's lymphoma--an alternative hypothesis to a vectored virus. *J. Natl. Cancer Inst.* **42,** 19–28 (1969).

220. Whittle, H. C. *et al.* T-cell control of Epstein-Barr virus-infected B cells is lost during *P. falciparum malaria*. *Nature* **312,** 449–50

221. Weidanz, W. P. Malaria and alterations in immune reactivity. *Br. Med. Bull.* **38,** 167–72 (1982).

222. Hänscheid, T., Egan, T. J. & Grobusch, M. P. Haemozoin: from melatonin pigment to drug target, diagnostic tool, and immune modulator. *Lancet Infect. Dis.* **7,** 675–85 (2007).

223. Brown, W. H. Malarial Pigment (so-called melanin): its nature and mode of production. *J. Exp. Med.* **13,** 290–9 (1911).

224. Shio, M. T., Kassa, F. A., Bellemare, M.-J. & Olivier, M. Innate inflammatory response to the malarial pigment hemozoin. *Microbes Infect.* **12,** 889–99 (2010).

225. Pagola, S., Stephens, P. W., Bohle, D. S., Kosar, A. D. & Madsen, S. K. The structure of malaria pigment beta-haematin. *Nature* **404,** 307–10 (2000).

226. Egan, T. J. Haemozoin formation. *Mol. Biochem. Parasitol.* **157,** 127–36 (2008).

227. Lew, V. L., Tiffert, T. & Ginsburg, H. Excess hemoglobin digestion and the osmotic stability of *Plasmodium falciparum*-infected red blood cells. *Blood* **101,** 4189–94 (2003).

228. Sullivan, D. J. Theories on malarial pigment formation and quinoline action. *Int. J. Parasitol.* **32,** 1645–53 (2002).

229. Hoang, A. N., Ncokazi, K. K., de Villiers, K. A., Wright, D. W. & Egan, T. J. Crystallization of synthetic haemozoin (beta-haematin) nucleated at the surface of lipid particles. *Dalton Trans.* **39,** 1235–44 (2010).

230. Oliveira, M. F. *et al.* Structural and morphological characterization of hemozoin produced by *Schistosoma mansoni* and *Rhodnius prolixus*. *FEBS Lett.* **579,** 6010–6 (2005).

231. Nakatani, K., Ishikawa, H., Aono, S. & Mizutani, Y. Heme-binding properties of heme detoxification protein from *Plasmodium falciparum*. *Biochem. Biophys. Res. Commun.* **439,** 477–480 (2013).

232. Brown, W. H. Malarial pigment (hematin) as a factor in the production of the malarial paroxysm. *J. Exp. Med.* **15,** 579–97 (1912).

233. Sherman, I. W. Amino acid metabolism and protein synthesis in malarial parasites. *Bull. World Health Organ.* **55,** 265–76 (1977).

234. Francis, S. E., Sullivan, D. J. & Goldberg, D. E. Hemoglobin metabolism in the malaria parasite *Plasmodium falciparum*. *Annu. Rev. Microbiol.* **51,** 97–123 (1997).

235. Loose, L. D., Cook, J. A. & Di Luzio, N. R. Malarial immunosuppression-a macrophage mediated defect. *Proc. Helminthol. Soc. Wash.* **39,** 484–91 (1972).

236. Schwarzer, E., Turrini, F., Giribaldi, G., Cappadoro, M. & Arese, P. Phagocytosis of *P. falciparum* malarial pigment hemozoin by human monocytes inactivates monocyte protein kinase C. *Biochim. Biophys. Acta* **1181,** 51–4 (1993).

237. Schwarzer, E. & Arese, P. Phagocytosis of malarial pigment hemozoin inhibits NADPH-oxidase activity in human monocyte-derived macrophages. *Biochim. Biophys. Acta* **1316,** 169–75 (1996).

238. Fiori, P. L. *et al.* Reduced microbicidal and anti-tumour activities of human monocytes after ingestion of *Plasmodium falciparum*-infected red blood cells. *Parasite Immunol.* **15,** 647–55 (1993).

239. Schwarzer, E., Alessio, M., Ulliers, D. & Arese, P. Phagocytosis of the malarial pigment, hemozoin, impairs expression of major histocompatibility complex class II antigen, CD54, and CD11c in human monocytes. *Infect. Immun.* **66,** 1601–6 (1998).

240. Schwarzer, E., Müller, O., Arese, P., Siems, W. G. & Grune, T. Increased levels of 4-hydroxynonenal in human monocytes fed with malarial pigment hemozoin. A possible clue for hemozoin toxicity. *FEBS Lett.* **388,** 119–22 (1996).

241. Schwarzer, E., Ludwig, P., Valente, E. & Arese, P. 15(S)-hydroxyeicosatetraenoic acid (15-HETE), a product of arachidonic acid peroxidation, is an active component of hemozoin toxicity to monocytes. *Parassitologia* **41,** 199–202 (1999).

242. Schwarzer, E., Kuhn, H., Valente, E. & Arese, P. Malaria-parasitized erythrocytes and hemozoin nonenzymatically generate large amounts of hydroxy fatty acids that inhibit monocyte functions. *Blood* **101,** 722–8 (2003).

243. Skorokhod, O. a, Alessio, M., Mordmüller, B., Arese, P. & Schwarzer, E. Hemozoin (malarial pigment) inhibits differentiation and maturation of human monocyte-derived dendritic cells: a peroxisome proliferator-activated receptor-gamma-mediated effect. *J. Immunol.* **173,** 4066–74 (2004).

244. Skorokhod, O., Schwarzer, E., Grune, T. & Arese, P. Role of 4-hydroxynonenal in the hemozoin-mediated inhibition of differentiation of human monocytes to dendritic cells induced by GM-CSF/IL-4. *Biofactors* **24,** 283–9 (2005).

245. Giribaldi, G. *et al.* Hemozoin- and 4-hydroxynonenal-mediated inhibition of erythropoiesis. Possible role in malarial dyserythropoiesis and anemia. *Haematologica* **89,** 492–3 (2004).

246. Skorokhod, O. A. *et al.* Inhibition of erythropoiesis in malaria anemia: role of hemozoin and hemozoin-generated 4-hydroxynonenal. *Blood* **116,** 4328–37 (2010).

247. Skorokhod, A., Schwarzer, E., Gremo, G. & Arese, P. HNE produced by the malaria parasite *Plasmodium falciparum* generates HNE-protein adducts and decreases erythrocyte deformability. *Redox Rep.* **12,** 73–5 (2007).

248. Uyoga, S. *et al.* Transfer of 4-hydroxynonenal from parasitized to non-parasitized erythrocytes in rosettes. Proposed role in severe malaria anemia. *Br. J. Haematol.* **157,** 116–24 (2012).

249. Carney, C. K. *et al.* The basis of the immunomodulatory activity of malaria pigment (hemozoin). *J. Biol. Inorg. Chem.* **11,** 917–29 (2006).

250. Millington, O. R., Di Lorenzo, C., Phillips, R. S., Garside, P. & Brewer, J. M. Suppression of adaptive immunity to heterologous antigens during *Plasmodium* infection through hemozoin-induced failure of dendritic cell function. *J. Biol.* **5,** 5 (2006).

251. Giusti, P. *et al. Plasmodium falciparum*-infected erythrocytes and beta-hematin induce partial maturation of human dendritic cells and increase their migratory ability in response to lymphoid chemokines. *Infect. Immun.* **79,** 2727–36 (2011).

252. Were, T. *et al.* Naturally acquired hemozoin by monocytes promotes suppression of RANTES in children with malarial anemia through an IL-10-dependent mechanism. *Microbes Infect.* **11,** 811–9 (2009).

253. Ochiel, D. O. *et al.* Differential regulation of beta-chemokines in children with *Plasmodium falciparum malaria*. *Infect. Immun.* **73,** 4190–7 (2005).

254. Keller, C. C. *et al.* Suppression of a novel hematopoietic mediator in children with severe malarial anemia. *Infect. Immun.* **77,** 3864–71 (2009).

255. Keller, C. C. *et al.* Acquisition of hemozoin by monocytes down-regulates interleukin-12 p40 (IL-12p40) transcripts and circulating IL-12p70 through an IL-10-dependent mechanism: *in vivo* and *in vitro* findings in severe malarial anemia. *Infect. Immun.* **74,** 5249–60 (2006).

256. Ong'echa, J. M. *et al.* Increased circulating interleukin (IL)-23 in children with malarial anemia: *in vivo* and *in vitro* relationship with co-regulatory cytokines IL-12 and IL-10. *Clin. Immunol.* **126,** 211–21 (2008).

257. Pichyangkul, S., Saengkrai, P. & Webster, H. K. *Plasmodium falciparum* pigment induces monocytes to release high levels of tumor necrosis factor-alpha and interleukin-1 beta. *Am. J. Trop. Med. Hyg.* **51,** 430–5 (1994).

258. Sherry, B. A. *et al.* Malaria-specific metabolite hemozoin mediates the release of several potent endogenous pyrogens (TNF, MIP-1 alpha, and MIP-1 beta) *in vitro,* and altered thermoregulation in vivo. *J. Inflamm.* **45,** 85–96 (1995).

259. Giribaldi, G. *et al.* Involvement of inflammatory chemokines in survival of human monocytes fed with malarial pigment. *Infect. Immun.* **78,** 4912–21 (2010).

260. Jaramillo, M. *et al.* Hemozoin-inducible proinflammatory events *in vivo*: potential role in malaria infection. *J. Immunol.* **172,** 3101–10 (2004).

261. Jaramillo, M., Gowda, D. C., Radzioch, D. & Olivier, M. Hemozoin increases IFN-gamma-inducible macrophage nitric oxide generation through extracellular signal-regulated kinase- and NF-kappa B-dependent pathways. *J. Immunol.* **171,** 4243–53 (2003).

262. Jaramillo, M., Godbout, M. & Olivier, M. Hemozoin induces macrophage chemokine expression through oxidative stress-dependent and -independent mechanisms. *J. Immunol. (Baltimore, Md. 1950)* **174,** 475–84 (2005).

263. Prato, M. & Giribaldi, G. Matrix Metalloproteinase-9 and Haemozoin: Wedding Rings for Human Host and *Plasmodium falciparum* Parasite in Complicated Malaria. *J. Trop. Med.* **2011,** 628435 (2011).

264. Nagase, H. & Woessner, J. F. Matrix metalloproteinases. *J. Biol. Chem.* **274,** 21491–4 (1999).

265. Griffiths, M. J. *et al.* Genomewide analysis of the host response to malaria in Kenyan children. *J. Infect. Dis.* **191,** 1599–611 (2005).

266. Van den Steen, P. E. *et al.* Matrix metalloproteinases, tissue inhibitors of MMPs and TACE in experimental cerebral malaria. *Lab. Invest.* **86,** 873–88 (2006).

267. Prato, M., Giribaldi, G., Polimeni, M., Gallo, V. & Arese, P. Phagocytosis of hemozoin enhances matrix metalloproteinase-9 activity and TNF-alpha production in human monocytes: role of matrix metalloproteinases in the pathogenesis of falciparum malaria. *J. Immunol.* **175,** 6436–42 (2005).

268. Prato, M., Gallo, V., Giribaldi, G. & Arese, P. Phagocytosis of haemozoin (malarial pigment) enhances metalloproteinase-9 activity in human adherent monocytes: role of IL-1beta and 15-HETE. *Malar. J.* **7,** 157 (2008).

269. Giribaldi, G., Valente, E., Khadjavi, A., Polimeni, M. & Prato, M. Macrophage inflammatory protein-1alpha mediates matrix metalloproteinase-9 enhancement in human adherent monocytes fed with malarial pigment. *Asian Pac. J. Trop. Med.* **4,** 925–30 (2011).

270. Prato, M., Gallo, V., Giribaldi, G., Aldieri, E. & Arese, P. Role of the NF-κB transcription pathway in the haemozoin- and 15-HETE-mediated activation of matrix metalloproteinase-9 in human adherent monocytes. *Cell. Microbiol.* **12,** 1780–91 (2010).

271. Khadjavi, A., Valente, E., Giribaldi, G. & Prato, M. Involvement of p38 MAPK in haemozoin-dependent MMP-9 enhancement in human monocytes. *Cell Biochem. Funct.* (2013). doi:10.1002/cbf.2963

272. Polimeni, M. *et al.* Haemozoin induces early cytokine-mediated lysozyme release from human monocytes through p38 MAPK- and NF-kappaB-dependent mechanisms. *PLoS One* **7,** e39497 (2012).

273. Polimeni, M. *et al.* Human lysozyme as a potential diagnostic marker in malaria: a mechanistic study of haemozoin-induced monocyte degranulation. *Malar. J.* **11,** P80 (2012).

274. Prato, M., Giribaldi, G. & Arese, P. Hemozoin triggers tumor necrosis factor alpha-mediated release of lysozyme by human adherent monocytes: new evidences on leukocyte degranulation in *P. falciparum* malaria. *Asian Pac. J. Trop. Med.* **2,** 35–40 (2009).

275. Barrera, V. *et al.* Host fibrinogen stably bound to hemozoin rapidly activates monocytes via TLR-4 and CD11b/CD18-integrin: a new paradigm of hemozoin action. *Blood* **117,** 5674–82 (2011).

276. Coban, C. *et al.* Toll-like receptor 9 mediates innate immune activation by the malaria pigment hemozoin. *J. Exp. Med.* **201,** 19–25 (2005).

277. Jaramillo, M. *et al.* Synthetic *Plasmodium*-like hemozoin activates the immune response: a morphology - function study. *PLoS One* **4,** e6957 (2009).

278. Shio, M. T. *et al.* Malarial hemozoin activates the NLRP3 inflammasome through Lyn and Syk kinases. *PLoS Pathog.* **5,** e1000559 (2009).

279. Dostert, C. *et al.* Malarial hemozoin is a Nalp3 inflammasome activating danger signal. *PLoS One* **4,** e6510 (2009).

280. Griffith, J. W., Sun, T., McIntosh, M. T. & Bucala, R. Pure Hemozoin is inflammatory *in vivo* and activates the NALP3 inflammasome via release of uric acid. *J. Immunol.* **183,** 5208–20 (2009).

281. Wu, X., Gowda, N. M., Kumar, S. & Gowda, D. C. Protein-DNA complex is the exclusive malaria parasite component that activates dendritic cells and triggers innate immune responses. *J. Immunol.* **184,** 4338–48 (2010).

282. Parroche, P. *et al.* Malaria hemozoin is immunologically inert but radically enhances innate responses by presenting malaria DNA to Toll-like receptor 9. *Proc. Natl. Acad. Sci. U. S. A.* **104,** 1919–24 (2007).

283. Dasari, P. *et al.* Digestive vacuole of *Plasmodium falciparum* released during erythrocyte rupture dually activates complement and coagulation. *Blood* **119,** 4301–10 (2012).

284. Dasari, P. *et al.* Digestive vacuoles of *Plasmodium falciparum* are selectively phagocytosed by and impair killing function of polymorphonuclear leukocytes. *Blood* **118,** 4946–56 (2011).

285. Dasari, P. & Bhakdi, S. Pathogenesis of malaria revisited. *Med. Microbiol. Immunol.* **201,** 599–604 (2012).

286. Cambos, M. *et al.* The IL-12p70/IL-10 interplay is differentially regulated by free heme and hemozoin in murine bone-marrow-derived macrophages. *Int. J. Parasitol.* **40,** 1003–12 (2010).

287. Taramelli, D. *et al.* The heme moiety of malaria pigment (beta-hematin) mediates the inhibition of nitric oxide and tumor necrosis factor-alpha production by lipopolysaccharide-stimulated macrophages. *Exp. Parasitol.* **81,** 501–11 (1995).

288. Boura, M., Frita, R., Góis, A., Carvalho, T. & Hänscheid, T. The hemozoin conundrum: is malaria pigment immune-activating, inhibiting, or simply a bystander? *Trends Parasitol.* **29,** 469–476 (2013).

289. Marsh, K. & Kinyanjui, S. Immune effector mechanisms in malaria. *Parasite Immunol.* **28,** 51–60

290. Chen, M. M., Shi, L. & Sullivan, D. J. *Haemoproteus* and *Schistosoma* synthesize heme polymers similar to *Plasmodium* hemozoin and beta-hematin. *Mol. Biochem. Parasitol.* **113,** 1–8 (2001).

291. Coban, C. *et al.* The malarial metabolite hemozoin and its potential use as a vaccine adjuvant. *Allergol. Int. Off. J. Japanese Soc. Allergol.* **59,** 115–24 (2010).

292. Slater, A. F. *et al.* An iron-carboxylate bond links the heme units of malaria pigment. *Proc. Natl. Acad. Sci. U. S. A.* **88,** 325–9 (1991).

293. Keller, C. C. *et al.* Elevated nitric oxide production in children with malarial anemia: hemozoin-induced nitric oxide synthase type 2 transcripts and nitric oxide in blood mononuclear cells. *Infect. Immun.* **72,** 4868–73 (2004).

294. Pisciotta, J. M. & Sullivan, D. Hemozoin: oil versus water. *Parasitol. Int.* **57,** 89–96 (2008).

295. Coban, C. *et al.* Immunogenicity of whole-parasite vaccines against *Plasmodium falciparum* involves malarial hemozoin and host TLR9. *Cell Host Microbe* **7,** 50–61 (2010).

296. Mphande, F., Nilsson, S. & Bolad, A. in *Methods Malar. Res.* (Moll, K., Ljungström, I., Perlmann, H., Scherf, A. & Wahlgren, M.) 1–3 (2008).

297. Coban, C., Ishii, K. J., Sullivan, D. J. & Kumar, N. Purified malaria pigment (hemozoin) enhances dendritic cell maturation and modulates the isotype of antibodies induced by a DNA vaccine. *Infect. Immun.* **70,** 3939–43 (2002).

298. Bohle, D. S., Dinnebier, R. E., Madsen, S. K. & Stephens, P. W. Characterization of the Products of the Heme Detoxification Pathway in Malarial Late Trophozoites by X-ray Diffraction. *J. Biol. Chem.* **272,** 713–716 (1997).

299. Egan, T. J. & Tshivhase, M. G. Kinetics of beta-haematin formation from suspensions of haematin in aqueous benzoic acid. *Dalton Trans.* 5024–32 (2006). doi:10.1039/b610866k

300. Skorokhod, O. a, Schwarzer, E., Ceretto, M. & Arese, P. Malarial pigment haemozoin, IFN-gamma, TNF-alpha, IL-1beta and LPS do not stimulate expression of inducible nitric oxide synthase and production of nitric oxide in immuno-purified human monocytes. *Malar. J.* **6,** 73 (2007).

301. Schwarzer, E. *et al.* Hemozoin stability and dormant induction of heme oxygenase in hemozoin-fed human monocytes. *Mol. Biochem. Parasitol.* **100,** 61–72 (1999).

302. Bain, B. *Blood cells: a practical guide*. 23–24 (Oxford: Blackwell Science, 1995).

303. Hänscheid, T., Frita, R., Längin, M., Kremsner, P. G. & Grobusch, M. P. Is flow cytometry better in counting malaria pigment-containing leukocytes compared to microscopy? *Malar. J.* **8,** 255 (2009).

304. De Grooth, B. G., Terstappen, L. W., Puppels, G. J. & Greve, J. Light-scattering polarization measurements as a new parameter in flow cytometry. *Cytometry* **8,** 539–44 (1987).

305. Frita, R. *et al.* Simple flow cytometric detection of haemozoin containing leukocytes and erythrocytes for research on diagnosis, immunology and drug sensitivity testing. *Malar. J.* **10,** 74 (2011).

306. Hänscheid, T., Valadas, E. & Grobusch, M. P. Automated malaria diagnosis using pigment detection. *Parasitol. Today* **16,** 549–51 (2000).

307. Mendelow, B. V *et al.* Automated malaria detection by depolarization of laser light. *Br. J. Haematol.* **104,** 499–503 (1999).

308. Orjih, A. U. & Fitch, C. D. Hemozoin production by *Plasmodium falciparum*: variation with strain and exposure to chloroquine. *Biochim. Biophys. Acta* **1157,** 270–4 (1993).

309. Gordon, S. & Taylor, P. R. Monocyte and macrophage heterogeneity. *Nat. Rev. Immunol.* **5,** 953–64 (2005).

310. Passlick, B., Flieger, D. & Ziegler-Heitbrock, H. W. Identification and characterization of a novel monocyte subpopulation in human peripheral blood. *Blood* **74,** 2527–34 (1989).

311. Petkova, S. B. *et al.* Genetic influence on immune phenotype revealed strain-specific variations in peripheral blood lineages. *Physiol. Genomics* **34,** 304–14 (2008).

312. Kremsner, P. G. *et al.* Prognostic value of circulating pigmented cells in African children with malaria. *J. Infect. Dis.* **199,** 142–50 (2009).

313. Mordmüller, B., Turrini, F., Long, H., Kremsner, P. G. & Arese, P. Neutrophils and monocytes from subjects with the Mediterranean G6PD variant: effect of *Plasmodium falciparum* hemozoin on G6PD activity, oxidative burst and cytokine production. *Eur. Cytokine Netw.* **9,** 239–45 (1998).

314. Zimmerman, P. A., Thomson, J. M., Fujioka, H., Collins, W. E. & Zborowski, M. Diagnosis of malaria by magnetic deposition microscopy. *Am. J. Trop. Med. Hyg.* **74,** 568–72 (2006).

315. Mens, P. F., Matelon, R. J., Nour, B. Y. M., Newman, D. M. & Schallig, H. D. F. H. Laboratory evaluation on the sensitivity and specificity of a novel and rapid detection method for malaria diagnosis based on magneto-optical technology (MOT). *Malar. J.* **9,** 207 (2010).

316. Yuen, C. & Liu, Q. Magnetic field enriched surface enhanced resonance Raman spectroscopy for early malaria diagnosis. *J. Biomed. Opt.* **17,** 017005 (2012).

317. Rebelo, M., Shapiro, H. M., Amaral, T., Melo-Cristino, J. & Hänscheid, T. Haemozoin detection in infected erythrocytes for *Plasmodium falciparum* malaria diagnosis-prospects and limitations. *Acta Trop.* **123,** 58–61 (2012).

318. Krämer, B., Grobusch, M. P., Suttorp, N., Neukammer, J. & Rinneberg, H. Relative frequency of malaria pigment-carrying monocytes of nonimmune and semi-immune patients from flow cytometric depolarized side scatter. *Cytometry* **45,** 133–40 (2001).

319. Chimma, P. *et al.* A distinct peripheral blood monocyte phenotype is associated with parasite inhibitory activity in acute uncomplicated *Plasmodium falciparum* malaria. *PLoS Pathog.* **5,** e1000631 (2009).

320. Strauss-Ayali, D., Conrad, S. M. & Mosser, D. M. Monocyte subpopulations and their differentiation patterns during infection. *J. Leukoc. Biol.* **82,** 244–52 (2007).

321. Schofield, L. & Grau, G. E. Immunological processes in malaria pathogenesis. *Nat. Rev. Immunol.* **5,** 722–35 (2005).

322. White, N. J., Turner, G. D. H., Medana, I. M., Dondorp, A. M. & Day, N. P. J. The murine cerebral malaria phenomenon. *Trends Parasitol.* **26,** 11–5 (2010).

323. Van den Steen, P. E. *et al.* Immunopathology and dexamethasone therapy in a new model for malaria-associated acute respiratory distress syndrome. *Am. J. Respir. Crit. Care Med.* **181,** 957–68 (2010).

324. Metzger, W. G., Mordmüller, B. G. & Kremsner, P. G. Malaria pigment in leucocytes. *Trans. R. Soc. Trop. Med. Hyg.* **89,** 637–8

325. Nguyen, P. H., Day, N., Pram, T. D., Ferguson, D. J. & White, N. J. Intraleucocytic malaria pigment and prognosis in severe malaria. *Trans. R. Soc. Trop. Med. Hyg.* **89,** 200–4 (1995).

326. Ogonda, L. A. *et al.* The levels of CD16/Fc gamma receptor IIIA on CD14+ CD16+ monocytes are higher in children with severe *Plasmodium falciparum* anemia than in children with cerebral or uncomplicated malaria. *Infect. Immun.* **78,** 2173–81 (2010).

327. Schwarzer, E., Bellomo, G., Giribaldi, G., Ulliers, D. & Arese, P. Phagocytosis of malarial pigment haemozoin by human monocytes: a confocal microscopy study. *Parasitology* **123,** 125–31 (2001).

328. Day, N. P. *et al.* Clearance kinetics of parasites and pigment-containing leukocytes in severe malaria. *Blood* **88,** 4694–700 (1996).

329. Levesque, M. A., Sullivan, A. D. & Meshnick, S. R. Splenic and hepatic hemozoin in mice after malaria parasite clearance. *J. Parasitol.* **85,** 570–3 (1999).

330. Stephens, R., Culleton, R. L. & Lamb, T. J. The contribution of *Plasmodium chabaudi* to our understanding of malaria. *Trends Parasitol.* **28,** 73–82 (2012).

331. Deroost, K. *et al.* Improved methods for haemozoin quantification in tissues yield organ-and parasite-specific information in malaria-infected mice. *Malar. J.* **11,** 166 (2012).

332. Massie, H. R., Aiello, V. R. & Sternick, S. M. Comparative survival of C57BL/6J mice on two commonly used mouse diets. *Age (Omaha).* **14,** 53–56 (1991).

333. Sullivan, A. D., Ittarat, I. & Meshnick, S. R. Patterns of haemozoin accumulation in tissue. *Parasitology* **112 (Pt 3,** 285–94 (1996).

334. Menezes, R. G. *et al.* Autopsy discoveries of death from malaria. *Leg. Med. (Tokyo).* **14,** 111–5 (2012).

335. Valerie A. White. Malaria in Malawi: Inside a Research Autopsy Study of Pediatric Cerebral Malaria. (2011). at <http://www.archivesofpathology.org/doi/full/10.1043/1543-2165-135.2.220>

336. Casals-Pascual, C. *et al.* Suppression of erythropoiesis in malarial anemia is associated with hemozoin in vitro and in vivo. *Blood* **108,** 2569–77 (2006).

337. Kaufmann, S. H. E., Ladel, C. H. & Flesch, I. E. A. T cells and cytokines in intracellular bacterial infections: experiences with *Mycobacterium bovis* BCG. *Ciba Found. Symp.* **195,** 123–32; discussion 132–6 (1995).

338. Cunnington, A. J., de Souza, J. B., Walther, M. & Riley, E. M. Malaria impairs resistance to *Salmonella* through heme- and heme oxygenase-dependent dysfunctional granulocyte mobilization. *Nat. Med.* **18,** 120–7 (2012).

339. Achtman, A. H., Stephens, R., Cadman, E. T., Harrison, V. & Langhorne, J. Malaria-specific antibody responses and parasite persistence after infection of mice with *Plasmodium chabaudi chabaudi*. *Parasite Immunol.* **29,** 435–44 (2007).

340. Cattadori, I. M., Boag, B. & Hudson, P. J. Parasite co-infection and interaction as drivers of host heterogeneity. *Int. J. Parasitol.* **38,** 371–80 (2008).

341. Maude, R. J., Buapetch, W. & Silamut, K. A simplified, low-cost method for polarized light microscopy. *Am. J. Trop. Med. Hyg.* **81,** 782–3 (2009).

342. Wilson, B. K., Behrend, M. R., Horning, M. P. & Hegg, M. C. Detection of malarial byproduct hemozoin utilizing its unique scattering properties. *Opt. Express* **19,** 12190–6 (2011).

343. Frita, R., Carapau, D., Mota, M. M. & Hänscheid, T. *In Vivo* Hemozoin Kinetics after Clearance of Plasmodium berghei Infection in Mice. *Malar. Res. Treat.* **2012,** 373086 (2012).

List of Publications

Peer-reviewed articles

The hemozoin conundrum: is malaria pigment immune-activating, inhibiting, or simply a bystander?

Boura M[1], Frita R[1], Góis A[1], Carvalho T[1], Hänscheid T[1].

[1]*Instituto de Medicina Molecular, Faculdade de Medicina da Universidade de Lisboa, 1649-028 Lisbon, Portugal*

Published in Trends in Parasitology. October 29 2013, vol 29

***In Vivo* Hemozoin Kinetics after Clearance of *Plasmodium berghei* Infection in Mice**

Frita R[1], Carapau D[1], Mota MM[1], and Hänscheid T[1]

[1]*Instituto de Medicina Molecular, Faculdade de Medicina da Universidade de Lisboa, 1649-028 Lisbon, Portugal*

Published in Malaria Research and Treatment, vol. 2012.

Simple flow cytometric detection of haemozoin containing leukocytes and erythrocytes for research on diagnosis, immunology and drug sensitivity testing.

Frita R[1], Rebelo M[1], Pamplona A[1], Vigario AM[1], Mota MM[1], Grobusch MP[1], Hänscheid T[1]

[1]*Instituto de Medicina Molecular, Faculdade de Medicina de Lisboa, Lisbon, Hospital Universitário de Santa Maria, Av, Prof, Egas Moniz, P-1649-028 Lisboa, Portugal*.

Published in Malaria Journal, March 31 2011, vol 10

Is flow cytometry better in counting malaria pigment-containing leukocytes compared to microscopy?

Hänscheid T[1], Frita R[1], Längin M[1], Kremsner PG[1], Grobusch MP[1]

[1]*Medical Research Unit, Hôpital Albert Schweitzer, Lambaréné, Gabon.*

Published in *Malaria Journal,* November 16 2009, vol 87

Manuscripts in preparation

Malaria pigment promotes increased intracellular bacterial survival due to impaired cellular functions.

Rosangela Frita[±1], Márcia Boura[±1], Ana Góis[1], Tânia Carvalho[1], Maria M. Mota[1], Thomas Hänscheid[1]

[1]*Instituto de Medicina Molecular, Faculdade de Medicina da Universidade de Lisboa, 1649-028 Lisbon, Portugal*

Proposed journal: PLOS Pathogens

***In-vivo* Tuberculosis co-infection during *P. chabaudi* acute and chronic infection.**

Rosangela Frita[±1], Tânia Carvalho[1], Maria M. Mota[1], Thomas Hänscheid[1]

[1]*Instituto de Medicina Molecular, Faculdade de Medicina da Universidade de Lisboa, 1649-028 Lisbon, Portugal*

Communications

Oral presentations

V Congresso Pandemias na Era da Globalização e III Simpósio Nacional de Medicina do Viajante. Coimbra 2013.

'Co-infecção Malaria e Tuberculose: o papel da hemozoína.'

22 nd European Congress of Clinical Microbiology and Infectious Diseases. London, 2012

'Effect of malaria pigment (haemozoin) on infection and immunity'

IV Congresso Nacional Pandemias na era da Globalização e 2º Simpósio Nacional da Medicina do Viajante. Coimbra 2011.

'Pigmento malárico como possível adjuvante numa vacina com esporozoítos irradiados'

Poster presentations

VIII Congresso Nacional da Sida e X Congresso Nacional de Doenças infecciosas. Coimbra, 2010

'Malaria e Tuberculose: o papel do pigmento malárico'

Major Conferences Attended

22 nd European Congress of Clinical Microbiology and Infectious Diseases. London, 2012

'Effect of malaria pigment (haemozoin) on infection and immunity'

Awards

2010: Portuguese Society of Infectious Diseases. Best poster award on the VIII National AIDS congress and X National congress of Infectious Diseases, Coimbra, Portugal

2009: Glaxo Smith Kline Foundation on Health Sciences. Support grant for a doctorate in Infectious Pathology.

APPENDIX - Related Publications

In agreement with the Decreto-Lei 388/70, art. 8º, parágrafo 2, the results presented here were published or are currently being prepared for publication in the following scientific journals:

Chapter I

Hemozoin production and characterization

The hemozoin conundrum: is malaria pigment immune-activating, inhibiting, or simply a bystander?

Boura M, Frita R, Góis A, Carvalho T, Hänscheid T.

Trends Parasitol. 2013 Oct;29(10):469-76

CHAPTER II

1. **Detection of Hz-containing cells using flow-cytometry**

Simple flow cytometric detection of haemozoin containing leukocytes and erythrocytes for research on diagnosis, immunology and drug sensitivity testing.

Frita R, Rebelo M, Pamplona A, Vigario AM, Mota MM, Grobusch MP, Hänscheid T

Malar J. 2011 Mar 31;10:74.

CHAPTER III

Long term kinetics of hemozoin in mice organs

***In Vivo* Hemozoin Kinetics after Clearance of *Plasmodium berghei* Infection in Mice**

Frita R, Carapau D, Mota MM, and Hänscheid T

Malar Res Treat. 2012;2012:373086